博士論文

Analyses of water in silicate glass surface by ATR-IR spectroscopy

（ATR-IR分光法によるシリケートガラス表面に導入された水の分析）

安間　伸一

Table of Contents

Abstract

Surface region of industrially produced silicate glass often contains much higher water content due to reaction with its surrounding atmosphere or solution compared with its bulk region. Although various hydrous species, such as molecular water (H_2O) and/or hydroxyl group (SiOH) which have different degree of hydrogen bonding, have different influences on the properties of glass, there was no study to differentiate the associated speciation of hydrous species in glass surface. It's because surface-sensitive spectroscopic method which can probe the water in thin surface region has not been known previously.

In this study, we evaluated attenuated total reflection (ATR) – infrared (IR) spectroscopy as an analytical method for hydrous species introduced in surface of silicate glass monoliths and applied the method to understand effect of the surface treatment method, fictive temperature and glass composition on existing state of the species in conjunction with several surface analyze technique including X-ray photoelectron spectroscopy (XPS), secondary ion mass spectrometry (SIMS), specular reflectance IR and nano-indentation.

In chapter 2 and 3, several industry relevant, surface-treated samples, such as as-produced float glass, polished glass, leached glass by acid, and treated glass by SO_2 gas were studied. Ion-exchange between hydrogen in environment and sodium in glass was observed through SIMS and XPS depth profiling in the surfaces of the samples and ATR-IR analysis revealed that the relative speciation of the introduced hydrous species in these surfaces were completely different from those in bulk region and varied due to different surface treatment. Especially, SO_2 gas-treated glass surface was compared with acid-leached one in detail and found to have higher ratio of SiOH which possess weak

hydrogen bonding to molecular water, compared with acid-leached glass surface.

To understand the mechanism which cause different water speciation, the influence of the thermal history, especially fictive temperature, of glasses on water speciation was investigated in chapter 4. ATR-IR analyses showed the fictive temperature of the glass before leaching affect the relative amounts of SiOH (with weak hydrogen bonding) and molecular H_2O but the effect on the water speciation was not significant enough to explain the difference between SO_2 gas-treated and acid-leached surface. Therefore the difference in water speciation is expected to be due to the other parameters such as concentration of the hydrous species and/or treatment temperature.

In chapter 5, influence of the glass composition, especially aluminum content in silicate glasses, on formation of the altered layer through reaction with strong acid were studied. It was showed that in the glass with high aluminum content not only mobile alkali ion, such as sodium ion, but also aluminum were leached out from surface. Nano indenter experiments indicated that larger decrease of hardness was observed after acid treatment in the glass containing high amount of aluminum compared with other glasses with less aluminum including soda lime glass. ATR-IR spectra revealed that relative amount of weakly associated SiOH decreased and molecular water are increased among hydrous species with aluminum content. Moreover our results obtained through multiple surface analyses indicated that characteristics of the elemental composition and water speciation in the leached layer is similar to those in silica gel. For further investigation other analysis with a method which can probe network structure in glass surface, such as UV Raman spectroscopy, is needed. This study demonstrated that glass composition affect the formation of altered layer through the glass's reaction with solution.

In this work, we showed the combined analyses including ATR-IR and other surface-

sensitive method can provide quantitative and qualitative information of the hydrous species in surface of glass monolith, such as SiOH and molecular water. This technique was found to be useful to understand a mechanism how hydrous species in glass surface affect the properties of glass.

List of Figures

1 Introduction

1.1 Water in Bulk and Surface of Glass

While water of hundreds of parts per million are typically retained in bulk of commercial silicate glasses from water vapor in the melting atmosphere or from raw materials [1], concentration of water introduced to surface of the glasses through reaction with ambient humidity and aqueous solutions, especially under acid conditions, or certain gas species can be one or two orders of magnitude higher, which is up to several percent [2,3]. A typical diffused depth of the water in glass surface ranged from several nanometer to hundreds of nanometer. In this thesis, the term “water in glass surface” is referred to these hydrous species existing in outermost and inner surface of glass with the depth of up to several hundreds of nanometer.

Water in bulk of glasses have been analyzed through several methods and reported that the water can exist as a hydroxyl group (SiOH) or as interstitial molecular water (H_2O) [4,5] which have different impacts on glass properties as explained in the session 1.2. Although the concentration of water in glass surface is usually much higher than that in the bulk and it should cause critical influence on properties of the overall materials, there has not been study revealing the speciation of the water in surface region. This should be due to absence of surface sensitive spectroscopy which can detect hydrous species existing in glass surface regions.

1.2. Effects of Different Hydrous Species in Glass on Its Properties

Incorporated hydrous species in glass influence glass structure, and thereby, glass properties [1]. Since the hydroxyl species (SiOH) and the molecular water (H_2O) in glass have different effects as explained below, on glass properties, it is important to understand both concentration and speciation of hydrous species for prediction and control of the glass properties. .

The effect of water on the viscosity is significant. 5 wt% of water can cause decrease of as much as 40 % for glass transition temperature for same glass compositions (Fig. 1-1) [6]. This effect is considered as due to weakening of the Si-O-Si network by depolymerization through generation of hydroxyl groups upon incorporation of water, i.e., the bridging oxygen are converted to non-bridging hydroxyl. Diffused hydrous species into silica glass can promote structural relaxation. In this case, small quantity of molecular water was suggested to have important role in the relaxation rather than hydroxyl groups [7]. These are the examples where the hydroxyl species (SiOH) and the molecular water (H_2O) cause different influence in glass properties.

The effect of water on absorption in the infrared (IR) region is known to be very important in IR transmitting materials such as optical glass fibers for telecommunication systems. Molecular water and hydroxyl species cause absorption in different wavelength, respectively, which are extremely detrimental to the application of these fibers requiring extremely low loss.

Water also influences the mechanical properties of glass through reaction between glass network and water from environment. Michalske and Freiman suggested that

subcritical crack growth is caused by so-called stress corrosion, which is associated with the stress-enhanced thermal activation of a dissociative hydrolysis reaction represented in Fig. 1-2 for the case of silica glass [8]. This reaction is initiated by the penetration of the molecular water from environment to around crack tip while hydrolysis which break the Si–O–Si resulted in a couple of hydroxyl groups as the reaction below.

$$Si - O - Si + H_2O \rightarrow 2\,SiOH$$

Therefore existence of the molecular water and hydroxyl groups have different meanings in this scheme, it is important to differentiate the hydrous species in glass surface and crack tip. There have been lots of examples about the influence of hydrous species in glass on its mechanical properties in various aspects as well. For example, water adsorption and surface hydroxylation were reported to affect mechanical strength [9–12], the residual surface compressive stress in chemically strengthened glass can be relaxed at a faster rate in the presence of water [13] and diffused water from environment are suggested to generate a swollen zone around crack tip resulting in static fatigue of glass [14,15]

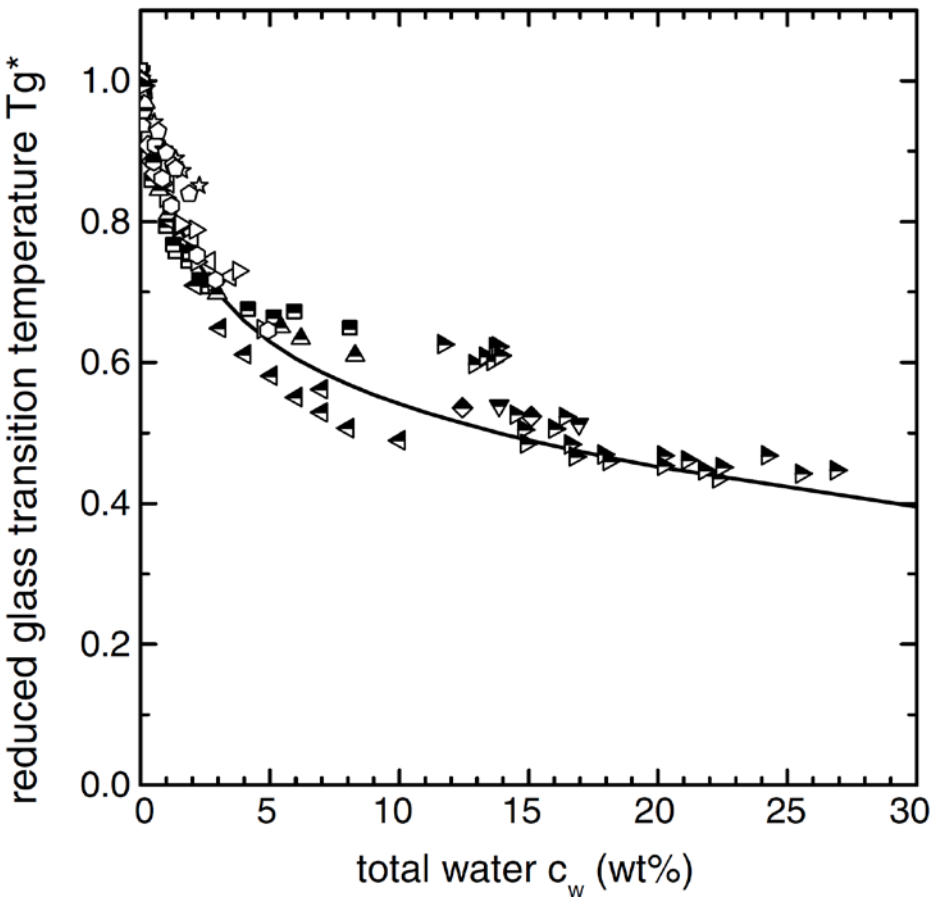

Fig. 1-1 Reduced glass transition temperature $T_g^* = T_g / T_g^{GN}$ as a function of the total water content c_w where T_g^{GN} is the glass transition temperature of glass with very low water content (c_w = 0.02wt %) [6]

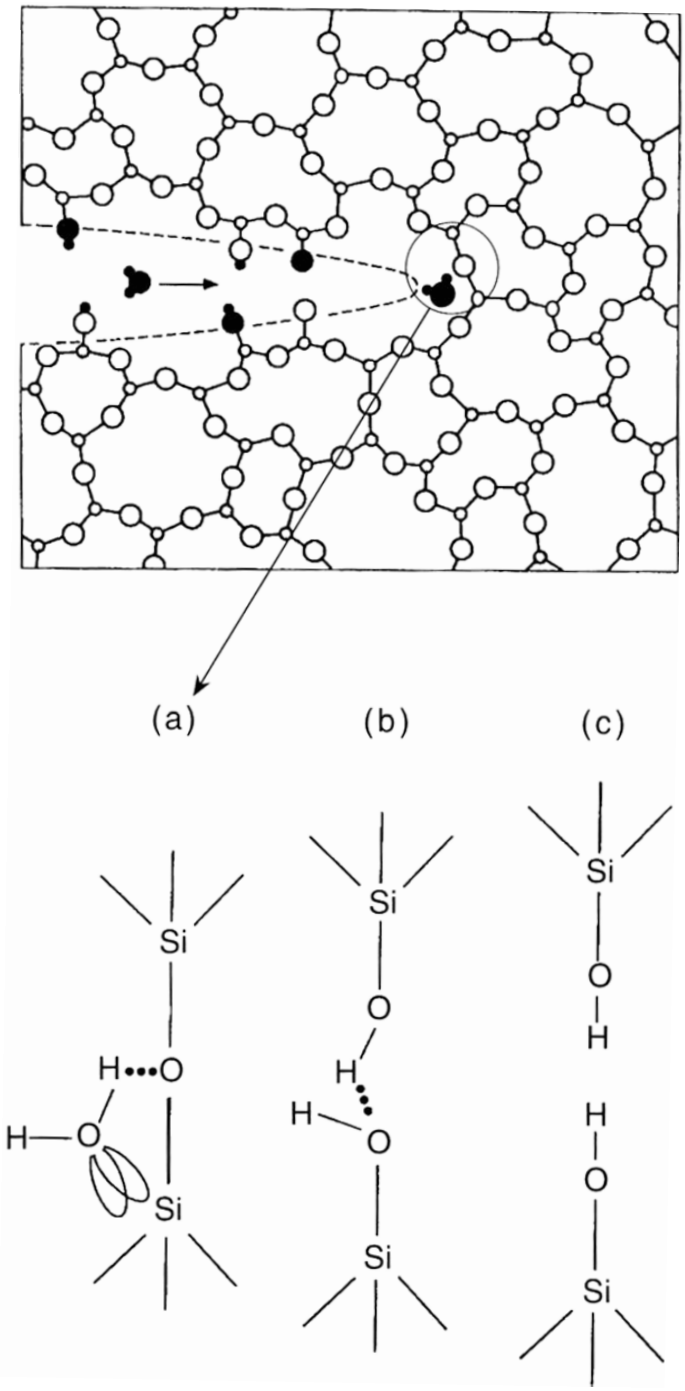

Fig. 1-2 Basic mechanism of the stress-corrosion reaction [8]

1.3. Analyses of Water in Glass Bulk

Several methods have been reported for the analysis of water and hydrogen in glass, but to identify and quantify the hydrous species, such as molecular water and hydroxyl group in glass, vibrational spectroscopies such as IR and Raman spectroscopies have been mainly utilized. The hydroxyl and molecular water in bulk of glasses can be detected by the transmission IR spectroscopies between 8000 and 800 cm^{-1}. The most accepted band assignments are those for silica glass reported by Davis and Tomozawa in Fig. 1-3[4]. For other multicomponent glasses, several groups studied peak assignment [16–20].

The most convenient way to estimate relative water concentration in glass bulk is to obtain transmission IR spectrum. The broad band attributed to the OH stretching vibration (ν_{OH}) of OH and H_2O is observed middle IR region within the 3700 - 2500 cm^{-1}. But this band is caused by both the hydroxyl species (SiOH) and the molecular water (H_2O) in glass. So to estimate each abundance of these species, combination band observed in near IR region were needed to be evaluated.

Stuke studied the relative concentration of SiOH and H_2O in bulk of soda lime glass by analyzing 4500 cm^{-1} band assigned to the combination of OH stretching and bending modes of SiOH with weak hydrogen bonding and 5250 cm^{-1} band assigned to the combination band of stretching and bending modes of molecular water groups (Fig. 1-4)[5]. The ratio of SiOH to molecular water depends on their concentration or composition of glass matrix. As shown in Fig. 1-5, when the total water concentration is less than 1 wt% in the bulk, the majority of water exist as SiOH, while at higher concentration interstitial molecular water is dominant.

Raman spectroscopy can provide important insight of the water speciation in the bulk of glasses as well as impacts of water on the glass network. For instance, Le Losq et al. demonstrated that temperature has important role in the water speciation in aluminosilicate melts and glasses by in situ high temperature Raman experiment. Their experiments show the dissociation of molecular water into its ionic products H^+ and OH^- determines the observed evolution of the measured water speciation between hydroxyl (OH) groups and molecular water in the melt [21].

^1H nuclear magnetic resonance (NMR) spectroscopy can also be utilized to analyze the water speciation in bulk of glass. Yamashita reported analysis of the water speciation in several sodium silicate glasses by ^1H NMR in conjunction with transmission IR spectroscopy with in near IR region [22].

Although the speciation of the bulk water can be evaluated through those analytical method, such as transmission IR spectroscopy, Raman spectroscopy and NMR, it lacks the surface sensitivity to reveal the speciation of water in the surface region of a flat silicate glass plate.

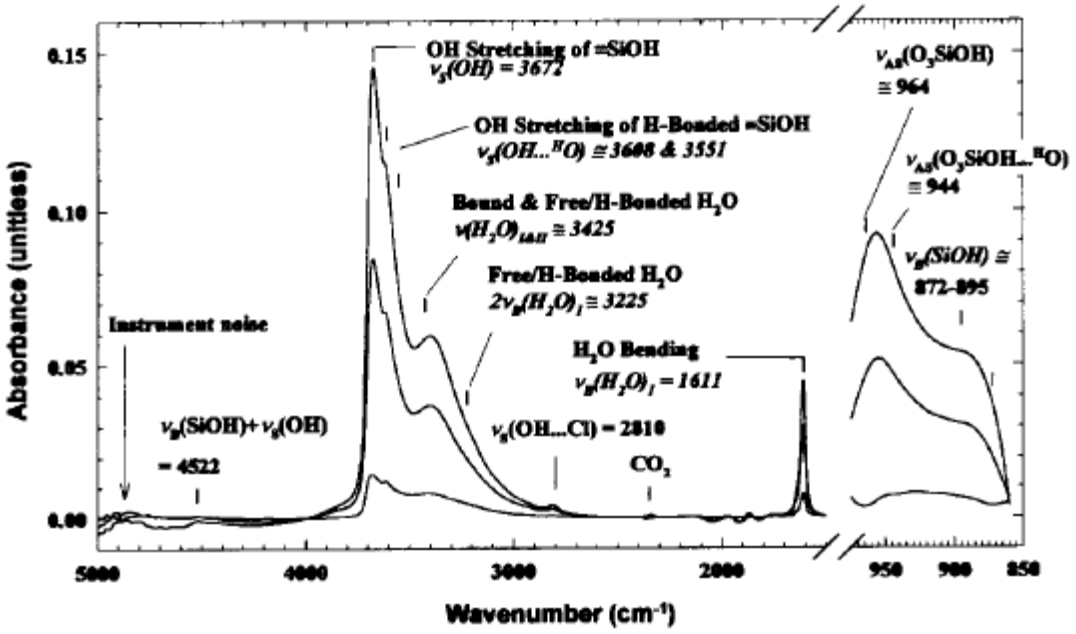

Fig. 1-3 IR difference spectra of a thin Suprasil W2 (silica glass) specimen hydrated for 4, 58.5 and 144 h at 250°C in saturated water vapor (39.2 atm).

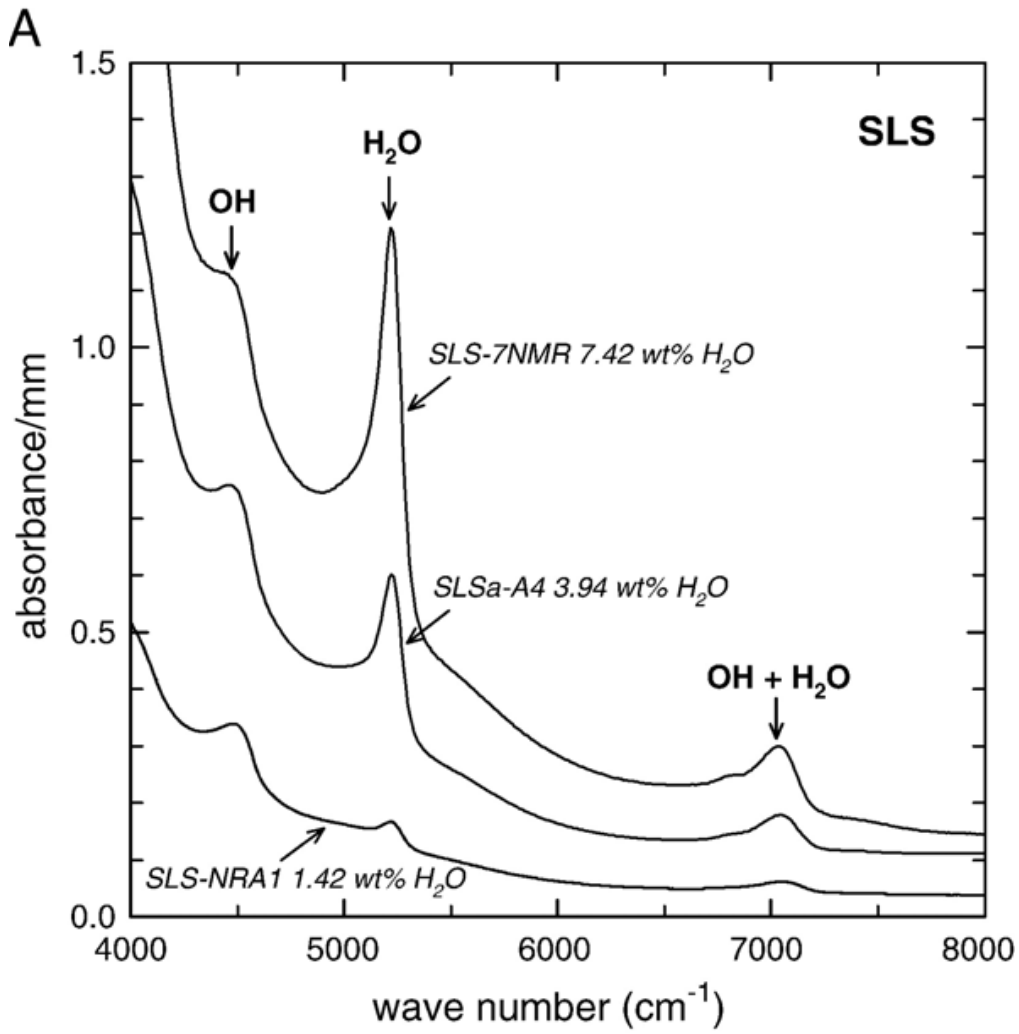

Fig. 1-4 Near-infrared absorption spectra of soda-lime silica glass [5]

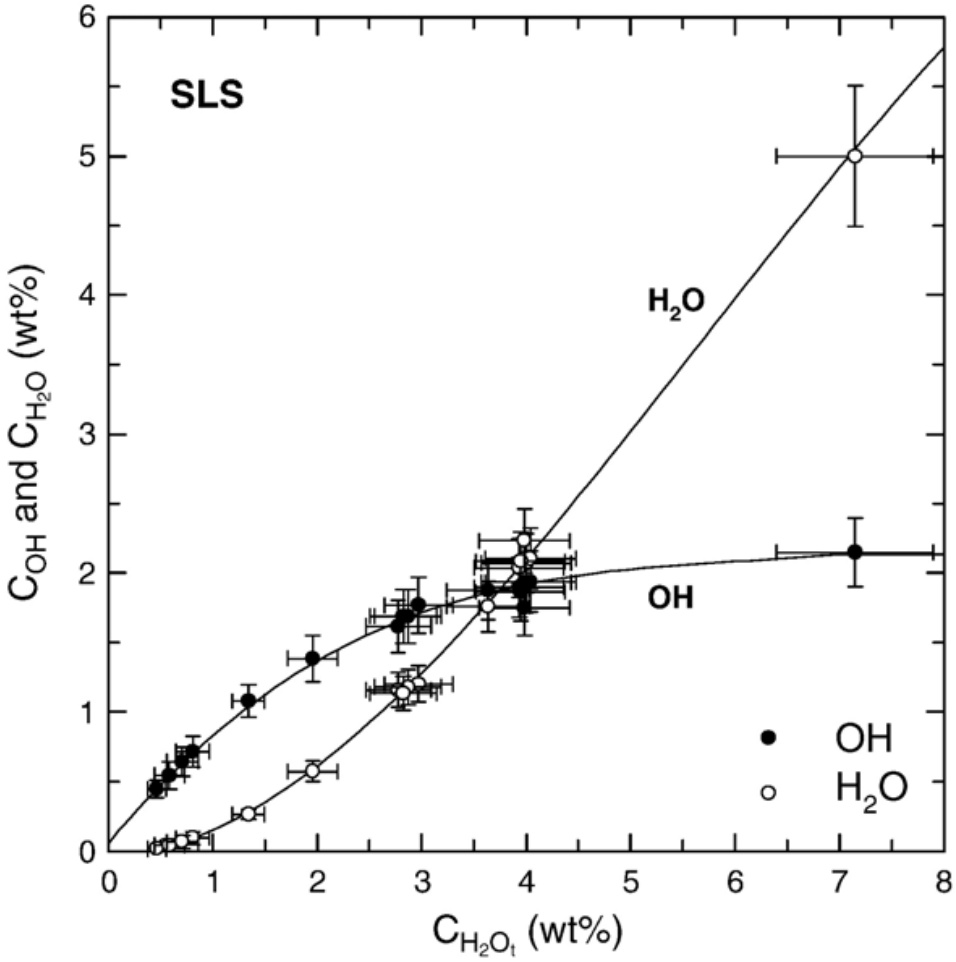

Fig. 1-5 Concentrations of OH groups and H_2O molecules as a function of total water content for soda lime silica glass [5]

1.4. Analyses Methods for Glass Surface

As an analytical method for glass surface, X-ray photoelectron spectroscopy (XPS) and secondary ion mass spectrometry (SIMS) have been typically employed for evaluation of glass surface composition. XPS is spectroscopy which measures the kinetic energy of photoelectron escaped from each element in materials surface irradiated with a beam of X-rays. Since the kinetic energy depends on binding energy of the electron which is specific to element, XPS can be utilized to analyze the elements in the surface. Moreover it can obtain distinctive information from the chemical or electronic state of the surface atoms by analyzing peak shift (chemical shift) in the spectra, because the binding energy is changed due to the chemical state of the element. Since only photoelectron in the depth within typically 10nm can escape from the surface, XPS possess high surface-sensitivity, which means it can obtain from very shallow region of the surface. The detection limit of XPS is typically around 0.1 at%, depending on the element. Combined with Ar ion sputtering of the surface atoms, depth profiling of the elemental composition is possible. Although there is a limitation for depth profiling due to the Ar ion sputtering damage on glass surface such as the concentration change of mobile (alkali and alkaline- earth) ions, by using C_{60} ion as sputtering gas the precise depth profile with the suppression of the migration of mobile ions can be obtained [2,23].

However, XPS doesn't have capability to analyze speciation of hydrous species existing in the depth of several hundreds of nanometer in glass surface because of its characteristics. To reveal the speciation of hydrous species in glass surface XPS needs to depend on information from chemical state of oxygen ion as a probe since it cannot analyze hydrogen ion which does not emit photoelectron. The speciation of water within

XPS information depth (typically 10 nm) of the surface region can be analyzed through evaluation of oxygen 1s peak which shifts due to the chemical state of oxygen, such as bridging oxygen in glass network (Si-O-Si), non-bridging oxygen ($Si-O^-$), oxygen in silanol (SiOH) and oxygen in water molecule (H-O-H) [24,25]. Although the chemical state of the oxygen in deeper region than the information depth needs to be analyzed in combination with the ion sputtering, chemical state of elements can be altered by the sputtering [26], which make difficult to obtain the information of the original distribution of the hydrous species by XPS.

SIMS is another way to obtain the depth profile of elements in glass in combination of ion sputtering. In SIMS, materials surface is irradiated with a focused primary ion beam and secondary ion ejected by sputtering is collected and analyzed with a mass spectrometer to determine the elemental composition of the surface. Especially, the technique make possible of depth profiling of elemental composition in several tens of um with detection limit of as low as ppm to ppb since it uses the atoms which comprise the surface as signals. It detect the atoms through mass spectroscopy, which enables to analyze the profile of all elements including hydrogen which cannot be detected by XPS. However, this method still does not reveal the speciation of water in deeper region with the ion sputtering because, again, the sputtering can change the chemical state of it.

Nuclear reaction analysis (NRA) can also analyze the profile of hydrogen but we cannot know the water speciation through this method because this method uses a resonant nuclear reaction as a probe for hydrogen.

Diffuse reflectance infrared Fourier transform spectroscopy (DRIFTS) [27] is an IR spectroscopic technique that is applicable to glass materials with high surface area, such as powder or fiber. IR beam incident onto a sample may be partly reflected regularly

(specular reflection) by the sample surface, but mainly scattered diffusely and penetrates into the sample. In DRIFTS, diffusely scattered light in all directions are collected and utilized for an analysis. This technique is quite sensitive to the surface and, however, is difficult to apply to glass monolith sample which is important in industrialized glass product. Moreover, there is no linear relation between the reflected light intensity (band intensity) and concentration, in contrast to traditional transmission spectroscopy in which the band intensity is directly proportional to concentration. Therefore, quantitative analyzes by DRIFTS are rather complicated.

Although the several methods have been utilized to analyze surface region of glass as reviewed in this section, existing state of hydrous species in the surface region of flat glass cannot be probed by these methods.

1.5. Attenuated Total Reflection (ATR) – IR Spectroscopy

Attenuated total reflection (ATR) - IR spectroscopy is a method that can provide surface-sensitive analysis in the outermost micron of the surface of materials [28]. It utilizes a crystal made with high-refractive-index materials, such as diamond, germanium or ZnSe, through which light is passed. If the crystal is in direct contact with a sample of lower refractive index, the light is totally reflected at the interface and the evanescent wave of the reflected light penetrates into the sample in contact with the crystal surface. The absorption of this evanescent wave by the sample attenuates the total reflection of the light at the interface, which is recorded as a function of the wavelength of the reflected light.

The evanescent wave decays exponentially with the distance from the surface within the sample. Its penetration depth is usually expressed as the distance at which the electric field intensity in the sample falls to 37 % (e^{-1}) of the surface value, and is calculated as shown below for the case of a media with a low extinction coefficient, *k*:

$$d_p = \lambda \Big/ \left\{ 2\pi n_1 \left[\sin^2\theta - (n_2/n_1)^2 \right]^{1/2} \right\} \quad \cdots (1)$$

where λ = wavelength of the IR beam, θ = incident angle of the IR beam, n_1 = the refractive index of the internal reflection crystal, and n_2 = the refractive index of the sample. Since the *k* value is very low (~10^{-5}) and the refractive index changes only slightly in the wavenumber range between 4000 and 1600 cm^{-1} for soda lime glasses [29], the ATR spectra of silicate glasses are readily obtained. When diamond crystal with a refractive index of around 2.4 is used as the crystals, the penetration depth of the

evanescent wave in soda lime glass is about several hundreds of nanometer, which is comparable with the diffused depth of the hydrous species in surfaces of acid-leached glass [3] and float glass [2]. Therefore, ATR - IR is expected to be appropriate method to analyze the existing state of the hydrous species in glass surfaces. There are a few reports of ATR-IR for inorganic glasses [30–32], but none address the speciation of water in the near surface region. Uchino reported ATR-IR spectra of hydrated Na_2O-SiO_2 glasses but didn't discussed the speciation of hydrous species but vibration in Si-O network [30]. Lowenstern studied water concentration in quartz and melt inclusions in it using ATR-IR. They obtained a mapping of the concentration with ATR micro-FTIR which utilized small ATR crystal tip of 350 um diameter but didn't mentioned the effect of surface treatment methods on the speciation of the hydrous species.

1.6. Scope of This Thesis

Glass surface often contains much higher water content compared to its bulk region, which is due to reaction with its environmental atmosphere or solution. Although different hydrous species, such as hydroxyl group (SiOH) and/or molecular water (H_2O) which have different degree of hydrogen bonding, in glass surface have different effects on properties of the material, the speciation of hydrous species in glass surfaces with a depth of several hundred nanometer has not been studied well so far because adequate surface-sensitive spectroscopic method which can probe the species has not been known.

In this research, we first attempted to evaluate ATR-IR spectroscopy as a surface-sensitive analytical method to investigate water in glass surface. We also compared the hydrogen profiles in leached glasses obtained with SIMS for quantitative analysis of the OH peak intensity in the ATR spectra (Chapter 2). Then, we measured and evaluated the ATR-IR spectra of various surface treated float glass samples (as-produced, polished, leached by acid, treated by SO_2 gas, and strengthened by thermal or chemical methods) to understand the water speciation in there surface (Chapter 3). To understand the mechanism which cause different water speciation in acid-leached and SO_2 gas-treated glass surface, we investigated the effect of fictive temperature of glasses on water speciation (Chapter 4). Influence of the glass composition, especially aluminum content in silicate glasses, on reaction with strong acid were studied through glass surface analyses through SIMS, XPS, ATR-IR and nano-indenter experiments. Correlation between hardness and composition of reacted layer were discussed (Chapter 5). Chapter 6 summarized this study.

2 Evaluation of ATR – IR Spectroscopy as Analysis Method of Glass Surface

2.1. Introduction

Characterization of the chemical structure of the surface and subsurface region of silicate glass is very important. Among various analytical techniques, infrared (IR) spectroscopy has been widely used for this purpose. IR can probe BO, and NBO groups as well as Si-OH and H_2O species inside the glass [33–37].

In order to obtain the surface information, IR analysis of glass must be carried out in a specular reflection (SR) or attenuated total reflection (ATR) configuration, rather than typical transmission mode [38].

Fig. 2-1 schematically compares these three methods. In the transmission mode, the signal intensity is often expressed as absorbance (A) which is defined as $-log(I_t/I_o)$ where I_o and I_t are the intensities of the incident and transmitted IR beams, respectively. The absorbance follows the Beer-Lambert law, $A = abc$ where a is specific absorptivity, b is sample thickness, and c is concentration of the species of interest. Since the thickness of the surface region affected by glass manufacturing processes or environmental corrosion is much thinner than the total thickness of the sample ($b_{surface} << b_{bulk}$), the transmission signal is always dominated by the bulk species.

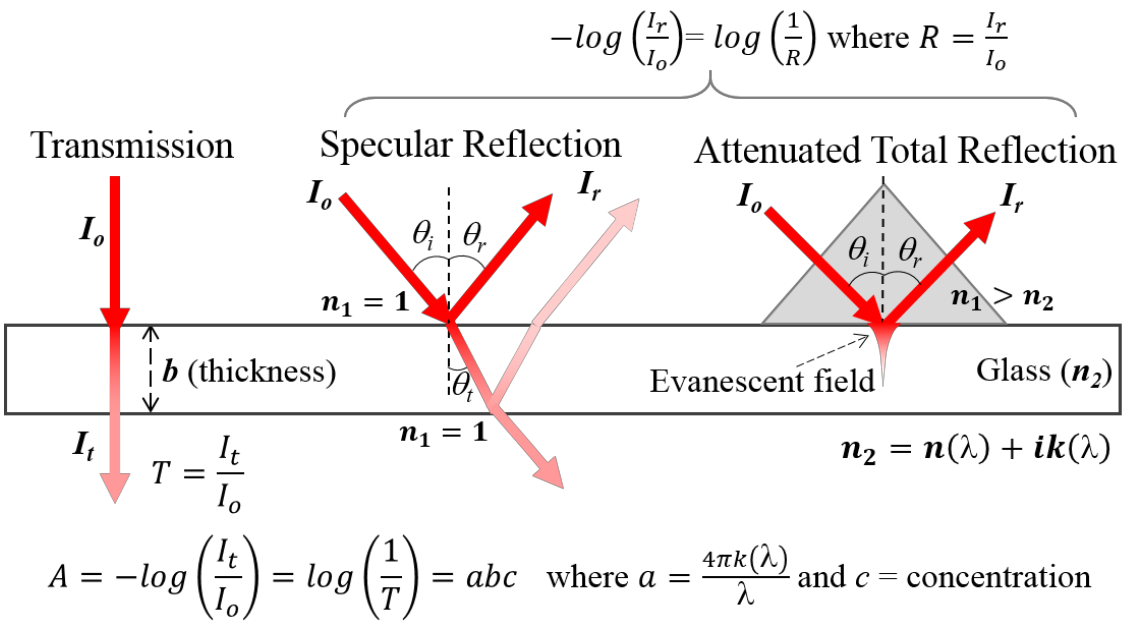

Fig. 2-1 Schematic illustration of transmission, specular reflection (SR), and attenuated total reflection (ATR) IR spectroscopy of a flat glass sample

In SR-IR, the intensity of the reflected beam (I_r) is measured and expressed as a reflectance ($R=I_r/I_o$), which is *dimensionally equivalent* to the transmittance (I_t/I_o) in the transmission mode experiment. When the IR frequency resonates with the absorption band of the sample, the reflected beam intensity is enhanced in SR-IR. Thus, the peak in the R vs. wavenumber (cm^{-1}) plot of SR-IR is positive, while the peak in transmission IR is negative when plotted in the percent transmission ($I_t/I_o \times 100\%$) scale.

In the case of ATR-IR, a crystal with a refractive index (n_1) higher than that of sample of interest (n_2) is in intimate contact with the sample surface and the IR probe beam is irradiated through this crystal. When the IR incidence angle (θ_i) is higher than the critical angle ($\theta_c=\arcsin(n_2/n_1)$), then IR is totally reflected from the crystal/sample interface and only an evanescent wave penetrates into the sample. The interaction of this evanescent wave and the absorption band of the sample attenuates the total reflection. When the measured reflectance (R) is plotted as log(1/R), then it is *dimensionally equivalent* to the absorbance; thus, peaks in ATR-IR spectra are often interpreted as absorption bands as in the case of transmission spectra.

However, it should be noted that peaks in the transmission IR spectra are governed by the absorptivity (a) which is a function of the imaginary (k) part of the complex refractive index of glass ($n+ik$) [i.e., $a = 4\pi k/\lambda$ where λ is the IR wavelength], while those in the SR-IR and ATR-IR spectra are governed by both the real (n) and imaginary (k) parts that vary over a large range [29]. As shown in Fig. 2-2 [29], the real part of the glass refractive index is not constant; due to the Kronig-Kramers relationship [39,40], n varies significantly along with k especially near the absorption band region. Thus, the SR-IR and ATR-IR spectra of glass cannot be interpreted in the same manner as the transmission IR peaks. The peak position, shape, and relative intensity can be drastically

different in the SR-IR and ATR-IR spectra of glass.

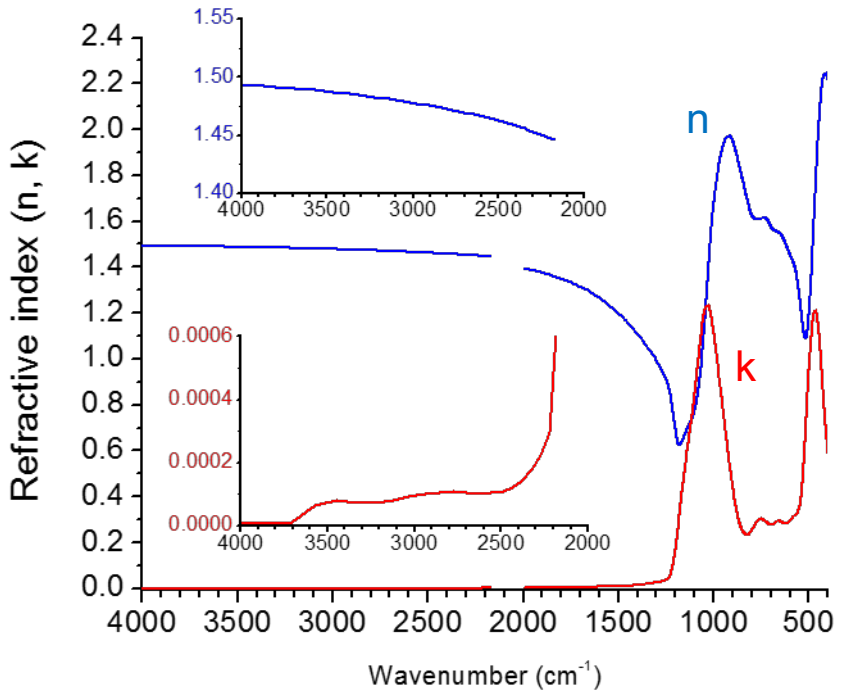

Fig. 2-2 Real (n) and imaginary (k) components of refractive index of soda lime glass shown in blue and red line, respectively [29].

Although ATR-IR spectroscopy is a useful and convenient method for evaluation of glass surface because it can be more surface sensitive than transmission IR analysis, only few studies on ATR-IR for inorganic glasses have been reported [30–32,41] and none of them discussed the comparison between theoretical and experimental spectra from glass surface. This chapter aims to provide clear explanations of how the spectral features in both SR-IR and ATR-IR spectra of glass are altered at various measurement conditions and how they should be interpreted. Spectral changes in as-produced float glass and acid treated soda lime glass are discussed; the same principles can be applied to other types of glass.

2.2. Experiment

2.2.1 Sample preparation

Soda lime float glasses (0.7 mm-thick) were used in this study as as-produced sample, which were supplied by AGC Inc. in Japan. The bulk composition of the glasses was analyzed by x-ray fluorescence (XRF) and is shown in Table 2-1. In all reflection experiments, the air-side of the float glass was used as the top side where incident IR beam entered. Some float glass samples were remelted in a Pt crucible in an electric furnace and quenched on a carbon plate. The quenched glass blocks were annealed at 600 ^{o}C for 1 hour and cooled slowly at a cooling rate of 1 ^{o}C/min to remove residual stress. Annealed glasses were then cut and polished with SiC sandpaper and CeO_2 dispersed in water into 5.0 mm thick slabs. Before IR measurements, all samples were cleaned with distilled water and ethanol in an ultrasonic cleaner and then using an UV/ozone cleaner.

In order to study changes in the hydrous species and the glass network structure in the surface region, the remelted and polished glass samples were treated with a 0.1M HCl solution at 90 ^{o}C for 1, 5, 20, 80, and 320 hours. The surface area of each sample treated with 50 ml HCl solution was 7.5 cm^2.

Table 2-1 Glass composition determined by XRF

	SiO_2	Al_2O_3	MgO	CaO	Na_2O	K_2O	Fe_2O_3
mol%	70.8	1.0	6.2	9.1	12.5	0.4	0.04

2.2.2 SR-IR measurements

SR-IR spectra of both as-produced float glass with 0.7 mm thickness and polished and leached samples with 5.0 mm thickness were obtained by three instruments: (i) 20^{o} incidence angle from the surface normal direction using a Bruker Hyperion 3000 micro-FT-IR system equipped with a 15x infrared microscope objective lens (Bruker Optics Inc.), (ii) ~45^{o} incidence angle using a Thermo-Nicholet 670 FTIR system equipped with a custom-arranged optics, and (iii) 43^{o}, 53^{o}, 58^{o}, 63^{o}, and 68^{o} incidence angles using a Bruker Hyperion 3000 system equipped with a Pike VeeMAX II ATR accessory. SR-IR spectra were obtained in the range of 4000 – 500 cm^{-1}. Spectra were acquired for three spots per sample in 400 scan passes at a 4 cm^{-1} resolution. A gold mirror was used as a standard reference for all measurements.

2.2.3 ATR-IR measurements

A Bruker Vertex70 FT-IR system was used for ATR-IR analysis of both float (0.7mm thickness) and leached (5.0mm thickness) soda-lime glass samples using diamond and Ge ATR crystals. For the diamond ATR (MVP-Pro, Harrick Scientific Products), the IR beam incident angle was 45°. The sample was contacted against the ATR diamond crystal with a force of pushed by 420 N over a 1.5 mm^2 sampling area. For the Ge ATR (VariGATR, Harrick Scientific Products), the IR incident angle was set at 60°. The sample was contacted against the ATR germanium crystal with a force of pushed by 600 N over 1 cm^2 sampling area. Spectra were collected for 100 scans with a spectral resolution of 6 cm^{-1} from 4000 to 400 cm^{-1} for diamond ATR and from 4000 to 800 cm^{-1} in Ge ATR. The diamond ATR crystal absorbs IR in the 2300 and 2000 cm^{-1} region; so, this region cannot be probed. For the same reason, the Ge ATR-IR spectrum cuts off at 800 cm^{-1}. For the leached samples, peak heights in absorbance units were measured at their maximum values near 3450 cm^{-1} (A_{3450}) utilizing a straight baseline. The typical variance in the peak intensity was less than 5 % based on 3 measurements per sample.

2.2.4 Simulations of SR- and ATR- IR spectra

The reflectance of the IR beam was calculated using the Fresnel equations [42] and the refractive index of soda lime glass was taken from a literature (Fig. 2-2) [29]. The reflection coefficients of *p*-polarized and *s*-polarized beams (r_p and r_s, respectively) at an interface between media 1 and 2 are expressed as:

$$r_{p,12} = \frac{n_2 cos\theta_1 - n_1 cos\theta_2}{n_2 cos\theta_1 + n_1 cos\theta_2} \text{ and } r_{s,12} = \frac{n_1 cos\theta_1 - n_2 cos\theta_2}{n_1 cos\theta_1 + n_2 cos\theta_2} \quad (1)$$

where n_1 is the refractive index of the media 1, n_2 is the complex refractive index of media 2 ($n_2 = n(\lambda) + ik(\lambda)$ from Fig. 2-2 [29]), θ_1 is the incident angle (θ_i in Fig. 2-1) and θ_2 is the transmission angle (θ_t in Fig. 2-1) calculated from Snell's equation: $n_1 sin\theta_1 = n_2 sin\theta_1$. In the case of SR-IR, n_1 = 1 (air); in the case of ATR-IR, n_1 = ~2.4 diamond and ~4 for germanium. The exact n_1 value as a function of IR wavenumber can be found at for diamond [43] and for germanium [44]. Then, the reflectance of p-polarized (electric vector polarized parallel to the incidence plane) and s-polarized (perpendicular to the incidence plane) component of the IR beam are calculated as:

$$R_p = r_{p,12} r_{p,12}^* \text{ and } R_s = r_{s,12} r_{s,12}^* \quad (2)$$

and the total reflectance of the unpolarized beam is the average of these two values:

$$R = (R_p + R_s)/2 \quad (3)$$

Within the glass sample, the electric filed intensity of IR decreases with an exponential function of the distance from the surface. The characteristic attenuation or penetration distance is expressed as the distance required for the electric field amplitude (transmitted beam in SR-IR or evanescent wave in ATR-IR) to fall to 36.8% (e^{-1}) of its value at the surface. The penetration of depth of SR-IR [33] is defined as

$$d_{p,SR} = \lambda/4\pi k(\lambda) \quad (4)$$

The penetration depth in ATR-IR is expressed as

$$d_{p,ATR} = \lambda/\left(2\pi \text{Im}\left[\sqrt{n_2^2 - n_1^2 sin^2\theta_1}\right]\right) \quad (5)$$

where Im[] means the magnitude of the imaginary part [28]. Note that when $k(\lambda) \approx 0$,

then $d_{p,ATR}$ can be calculated using only the real part of n_2. The information depth from which most of IR signal comes from is three times the characteristic penetration depth which is wavelength dependent.

When the glass sample is thin, a small portion of the transmitted IR beam can be reflected from the backside of the sample and can be detected along with the beam reflected from the front surface (Fig. 2-1). In that case, the total reflectivity of SR-IR can be calculated as:

$$r_{p,121} = r_{p,12} + t_{p,12}r_{p,21}t_{p,21}e^{2i\beta} \text{ and } r_{s,121} = r_{s,12} + t_{s,12}r_{s,21}t_{s,21}e^{2i\beta} \quad (6)$$

where $t_{p,12}$ and $t_{s,12}$ is the transmission coefficients at the front surface for the beam entering from air, $r_{p,21}$ and $r_{s,21}$ is the reflection coefficient at the back surface, $t_{p,21}$ and $t_{s,21}$ is the transmission coefficient at the front surface for the beam reflected from the back surface, and $\beta = 2\pi b n_1 cos\theta_1/\lambda$ (where b = sample thickness; Fig. 2-1

Fig. 2-1) is the phase of the IR beam propagated through the glass. The transmission coefficients are calculated as:

$$t_{p,12} = \frac{2n_1 cos\theta_1}{n_2 cos\theta_1 + n_1 cos\theta_2} \text{ and } t_{s,12} = \frac{2n_1 cos\theta_1}{n_2 cos\theta_2 + n_1 cos\theta_1} \quad (7)$$

The $r_{p,21}$, $r_{s,21}$, $t_{p,21}$, and $t_{s,21}$ terms can be calculated by changing the subscript order in the $r_{p,12}$, $r_{s,12}$, $t_{p,12}$, and $t_{s,12}$ equations, respectively. Then, the total reflectance (R_{121}) from both front and back surfaces is calculated using the same equations (2) and (3) where $r_{p,121}$ and $r_{s,121}$, are used, instead of $r_{p,12}$ and $r_{s,12}$.

2.2.5 Secondary Ion Mass Spectroscopy (SIMS)

SIMS analyses of the leached samples were carried out using a PHI ADEPT1010 system. The Cs^+ primary beam impact energy was 3 keV and the beam current 200 nA. The scanning area was 400 um^2 for negative secondary ion detection with an incidence angle of 60° to the sample surface normal. The secondary ions, ^1H and ^{30}Si, were monitored during depth profiling. The samples were charge-neutralized with a metal mask on the sample at ground potential.

2.3. Results and Discussion

2.3.1 SR-IR and ATR-IR Spectra of Soda Lime Float Glass

Fig. 2-3 compares the SR-IR and ATR-IR spectra of the soda lime float glass samples with 0.7 mm thickness. Two positive peaks at ~1064 cm^{-1} and ~766 cm^{-1} in SR-IR spectra in Fig. 2-3 (a) are attributed to asymmetric and symmetric vibration modes of the Si-O-Si (BO) network [33,38]. The shoulder at ~950 cm^{-1} corresponds to the stretching vibration of the $Si\text{-}O^-$ (NBO) group in the glass [33,35]. It is noted that the BO peak at ~1064 cm^{-1} appears to be missing or red-shifted to ~1000 cm^{-1} in the Ge-ATR spectrum and ~910 cm^{-1} in the diamond-ATR spectrum shown in Fig. 2-3 (b). ATR-IR also shows a broad peak spanning from 3650 cm^{-1} to ~2500 cm^{-1} corresponding to stretching vibrations of the hydrogen-bonded Si-OH and H_2O species, and a sharp peak at ~1650 cm^{-1} corresponding to the bending vibration of the molecular H_2O species.

Although the ingress of water into the soda lime glass surface is true, it is incorrect to interpret the absence or red-shift of the BO peak in ATR-IR compared to the SR-IR as changes in the Si-O-Si network structure. This will be explained theoretically in the next section.

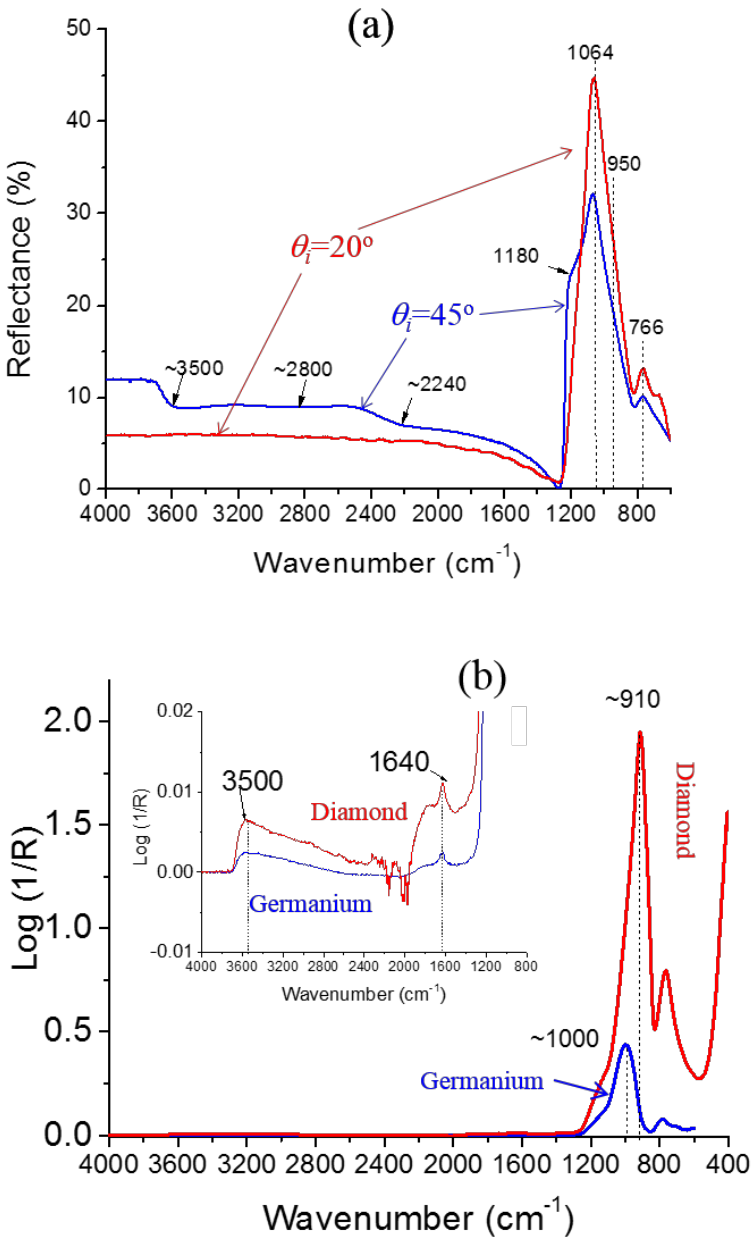

Fig. 2-3 (a) SR-IR spectra of soda lime float glass with 0.7 mm thickness obtained at an incidence angle of 20° (with a 15× IR objective lens) and 45°. (b) ATR-IR spectra of soda-lime float glass with 0.7 mm thickness obtained with diamond and Ge ATR crystals. The inset shows the 4000 - 1200 cm^{-1} region of the ATR-IR spectra.

It is also noted that the SR-IR spectrum of 0.7mm thickness float glass collected at the 45° incidence angle appears to show more spectral features than that of the same sample collected with the 15x objective lens in which the IR incidence angle is 20° (Fig. 2-3 (a)). The shoulder peak at ~1180 cm^{-1} and the negative peaks at ~2240 cm^{-1}, 2800 cm^{-1}, and 3500 cm^{-1} are observed only in the 45° SR-IR spectrum, but not in the 20° SR-IR spectrum.

In Fig. 2-3 (a), the negative peaks at ~2240 cm^{-1}, ~2800 cm^{-1}, and ~3400 cm^{-1} of the θ_i=45° spectrum could be puzzling since, as mentioned earlier, the absorption band in SR-IR should show up as a positive peak in the reflectance (R vs. cm^{-1}) plot. It is interesting to note that the peak positions of ~2800 cm^{-1} and ~3400 cm^{-1} agree well with the absorption bands in the transmission IR spectrum [45]. The ~2240 cm^{-1} is close to the peak reported for the Si-H (silane) group [1,46]. However, it should be noted that the peaks in SR-IR cannot be interpreted or assigned based on the coincidence of the SR-IR peak positions with the IR *absorption* bands of other materials.

2.3.2 Simulation of SR-IR and ATR-IR Spectra of Glass

In this section, the theoretical SR-IR and ATR-IR spectra are calculated using the equations (1) – (7) and the complex refractive index of diamond [43], germanium [44], and soda lime glass (Fig. 2-2) [29], and compared with the experimental spectra shown in Figure 2-3. This comparison clearly shows that anomaly or artifacts of the SR-IR and ATR-IR spectra of glass that should not be considered or interpreted as changes in absorption bands.

2.3.2a Comparison with simulated SR-IR spectra of glass

Fig. 2-4 displays the calculated SR-IR spectra for soda lime glass. The simulated spectra clearly show that the peak shape and position vary with the IR incidence angle, as observed experimentally. At near normal incidences ($\theta_i \leq 20^o$), the peak shape is very similar to the shape of the imaginary part (k) of the complex refractive index. However, as θ_i increases to the oblique angle, the peak shape changes drastically and the position of the maximum intensity is also blue-shifted. The BO band position is shifted from ~1065 cm^{-1} at the near-normal incidence angle to ~1080 cm^{-1} at higher incidence angles. Note that his blue shift is not due to the changes in the strength or energy of the Si-O-Si bond (changes in the position of the $k(\lambda)$ maximum); it is simply due to the anomaly caused by the change in the real part of the refractive index, $n(\lambda)$ in the wavenumber region. The nearly zero reflectance at 1300 cm^{-1} is simply because the refractive index of glass is the same as that of air at this wavelength (see Fig. 2-2).

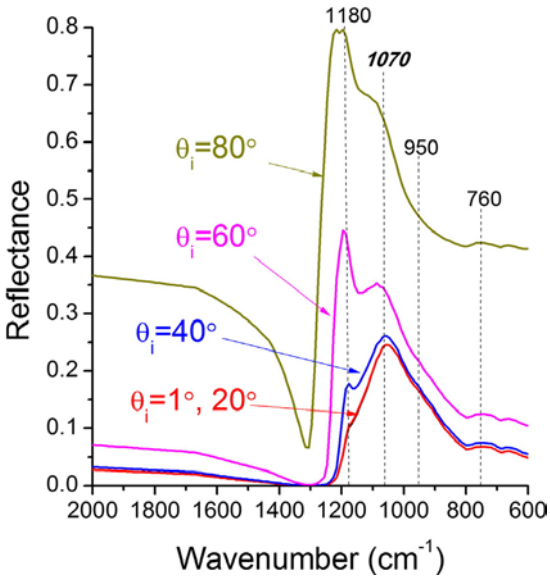

Fig. 2-4 SR-IR spectra of soda lime glass calculated with Eqs. (1)–(3) using the refractive index shown in Fig. 2-2 at different incidence angles (θ_i).

It is noted that as the incidence angle increases, the peak near 1180 - 1200 cm^{-1} grows. Fig. 2-5 displays the *s*- and *p*-polarized spectra of the polished soda lime glass sample measured as a function of the angle of incidence. The growth of the 1180~1200 cm^{-1} component is observed in both *s*- and *p*-polarized spectra. The simulated *s*- and *p*-polarized spectra from the refractive index shown in Fig. 2-2 reproduced the same trend observed in the experimental data (insets of Fig. 2-5). The small discrepancy in the peak shape must be due to the minor difference in the refractive index of the sample used in this study and the literature value shown in Fig. 2-2. This comparison clearly shows that the growth of the 1180 - 1200 cm^{-1} component is due to the anomaly caused by the change in the real part (n) of the complex refractive index. This position coincides with the minimum of $n(\lambda)$ in Fig. 2-2.

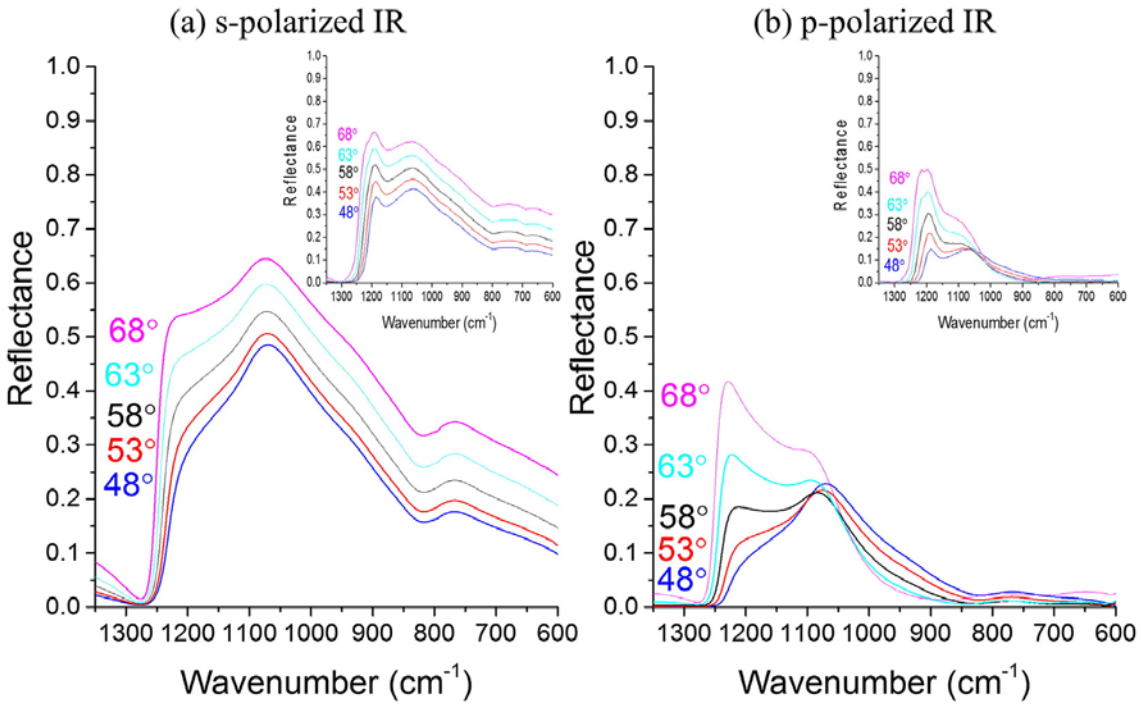

Fig. 2-5 Comparison of (a) s-polarized and (b) p-polarized SR-IR spectra of polished soda lime glass at incidence angles θ_i at the Brewster angle (58°) as well as ±5° and ±10°. The main panels are the experimental spectra and the insets are the spectra simulated with Eqs. (1)–(3) using the refractive index shown in Fig. 2-2.

This simple theoretical calculation of the SR-IR spectra of glass demonstrates how the peak shape and position vary with the IR incidence angle due to the wavelength dependence of the refractive index. It is not due to the new vibration modes or absorption band at an oblique incidence angle. If new absorption bands are involved, then there should be new peaks in $k(\lambda)$; but, the simulated spectra shown in the insets of Fig. 2-5 are all produced with the same $n(\lambda)$ and $k(\lambda)$ data set of soda lime glass (Fig. 2-2).

In SR-IR analysis, the contribution from the backside reflection is sometimes ignored, which could lead to artifacts in the spectra. Fig. 2-6 (a) plots the IR penetration depth, d_p, calculated using $k(\lambda)$ in Fig. 2-2. The penetration depth varies from ~0.65 μm at the BO absorption band position to ~2 cm in the >3700 cm^{-1} region. It is noted that when the sample thickness is 700 μm, then the >2200 cm^{-1} region of the IR beam can be reflected from the backside of the glass sample. This backside reflection can contribute to the signal intensity in the SR-IR experiment. When a microscope objective lens is used (θ_i=20° data shown in Fig. 2-3 (a)), the backside reflection is negligible since the focal depth of the objective lens is only on the order of several microns. However, in the typical SR-IR experiment with an elliptical mirror with a long focal distance (θ_i=45° data shown in Figure 2-3 (a)), the backside reflection should be taken into account.

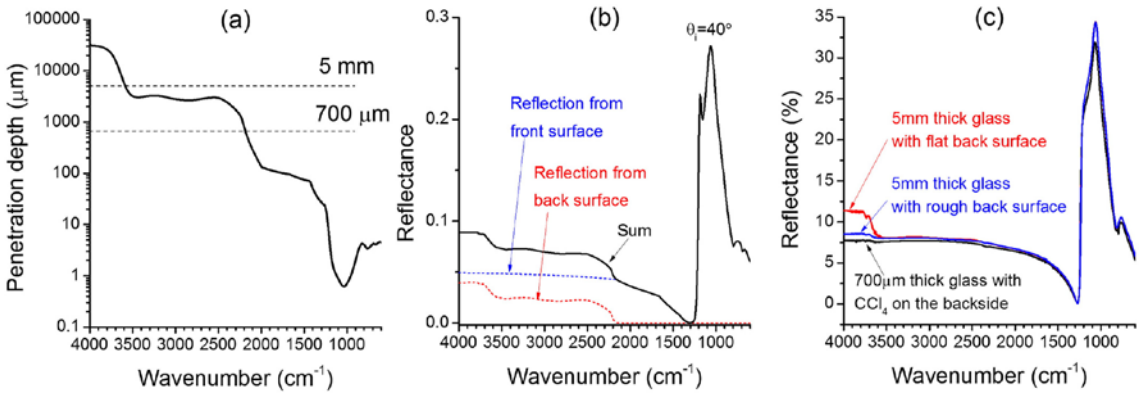

Fig. 2-6 (a) IR penetration depth, d_p, inside soda lime glass calculated with $k(\lambda)$ shown in Fig. 2-2. (b) SR-IR spectrum calculated for a 700 μm thick soda lime glass using Eqs. (1)–(7) at an incidence angle of 40°. The dotted lines are the components calculated for the reflection from the front and back surfaces. (c) Experimentally obtained SR-IR spectra of soda lime glass with different backside reflection conditions

Fig. 2-6 (b) shows how the backside reflection alters the SR-IR spectrum of a 700 μm thick float glass sample. When the IR beam is reflected from the front surface only, the SR-IR spectrum has no features at λ > 2000 cm^{-1}. The reflection from the backside has zero signal at λ < ~2240 cm^{-1}, but has non-zero signal at λ > ~2240 cm^{-1}. Since the front and backside reflected beams are spatially separated, the interference effect is negligible and the signals from these surfaces can be added. When these two components are added, the sum spectrum (solid line in Fig. 2-6 (b)) shows negative peaks at ~2240 cm^{-1}, ~2800 cm^{-1}, and ~3400 cm^{-1}, which is in good agreement with the experimentally observed spectrum (Fig. 2-3 (a), inset). This simulation clearly explains that the *apparent* peak at ~2240 cm^{-1} should not be interpreted as the silane (Si-H) species in the soda lime glass; it is simply the *onset* of the backside reflection contribution in SR-IR of a thin optically-flat glass sample. Note that the Si-H peaks are normally very sharp. The negative peaks at ~2800 cm^{-1} and 3400 cm^{-1} in the SR-IR spectrum are due to the absorption by hydrous species in the bulk. In this sense, the region above ~2240 cm^{-1} in the SR-IR spectrum is similar to the transmission absorption spectrum.

In order to further understand the backside reflection contribution in SR-IR, we conducted a few control experiments (Fig. 2-6 (c)). When the sample thickness is changed from 700 μm to 5 mm, then the onset of the backside contribution is shifted from ~2240 cm^{-1} to ~3600 cm^{-1}. When the backside of the 5mm thick sample is roughened, then this contribution is further suppressed. When CCl_4 is placed on the back of the 700 μm thick sample, then the backside reflection is completely suppressed since the refractive index of CCl_4 is very close to that of soda lime glass.

2.3.2b Comparison with simulated ATR-IR spectra of glass

In ATR-IR, the IR incident beam travels through the high refraction index crystal and is reflected from the crystal/glass interface; thus, the reflection behavior can be divided into two regimes: (i) $\theta_i < \theta_c$ (SR-IR region) and (ii) $\theta_i > \theta_c$ (ATR-IR region). The critical angle (θ_c) is ~38.7° for the diamond crystal and ~22.0° for the germanium crystal. When $\theta_i < \theta_c$, the peak shapes in the reflection spectra shown in Fig. 2-7 (a) and (b) appear to be governed mostly by the real part, $n(\lambda)$, of the glass refractive index (Figure 2). When $\theta_i > \theta_c$, the signal in the non-absorbing region (>1200 cm^{-1}) is almost zero since the IR beam undergoes total internal reflection (i.e., $R = I_r/I_o = 1$; $\log(1/R) \approx 0$). In the absorbing region (<1200 cm^{-1}), $k(\lambda)$ has non-zero value and the total internal reflection is attenuated (i.e., $R < 1$; $\log(1/R) > 0$). It is noted that the Si-O-Si peak position of the maximum intensity is not the same as the absorption band position in $k(\lambda)$; it is significantly red-shifted to ~910 cm^{-1} for the diamond-ATR data in Fig. 2-7 (a) and ~990 cm^{-1} for the Ge-ATR data in Fig. 2-7 (b). Such a red-shift in the absorption peak position is insignificant for organic materials since $k(\lambda)$ is very small and thus variance in $n(\lambda)$ is negligible. However, in the case of soda lime glass, both $n(\lambda)$ and $k(\lambda)$ vary over a large range, causing distortion of the peak shape in the ATR-IR spectrum. Thus, the difference in the peak positions of the SR-IR and ATR-IR spectra should not be interpreted as structural modification in the surface region [12]. These differences are simply due to the anomaly of the IR beam reflection resulting from changes in $n(\lambda)$.

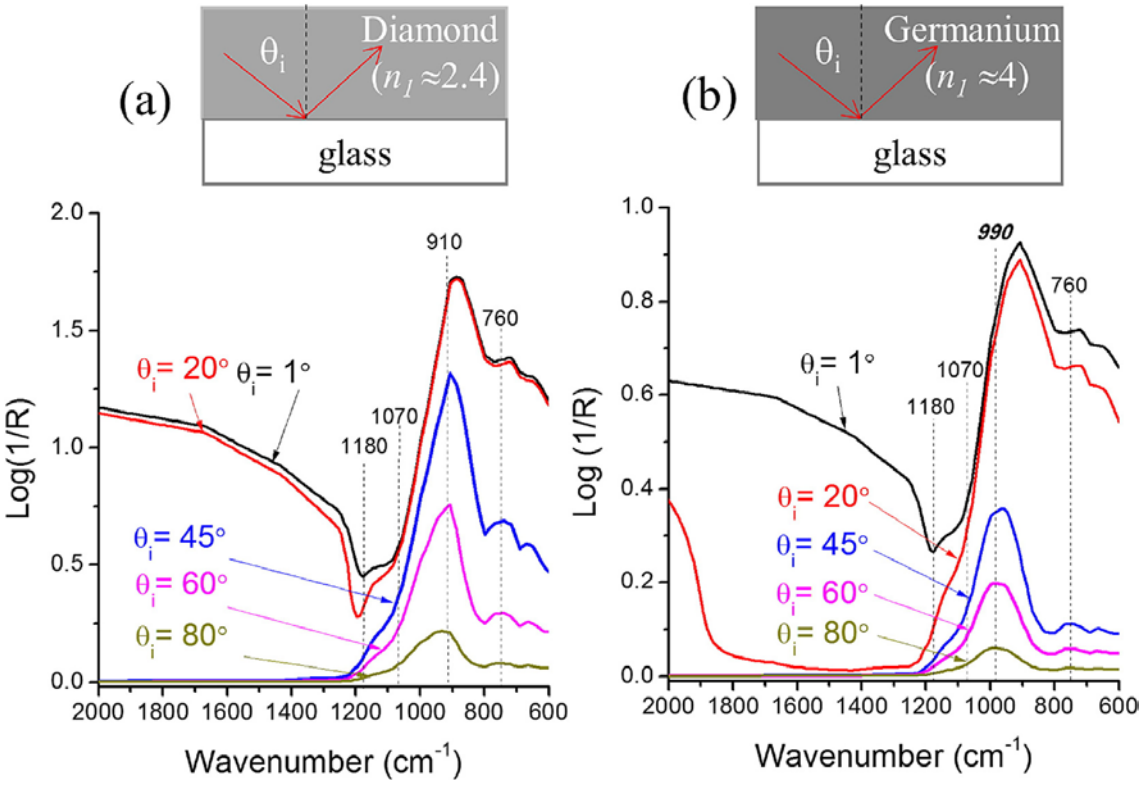

Fig. 2-7 (a) Diamond ATR-IR, and (b) Ge ATR-IR spectra of soda lime glass calculated with Eqs. (1)–(3) using the refractive index shown in Fig. 2-2 at different incidence angles (θ_i). Note that the calculated spectra for θ_i = 1° and 20° correspond to the SR-IR data since the incidence angle is lower than the critical angle (θ_c).

2.3.3 SR-IR vs. ATR-IR for Study of Si-O-Si Network Structure

The leaching of sodium via acid treatment is usually observed to shift and alter the shape of the broad band in the 1200 – 850 cm^{-1} region [33]. Fig. 2-8 compares the changes observed in the SR-IR and Ge ATR-IR spectra of the acid-treated soda lime glass surfaces. In the SR-IR spectra (Fig. 2-8 (a)), it can be seen that, upon acid treatments, the peak position of the BO band is slightly blue-shifted (from 1054 cm^{-1} to 1060 cm^{-1}) and the intensity of the NBO region (shoulder peak at ~950 cm^{-1}) is slightly increased. The change in the NBO region can be attributed to conversion of the NBO group to the Si-OH species upon leaching of Na^+ into solution and ingress of H^+ from the solution. Most divalent Ca^{2+} and Mg^{2+} ions remained in the surface region after leaching since they have less mobility than Na^+ [47]. Therefore, they have less effect on the peak position compared with leaching of Na^+. The glass samples also contain several hundred ppm of iron. Even if its oxidation state could be changed, its impact is negligible since its concentration is too low [48].

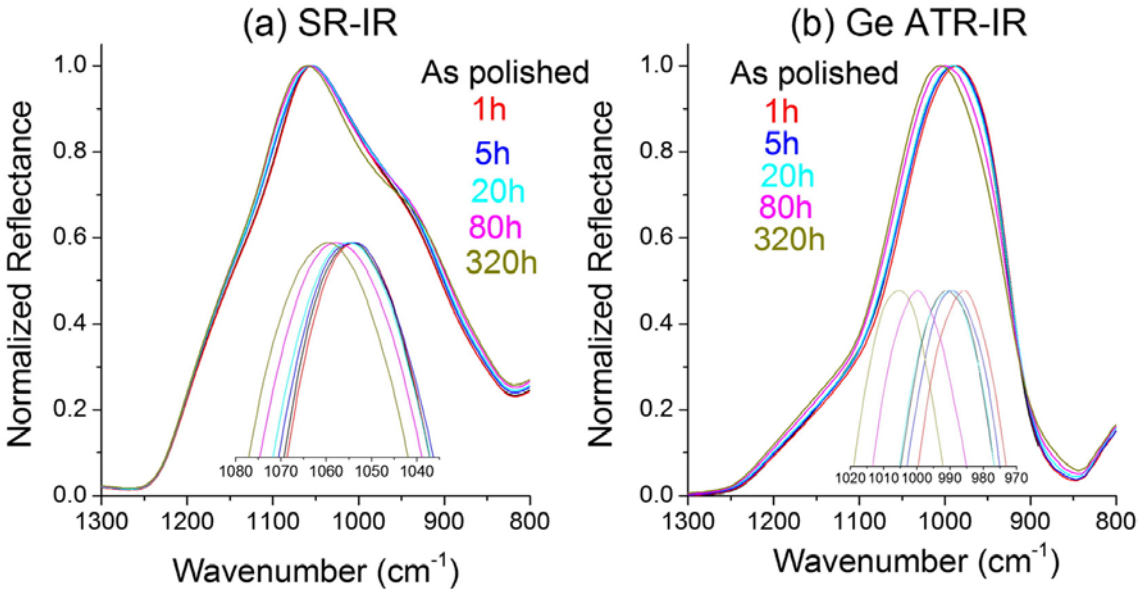

Fig. 2-8 SR-IR (θ_i =20°) and (b) Ge ATR-IR spectra of acid-treated soda lime glass samples for 0, 1, 5, 20, 80, and 320 hours.

The Ge ATR-IR spectra (Fig. 2-8 (b)) show larger blue-shift of the main peak from 990 cm^{-1} to 1010 cm^{-1}. And the intensity of the 950 cm^{-1} region decreases with acid treatment, which is opposite to the trend seen in SR-IR. One may attempt to interpret this observation in conjunction with the difference in the information depth of two methods: d_p = 650 nm at 1060 cm^{-1} in SR-IR and 490 nm at 1000 cm^{-1} in Ge ATR-IR. However, it should be noted that the peak shape and position of the Ge ATR-IR spectrum implies that the ~1000 cm^{-1} peak are affected by the convolution of $n(\lambda)$ and $k(\lambda)$. In other words, the anomaly effect of the complex refractive index of glass made the blue-shift larger in the Ge ATR-IR spectra, compared to the SR-IR spectra.

In the case of the diamond ATR-IR analysis, the peak position of the 910 cm^{-1} band (Fig. 2-2 (b) and Fig. 2-7 (a)) was blue-shifted by +1 cm^{-1} after 20 hours of acid etching and then red-shifted by -2 cm^{-1} after 320 hours (data not shown). This difference in the peak position change upon the acid etching treatment reiterated that the peaks in the Si-O-Si vibration region of the ATR-IR spectra of glass samples are altered by the anomaly effect originating from the complex refractive index of glass.

2.3.4 Diamond vs. Germanium ATR-IR for Detection of Hydrous Species

ATR-IR can be used to probe the hydrous species in the near surface region of soda lime glass [32,41]. The broad band within the 3800 - 2500 cm^{-1} region can be attributed to the OH stretching vibrations of Si-OH and H_2O species with varying degrees of hydrogen bonding interactions. Note that the 3450-3200 cm^{-1} region overlaps with the OH stretch vibrations of molecular water species in liquid or adsorbed layers [49]; but this does not mean that all peaks in the region can be assigned to the molecular water. The

OH stretch peak of molecular water as well as Si-OH could overlap depending on the degree of hydrogen bonding interactions [50]. The presence of the H-O-H bending vibration peak at ~1650 cm^{-1} indicates the presence of molecular water in the ATR-IR probe depth. Both Ge and diamond ATR-IR spectra clearly show these peaks (Fig. 2-9 (a) and (b)). Since the absorptivity of glass itself in this region is very small, the observed peaks can be interpreted as absorption bands of the Si-OH and H_2O species as in the case of transmission analysis. It is noted that the signal intensity is much weaker in the Ge ATR-IR spectra compared to the diamond ATR-IR spectra. This is mainly due to the difference in the penetration of the evanescent wave. The penetration depth ($d_{p,ATR}$) at 3400 cm^{-1} is calculated through equation (5) to be 600 nm for diamond ATR and 150 nm for Ge ATR. Thus, the Ge ATR-IR signal becomes saturated much faster than the diamond ATR-IR signal.

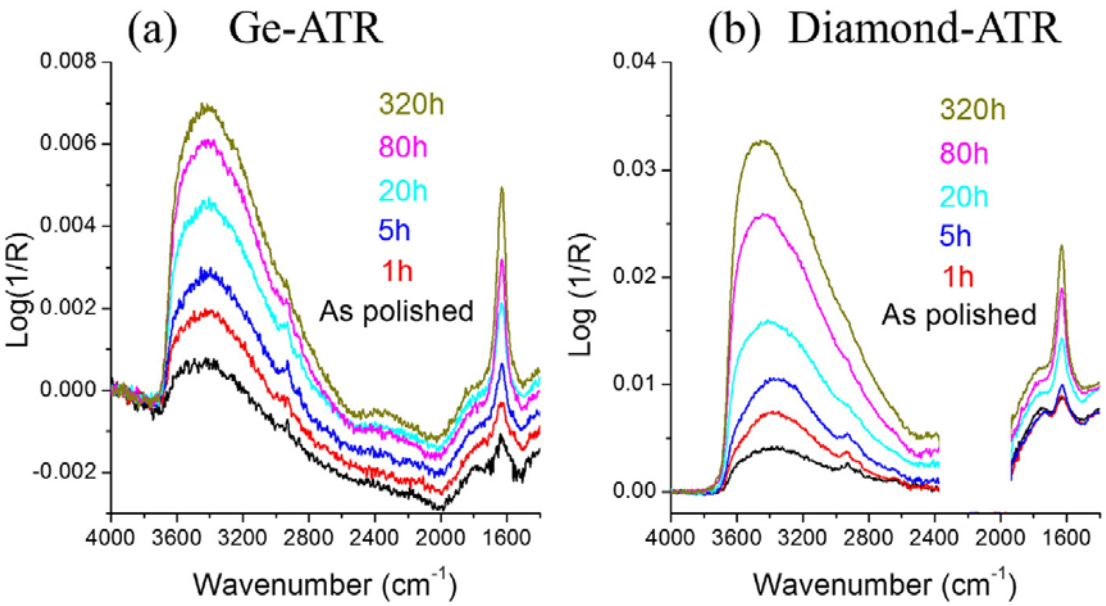

Fig. 2-9 ATR-IR spectra of acid-treated soda lime glass surfaces obtained with (a) germanium and (b) diamond crystals.

The penetration depth ($d_{p,ATR}$) in ATR-IR spectroscopy in various instrumental setting have been calculated through equation (5). Here, ATR crystal of diamond (n_1 =~ 2.4) and Ge (n_1 =~ 4.0) and incident angle of 45°, 60°, 80° have been considered, respectively. The results are shown in table 2-2. As clearly shown in table 2-2, shallower penetration depth can be realized by using the ATR crystal with higher refractive index and higher incident angle.

Table 2-2 Penetration depth in ATR-IR spectroscopy in various setting

$d_{p,ATR}$ (nm)		ATR crystal	
		diamond	Ge
incident angle	45°	588	189
	60°	324	145
	80°	255	125

2.3.5. Quantification of sub-surface OH/H_2O species using ATR-FTIR

To quantitatively evaluate the OH signal intensity in the ATR-IR spectra, leached samples with various depths of hydration were prepared using an acid solution (pH 1) at 90 °C for varying periods. Fig. 2-9 (b) shows the ATR-IR spectra from the leached samples. Peak shapes are similar to the polished sample for all leaching times up to 320 hours, while the peak intensities of both broad band around 3450 cm^{-1} and sharp band at 1625 cm^{-1} increase with leaching time.

The SIMS hydrogen depth profiles for the set of acid-leached samples are shown in Fig. 2-10 (a). The hydrated depth and amount of diffused hydrogen are presented in

Table 2-. The correlation between the 3450 cm^{-1} peak height in the ATR-IR spectra and the hydrogen amount from SIMS are plotted in Fig. 2-10 (b). The peak heights in ATR-IR can be used for Fig. 2-10 (b) since the peak shapes of the leached samples are almost the same, which means water speciation in the leached samples does not vary. The horizontal error bars in this graph are based on the accuracy of the SIMS data and the vertical error bars by the ATR-IR intensities. Although the data shows good linear relationship for the samples with the smaller hydrogen content and shallower hydrated depth, there is some deviation for the more deeply leached samples. This is because the electric field of the evanescence wave decreases exponentially as a function of distance from the surface and contribution to signal intensity by absorption in deeper region are weakened due to its attenuation. To understand this behavior, we need to consider the attenuation of evanescent wave in sample with depth as discussed below.

Table 2-3 Hydrated depth and hydrogen amount obtained from SIMS data

	leached sample				
	1h	5h	20h	80h	320h
Hydrated depth (nm)	18	32	54	101	163
Amount of hydrogen (a.u.)	0.74	2.24	3.68	8.51	12.23

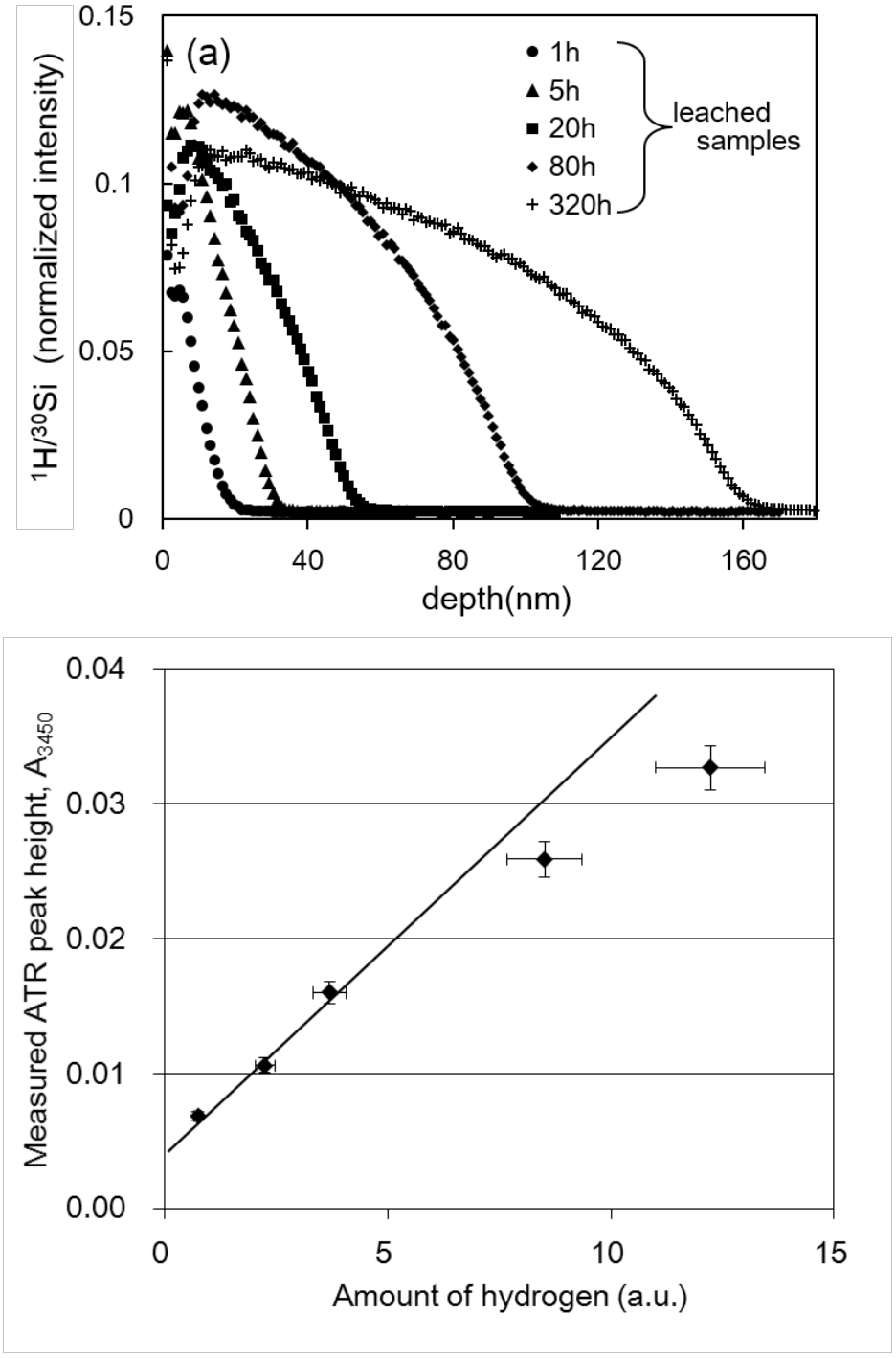

Fig. 2-10 (a) Hydrogen profiles obtained by SIMS of the polished and leached glass sample. (b) Correlation between the amount of hydrogen in the SIMS analysis and the measured ATR peak height at 3450 cm^{-1}. A line is a guide to the eye.

In a homogeneous sample, the absorption intensity in the ATR spectrum is proportional to the concentration of relevant species. However, if the sample has a compositional gradient in its surface, the amount of light absorbed at each depth in ATR-IR depends on both the concentration of the species and the intensity of the evanescent wave at each depth. Assuming constant refractive index and low extinction coefficient in the sample, the intensity of the peak in the ATR absorption spectrum, *I*, can be expressed as below [51],

$$I = \int_0^\infty k(x) \cdot \exp(-2x/d_p) dx \quad \cdot \cdot \cdot (8)$$

where x is depth in the sample, $k(x)$ is extinction coefficient as a function of depth, and d_p is the penetration depth of the evanescent wave. The term $\exp(-2x/d_p)$ gives the intensity of light at each depth, which is calculated as the square of the evanescent wave electric field, which decreases exponentially with distance from the surface.

If the species causing the IR absorption among a series of evaluated samples are identical, the extinction coefficient is proportional to the concentration of relevant species. Therefore equation (2) can be translated as:

$$I \propto \int_0^\infty C(x) \cdot \exp(-2x/d_p) dx \quad \cdot \cdot \cdot (9)$$

where $C(x)$ is the concentration profile of relevant species.

This is schematically illustrated in Fig. 2-11. Profiles of the hydrogen concentrations in the leached samples were obtained by SIMS (Fig. 2-10 (b)), while the

depth dependence of light intensity was calculated using the penetration depth obtained from equation (1). Although independent information about the absorption coefficients for water related species in the glass surface is not available, we can assume that they are constant because their relative abundance in ATR-IR spectra does not change substantially (Fig. 2-9 (a)). Then, the product of the hydrogen concentration (Fig. 2-11 (a)) and light intensity profiles (Fig. 2-11 (b)) yields the absorption intensity at each depth in the sample (Fig. 2-11 (c)). According to equation (3), the relative absorption in the ATR-IR spectra is calculated as the integral of absorption at each depth from surface to bulk (shaded area in Fig. 2-11 (c)).

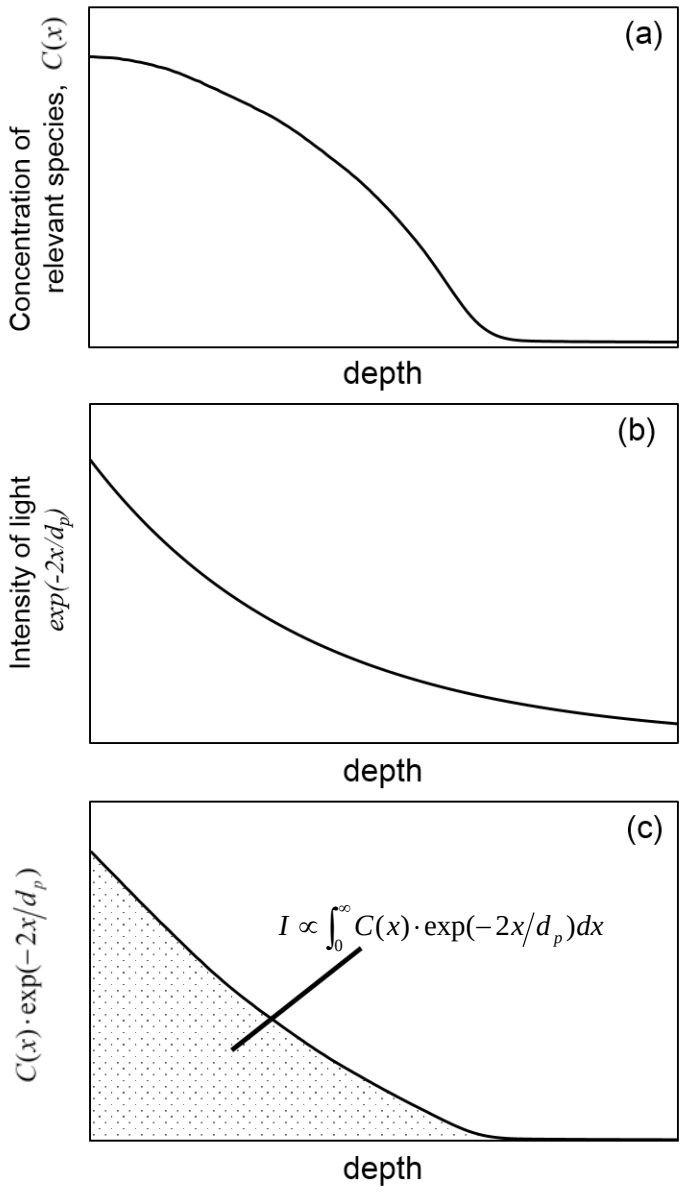

Fig. 2-11 Schematic illustration of ATR-IR absorption intensity calculation method. (a) Concentration profile of hydrogen species obtained by SIMS analysis. (b) Intensity profile of light at each depth (c) Absorption intensity at each depth is proportional to the product of concentration (a) and light intensity (b) at the depth. Relative absorption amount in ATR-IR spectra is calculated as the area under the curve.

To validate the absorption peak intensity for quantitative analysis of the ATR-IR spectra, the intensities of the 3450 cm^{-1} peak in the spectra of leached samples were simulated using the hydrogen profiles obtained by SIMS shown in Fig. 2-10(a), and then compared with the actual intensities in Fig. 2-9 (b) obtained with diamond ATR crystal. Although independent information about the absorption coefficients for water related species in the glass surface is not available, relative peak intensities can be calculated with equation (9) because the series of leached samples show similar shape in ATR-IR spectra, which means they have the same ratio of water-related species.

The correlation between the measured ATR-IR peak heights with diamond ATR crystal, A_{3450}, and the relative absorption intensities calculated with equation (9) is presented in Fig. 2-12. For same purpose, the correlation between the ATR-IR peak heights with obtained Ge ATR crystal and the relative expected absorption intensities is calculated with equation (9) and shown in Fig. 2-13. A very good linear relation with statistical correlation coefficient better than 0.99 is obtained which validates the quantitative relationship between the hydrogen concentration in the glass surface and the peak heights in the ATR-IR spectra for a specific hydrogen containing species.

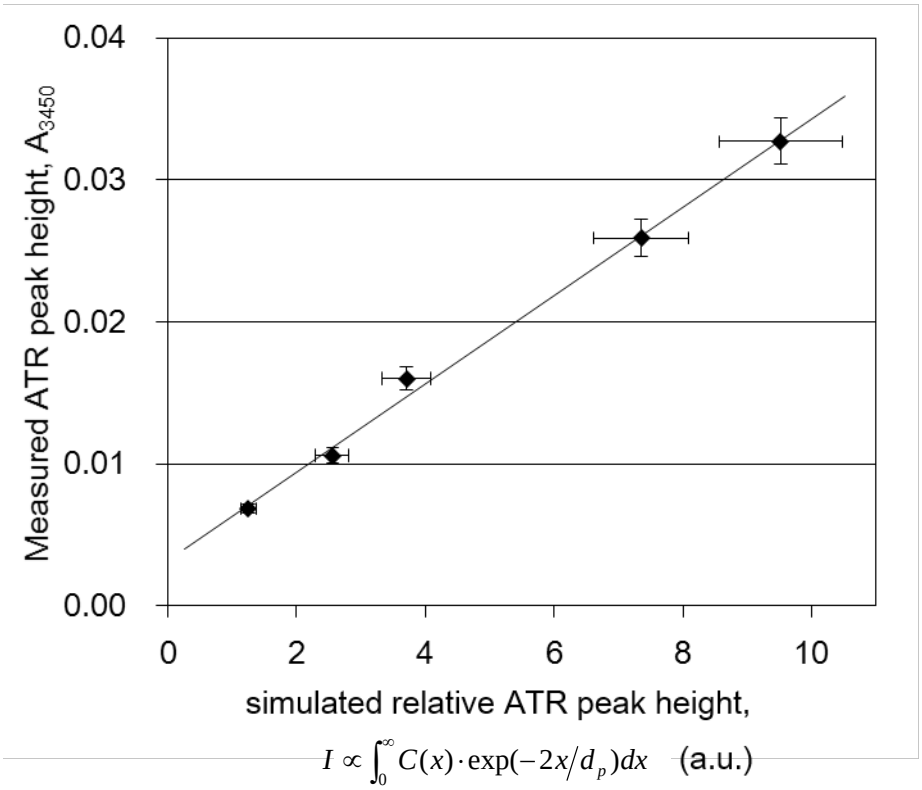

Fig. 2-12 Correlation between simulated and measured peak height in ATR spectra with diamond ATR crystal. A line is a guide to the eye.

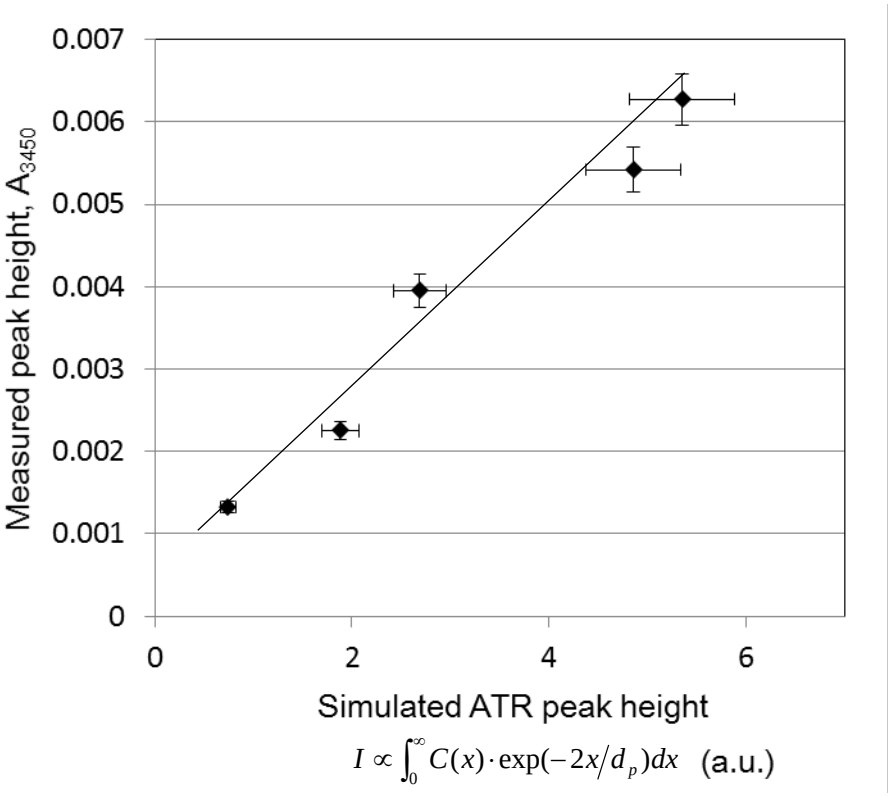

Fig. 2-13 Correlation between simulated and measured peak height in ATR spectra with Ge ATR crystal. A line is a guide to the eye.

Moreover, to evaluate surface-sensitivity of ATR-IR spectroscopy with various experimental setting, ratio of contribution in whole ATR-IR spectra due to the signal from the high concentration of water diffused into glass surface through surface treatment, I_1, and the one from the water which have pre-existed in bulk region of glass with low concentration before the treatment, I_2, can be calculated. Since the purpose of this study is to evaluate the exiting state of diffused water into glass surface, contribution originated from the water in surface to the whole spectra, that is $I_1/(I_1+ I_2)$, is preferred to be higher. Here, $I_1/(I_1+ I_2)$ will be calculated based on equation (9)

In the sample acid-leached for 320 hours, water concentration in deeper region than 300nm is stable at $^1H/^{30}Si = (2.3 \pm 0.03) \times 10^{-3}$. Here, surface region was defined as the region where water concentration is less than stable at $^1H/^{30}Si=2.39 \times 10^{-3}$, which is shallower region than 216 nm for the 320-hour leached sample. Thus $I_1/(I_1+ I_2)$ can be calculated as

$$I_1 \Big/ I_1 + I_2 = \int_0^{216} C(x) \cdot \exp(-2x/d_p)dx \Big/ \left(\int_0^{216} C(x) \cdot \exp(-2x/d_p)dx + \int_{216}^{\infty} C(x) \cdot \exp(-2x/d_p)dx \right)$$

This value was calculated for the sample with various treatment time in the case with d_p = 588 nm (diamond is used as ATR crystal and incident angle is 45 degree) and d_p = 125 nm (Ge crystal is used as ATR crystal and incident angle is 80 degree) and summarized in Table 2-4.

Table 2-4 Ratio of signal due to water diffused into glass surface contributed to in whole signal in ATR-IR spectra, $I_1/(I_1+ I_2)$

Treatment time	1h	5h	20h	80h	320h
Surface region	28nm	38nm	79nm	128nm	216nm
d_p=588nm	0.768	0.811	0.844	0.940	0.957
d_p=125nm	0.967	0.976	0.987	0.998	0.999

From this results, it is found that $I_1/(I_1+ I_2)$ is higher for the sample with longer treatment time (thicker surface region with high water concentration) or for the experimental setting with small information depth, d_p. In the case of the sample with shallower surface region than 100 nm analyzed with d_p of 588 nm, ratio of signal from low concentration of pre-existed water in bulk region is considerable, higher than 10%. To evaluate the speciation of water in surface region in the sample with shallower surface layer than 100 nm, smaller d_p, for example 125 nm, is preferred.

This method to evaluate the contribution of surface layer to the whole ATR-IR spectra can be applied to all cases where distribution of related chemical species are known. Experimental conditions, such as the refractive index of the ATR crystal and incident angle, should be carefully considered to realize appropriate surface-sensitivity for purpose of experiments.

2.3.6. Shape of ATR-IR Spectra and Hydrogen Concentration Profiles

Fig. 2-14 displays ATR-IR spectra obtained by normalizing ATR-IR spectra of the samples treated for various time shown in Fig. 2-9(b) by maximum intensities around 3450 cm^{-1}. Shapes of the normalized spectra roughly overlap with each other while shoulders around 3600 cm^{-1} of the spectra for longer treatment time slightly more

significant than those for short treatment time. This indicates that water speciation, which is distribution of hydrous species in some chemical states, in these samples are quite similar but relative ratio of the species corresponding to the region around 3600 cm^{-1} which is weakly hydrogen bonded SiOH [4] seems higher in the surfaces of the samples treated for longer periods.

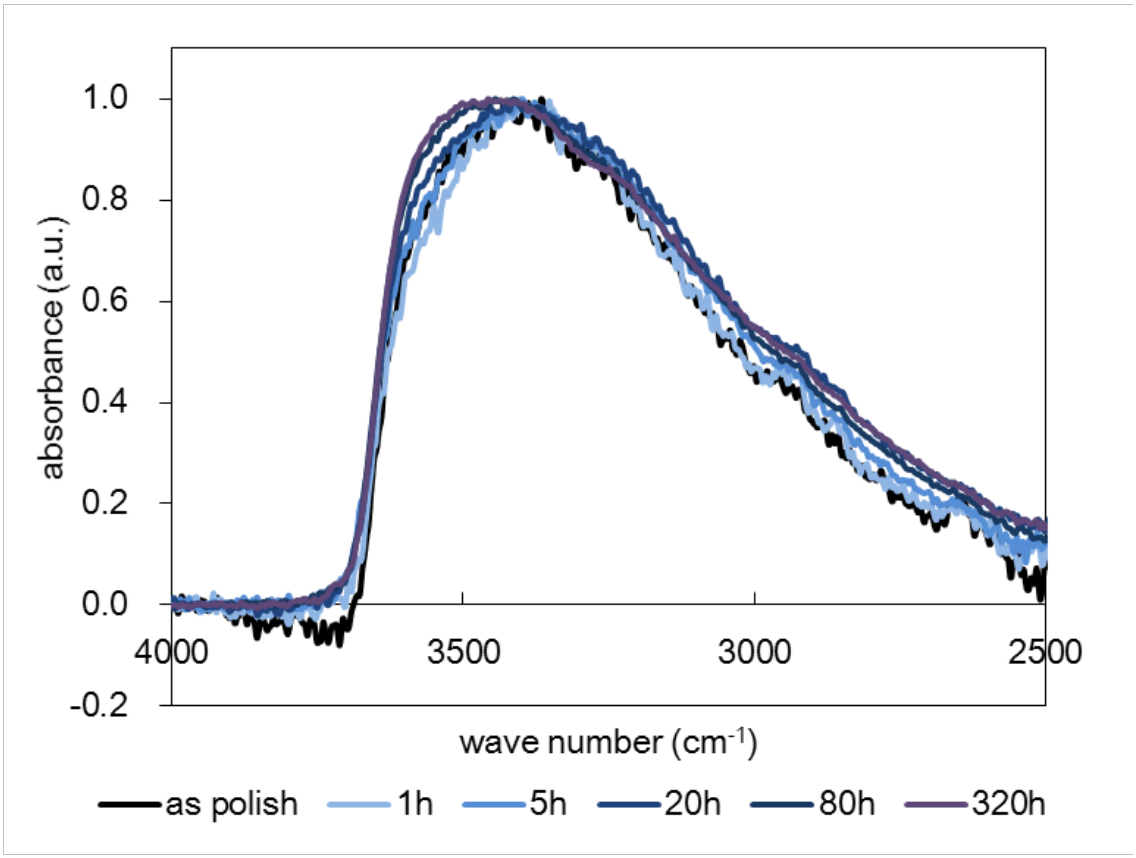

Fig. 2-14 Normalized ATR-IR spectra of various treatment time by diamond

Stuke et al. reported that speciation of water depends on total concentration of water; almost all water exist as SiOH in low total concentration (up to 1 wt%) and ratio of molecular water increase with the total water concentration and become dominant when the concentration is several percent [5]. In this study, since acid treatment of the samples have done for various treatment time in same temperature, a factor which can affect speciation of diffused water is the concentration of total water at each depth. Although the diffusion depth of water are quite different among the samples, if water concentration profiles are similar in shape it means that water speciation, distribution of hydrous species, among the samples are identical, which is consistent with similar ATR-IR spectra in shape.

To understand this point, we evaluate the similarity of the water concentration profiles obtained by SIMS (Fig. 2-10(a)). Although maximum concentration of hydrogen in SIMS profiles Fig. 2-10(a) vary in about 20 %, the actual maximum concentrations are expected to be similar among the samples. This is because accuracy of the concentration measured by SIMS is known as about 30 %, in acid leached samples hydrogen is introduced through ion-exchange between hydrogen or oxonium ions in solution and alkali ions in glass surfaces which originally same among the samples before leaching. Therefore, to make it easier to evaluate the similarity of them, the hydrogen profiles in Fig. 2-10(a) were normalized for maximum concentration near outermost surface to be 1 and shown in Fig. 2-15.

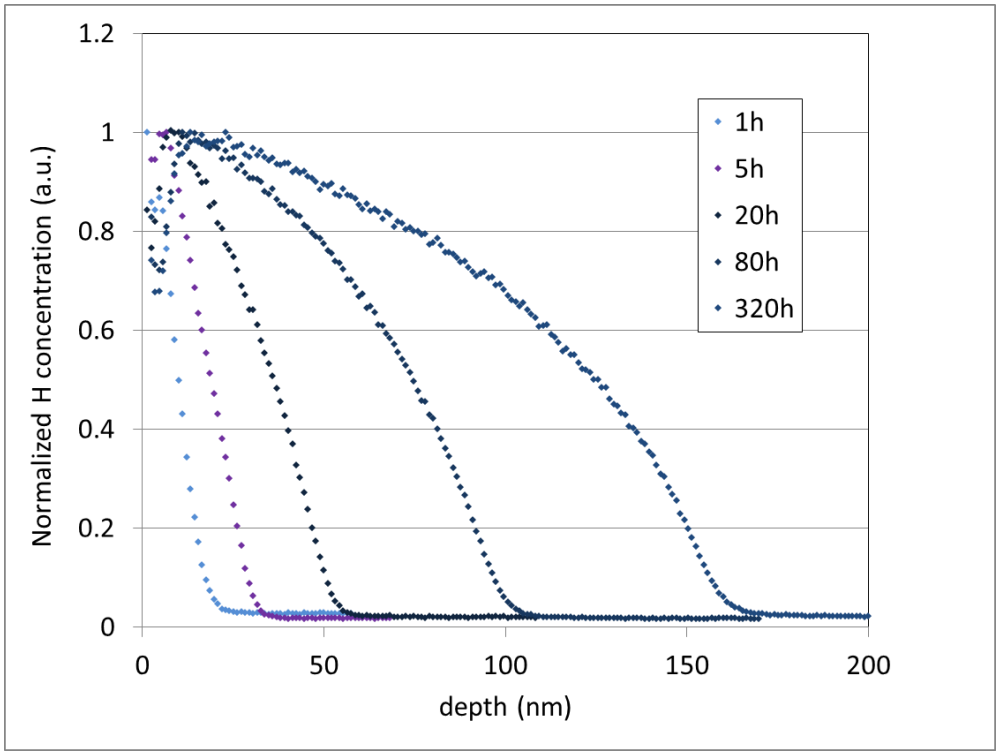

Fig. 2-15 Normalized hydrogen concentration profiles

Next, to normalized horizontal axis of the Fig. 2-15, depth is normalized for depth where normalized water concentration is 0.5 to be 1 and shown in Fig. 2-16.

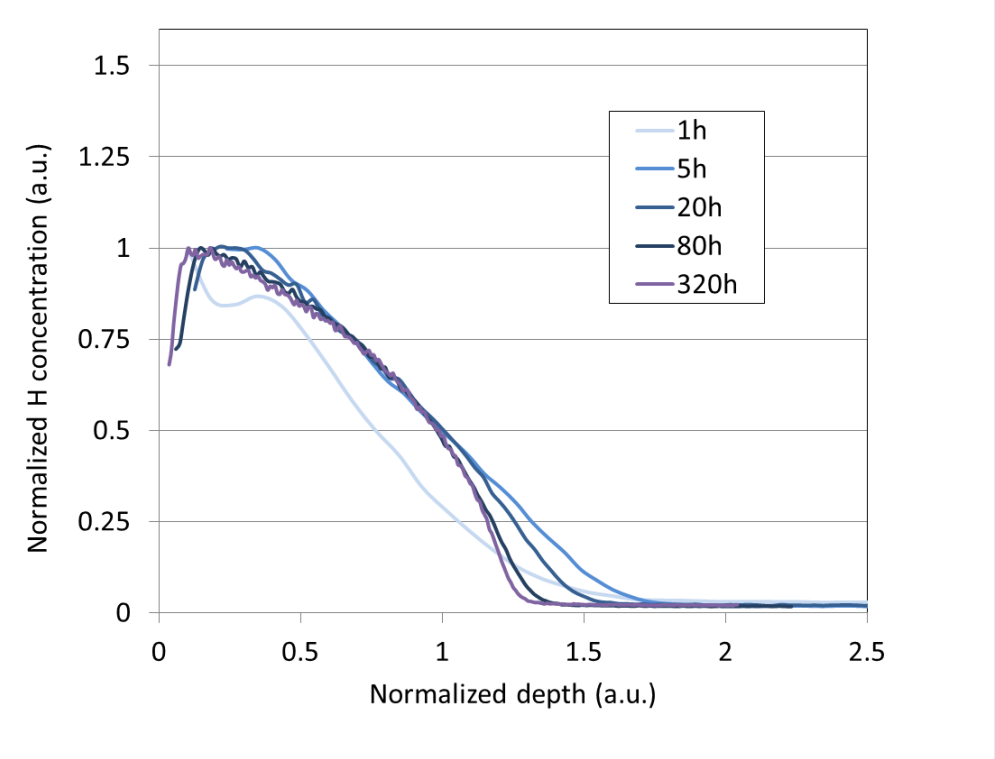

Fig. 2-16 hydrogen concentration profiles normalized both in vertical and horizontal axis.

From Fig. 2-16 the shape of hydrogen concentration profiles for 1 hour leached sample is found to be not consistent with the other profiles. This should be because experimental error in SIMS is relatively larger in near surface region and ratio for data obtained at shallow region are higher for the samples with shorter treatment time.

For the samples treated for longer than 5 hours, whereas the shapes of the profile are almost identical in the region where normalized concentration are higher than 0.5, the curves of the samples with longer treatment time seem steeper in the region where the normalized concentration are less than 0.5, which means the volume ratio of the region with low hydrogen concentration are smaller in the sample treated for longer time.

Although Fig. 2-14 indicates that water speciation in the samples with various treatment time are quite similar, Fig. 2-16 shows that the shape of SIMS hydrogen profiles vary in deeper region. The reason of this is estimated to be that the contribution to the ATR spectra from the water in the region with lower concentration is relatively small because amount of water itself is small in the region and evanescent wave used in ATR-IR is decayed in deeper region.

2.4. Summary

Infrared spectroscopy is an important and valuable tool for the characterization of glass structure, water in glass and water adsorption/reaction at surfaces. Although the fundamental vibrational state of the material is the desired information in all of these methods, the position, shape and intensity of the measured absorption peaks are influenced and sometimes distorted by differences and anomalies associated with how the data is acquired. In this study, SR and ATR have been used to acquire spectra of a commercial soda lime float glass, to describe and analyze the associated spectral features in detail. The observed differences in the wavenumber and shape of the important peaks for each method are explained using classical optical theory. The effects of incidence angle, backside reflections and information depth are highlighted. For example, the Si-O-Si BO peak is blue-shifted in SR-IR and red-shifted in ATR-IR simply due to the complex nature of the glass refractive index, not due to differences in probe depth. In the case of thin and flat glass samples, the IR reflection from the back surface can superimpose the transmission spectrum in the SR-IR spectrum in the wavenumber region where the bulk absorption coefficient is low. The effect of acid leaching on the Si-O-Si BO network should be analyzed by SR-IR, not by ATR-IR. When the ATR-IR intensity of the hydrous peaks (Si-OH and H_2O) is interpreted, the inhomogeneous depth profile of hydrogen and the IR penetration depth must be taken into account. Independent SIMS data for the leached samples established the quantitative relationship between the ATR signals and hydrogen concentration-depth profiles.

3 Analyses of Water in Several Surface-Treated Soda Lime Glass

3.1. Introduction

Water and hydroxyl species are often retained in commercial glass from the water vapor in the melting atmosphere or from the raw materials. Also, flat glass is sometimes surface treated with SO_2 gas in the annealing lehr zone during industrial float glass manufacture to precipitate sulfate powder on the glass surface for scratch protection from the rollers or to improve chemical durability by removing reactive alkali elements from glass surface [52,53]. Since the SO_2 surface treatment involves reactions with water to replace network modifier ions, such as sodium or calcium, with hydrogen derived from H_2SO_4, it can alter the hydration state of glass surfaces [2]. Ambient humidity and aqueous solutions, especially under acid conditions, can also introduce water and hydroxyl into the near surface [3].

In this chapter, we measured and evaluated the ATR-IR spectra of various surface treated float glass samples (as-produced, polished, leached by acid, treated by SO_2 gas, and strengthened by thermal or chemical methods) to understand the water speciation in there surface.

3.2. Experiment

3.2.1 Sample preparation

Soda lime silica glasses made by the float method were used in this study. The bulk composition of the glasses was analyzed by x-ray fluorescence (XRF) and is within the range shown in Table 3-1. These 3.9 mm thick float glass samples were supplied by AGC Inc. in Japan. These float glasses were treated by SO_2 gas in the production process and the composition-depth profiles obtained with x-ray photoelectron spectroscopy (XPS) and secondary-ion mass spectroscopy (SIMS) were reported previously [2].

Table 3-1 Evaluated glass composition by XRF

	SiO_2	Al_2O_3	MgO	CaO	Na_2O	K2O	Fe_2O_3
mol%	70.4-70.8	0.9-1.0	6.2-7.3	7.8-9.1	12.5-13.6	0-0.4	0.01-0.04

In this study, the float glass was evaluated ‘as produced’ and after various surface preparation treatments:

- Float glass sheets were re-melted in an electric furnace and poured onto carbon substrate. Following the annealing in the 600 ^oC and slowly cooling at a cooling rate of 1 ^oC/min to remove residual stress, glasses were lapped with SiC powder and polished with CeO_2 dispersed in water to 5.0 mm in thickness. All of the experiments described below were performed on this polished glass.
- Leached samples were prepared by acid treatment of the polished glass in a 90 ^oC HCl solution (0.1 mol/l) for 1, 5, 20, 80, 320 hours, respectively. The surface area of each sample was 7.5 cm^2 and the volume of HCl solution was 50ml.

- A lab-scale system for SO_2 treatment was used to treat the polished glasses in a fused quartz tube furnace (volume of 1700 cm^3) heated to 540 ^oC under a flowing mixture of 2.5 vol% SO_2, 78 vol% N_2 and 19.5 vol% O_2 at a constant flow rate of 1.6 l/min for 10 minutes. After this treatment, the furnace was purged with N_2 at 20 l/min for 5 min and then cooled to room temperature at ~40 ^oC /min. In this condition, surface coverage by sulfate precipitation after treatment is less than 10 %, which does not make crucial effect on diffusion or reaction between gas and glass surface.
- The thermally-tempered glass samples were also prepared in the lab. Polished glass of 5.0 mm thickness was cut to 30×30 mm and chamfered. The sample was hung in a conventional electrical furnace heated to 716°C and kept for 15 minutes for uniform heating and stress release. Then, the sample was removed from the furnace and then quenched with air. In this process, the surface compressive stress is expected to be 50 MPa with a case depth of 833 μm (1/6 of the thickness) which are typical values [54].
- The chemically-tempered glass was also prepared from polished glasses. The ion-exchange temperature and time were 425 ^oC and 2.5 hour, and the salt bath composition was 10 % $NaNO_3$ / 90 % KNO_3. The surface compression stress and case depth for this process were 450 MPa and 4.8 μm, which were determined directly with a surface stress meter (FSM-6000, Orihara Industry Inc., Japan)

3.2.2. Secondary Ion Mass Spectroscopy (SIMS)

SIMS analyses of the leached samples as well as ‘as-produced’ float glass samples

were carried out using a PHI ADEPT1010 system. The Cs^+ primary beam impact energy was 3keV and the beam current 200 nA. The scanning area was 400 um^2 for negative secondary ion detection with an incidence angle of 60° to the sample surface normal. The secondary ions, ^1H and ^{30}Si, were monitored during depth profiling. The samples were charge-neutralized with a metal mask on the sample at ground potential.

3.2.3. Fourier Transform Infrared Spectroscopy (FTIR)

A Bruker Vertex70 system equipped with a DTGS detector was used for both transmission and ATR FTIR analysis. For FTIR transmission analysis, 100 scans were collected for each sample with a spectral resolution of 6 cm^{-1}. Spectra were collected from 6000 to 1500 cm^{-1} and spectra were processed and evaluated as absorbance vs. wave number.

In the ATR-IR measurements, a 45° diamond crystal with a refractive index of 2.4 (MVP-Pro, Harrick Scientific Products) was used. For this condition, the penetration depth of the evanescent wave is about 600 nm at 3450 cm^{-1} and about 900 nm at 1650 cm^{-1}. Before the ATR-IR measurements, the samples were cleaned with distilled water and ethanol in an ultrasonic cleaner, followed by UV ozone cleaning. The sample was pressed against the ATR diamond crystal with a force of 420 N over a 1.5 mm^2 sampling area. Spectra were collected from 4000 to 1500 cm^{-1} and were processed and plotted as log of the inverse reflectance, log(*1/R*), which is equivalent to the absorbance (*A*). 100 scans were collected for each sample with a spectral resolution of 6 cm^{-1}.

3.3. Results and Discussion

3.3.1. Comparison of transmission FTIR and ATR FTIR

Fig. 3-1 (a) and (b) present the near-IR and mid-IR transmittance spectra for the float glass and polished glass. In Fig. 3-1 (a), only the 4500 cm^{-1} absorption band which is assigned to the combination band of stretching and bending modes of OH groups is observed in both float and polished glass, while the 5200 cm^{-1} absorption band corresponding to the combined stretching and bending modes of H_2O molecules is not observed. The broad background spanning from ~4700 cm^{-1} to 5700 cm^{-1} is due to the iron impurity in the glass [48]. Thus, it can be concluded that almost all the hydrogen in the bulk is not associated with molecular water, but with dissolved OH groups.

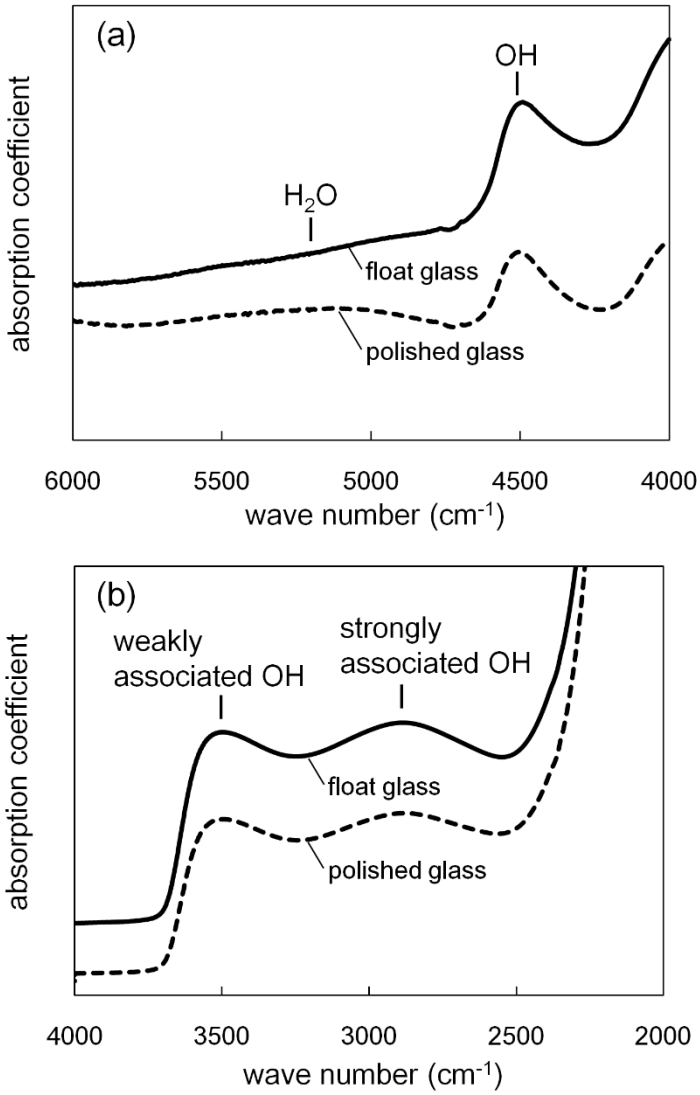

Fig. 3-1 Transmission spectra from float and polished samples in the (a) near-IR and (b) mid-IR regions.

The two broad peaks in Fig. 3-1 (b) centered at 3500 cm^{-1} and 2800 cm^{-1} are assigned to stretching vibrations of the Si-OH which are weakly and strongly bound to non-bridging oxygen sites in alkali silicates, respectively [16,20]. Utilizing the intensity of these two peaks, and published values for the relevant extinction coefficient [20], the amount of hydrogen (present as OH) in the bulk region can be calculated with the two-band method proposed by Scholze [16] to be around 2.3 - 2.8 × 10^{-3} as a H/Si ratio for both the float glass and the polished glass. For these low concentration values, it has been reported that almost all the hydrogen is not associated with molecular water, but with dissolved OH groups [5], which is consistent with the absence of 5200 cm^{-1} absorption band in near-IR transmission spectra shown in Fig. 3-1 (a).

The hydrogen content in the surface region is much higher than in the bulk region. Fig. 3-2 shows the hydrogen depth profiles of the as-received float glass surfaces (both air- and tin-sides) and the glass surface prepared by polishing and leaching with acid for 5 hours. The data shows that for the as-received float glass, the H/Si ratio of the surface region is about one order of magnitude higher than the bulk value determined from the transmission FTIR. In the case of the leached glass, the thickness of the hydrogen-enrichment region is much thinner than the as-received float glass, but its local maximum just beneath the surface is much higher than that the as-received glass.

Here, origin of the hydrogen concentration profile is discussed in terms of diffusion coefficient. Although the soda lime glasses were treated by SO_2 gas at high temperature around glass transition temperature, 540 ^oC, diffusion coefficient of water, D_{H2O}, in soda lime glass around the temperature range are not reported previously. Therefore, we reference D_{H2O} in rhyolitic glass which is similar to soda lime glass in that it contains more than 70 mol% of SiO_2 and other elements constitutes the glass are Al_2O_3 and alkali

and alkaline earth elements. D_{H2O} in rhyolitic glass reported by Zhang et al. as 1.1×10^{-12} (m^2/s) < D_{H2O} < 1.1×10^{-14} (m^2/s) [55]. Moreover, as index of diffusion distance after 600 seconds, $\sqrt{D_{H2O}t}$ is calculated as 2.6 (um) < $\sqrt{D_{H2O}t}$ < 2.6×10 (um).

Hydrogen concentration in Fig. 3-2 is decreased by half at 50 nm, which is deeper than that of 5 hour acid-leached sample because of higher treatment temperature in SO_2 gas treatment but seems much shorter than expected from the value of $\sqrt{D_{H2O}t}$ calculated above. This is possibly because the diffused water would be evaporated from the sample to atmosphere since the sample was exposed to dry air after SO_2 gas treatment in the process.

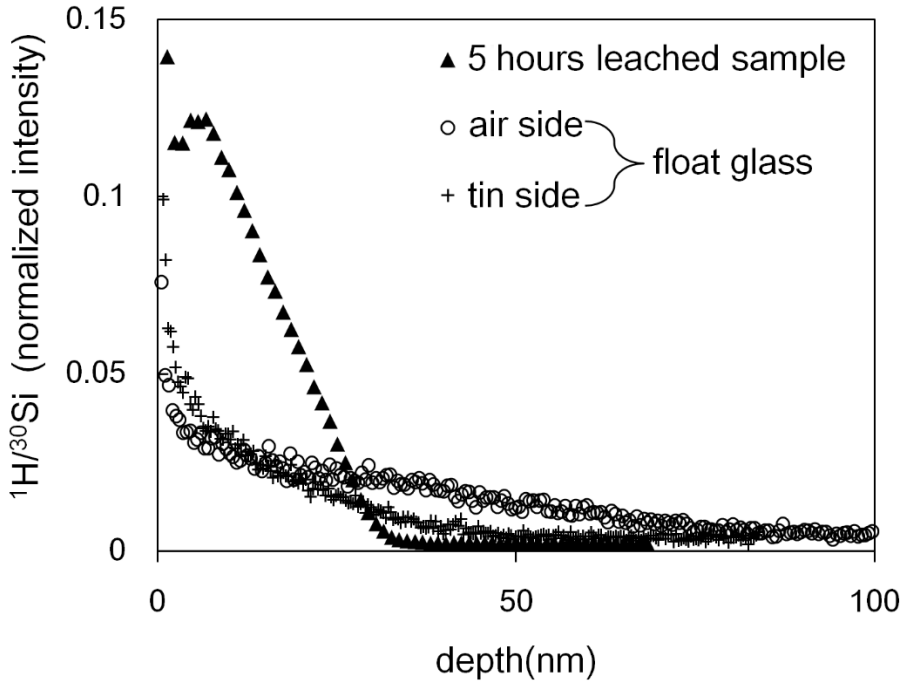

Fig. 3-2 Hydrogen concentration profiles evaluated by SIMS for the air- and tin-side surfaces of float glass and the polished and acid-leached glass sample. The data for an as-produced float sample was taken from Ref. [2].

The corresponding ATR-FTIR spectra obtained from each side (air and tin) of the float glass and the polished sample leached for 5 hours are presented in Fig. 3-3 (a) and (b), respectively. The ATR-IR spectra in the region between 2300 and 1900 cm^{-1} were deleted in the plot because the IR transmission in this region is very weak due to the absorption by the diamond ATR crystal itself. In Fig. 3-3 (a), the air side of float glass shows a larger OH peak than the tin side, which agrees well with the SIMS data shown in Fig. 3-2 [2]. Since these surfaces were treated by SO_2 gas and only briefly exposed to humidity, this difference in OH could be attributed mainly to surface dealkalization and ion exchange reaction due to SO_2 gas treatment. A difference is noted in the shape of the broad peak at the 3700-2500 cm^{-1} and the sharp peak at the 1650 cm^{-1} for the as-received float glass (Fig. 3-3 (a)) and the polished and leached sample (Fig. 3-3 (b)). These differences are discussed in detail in the next section.

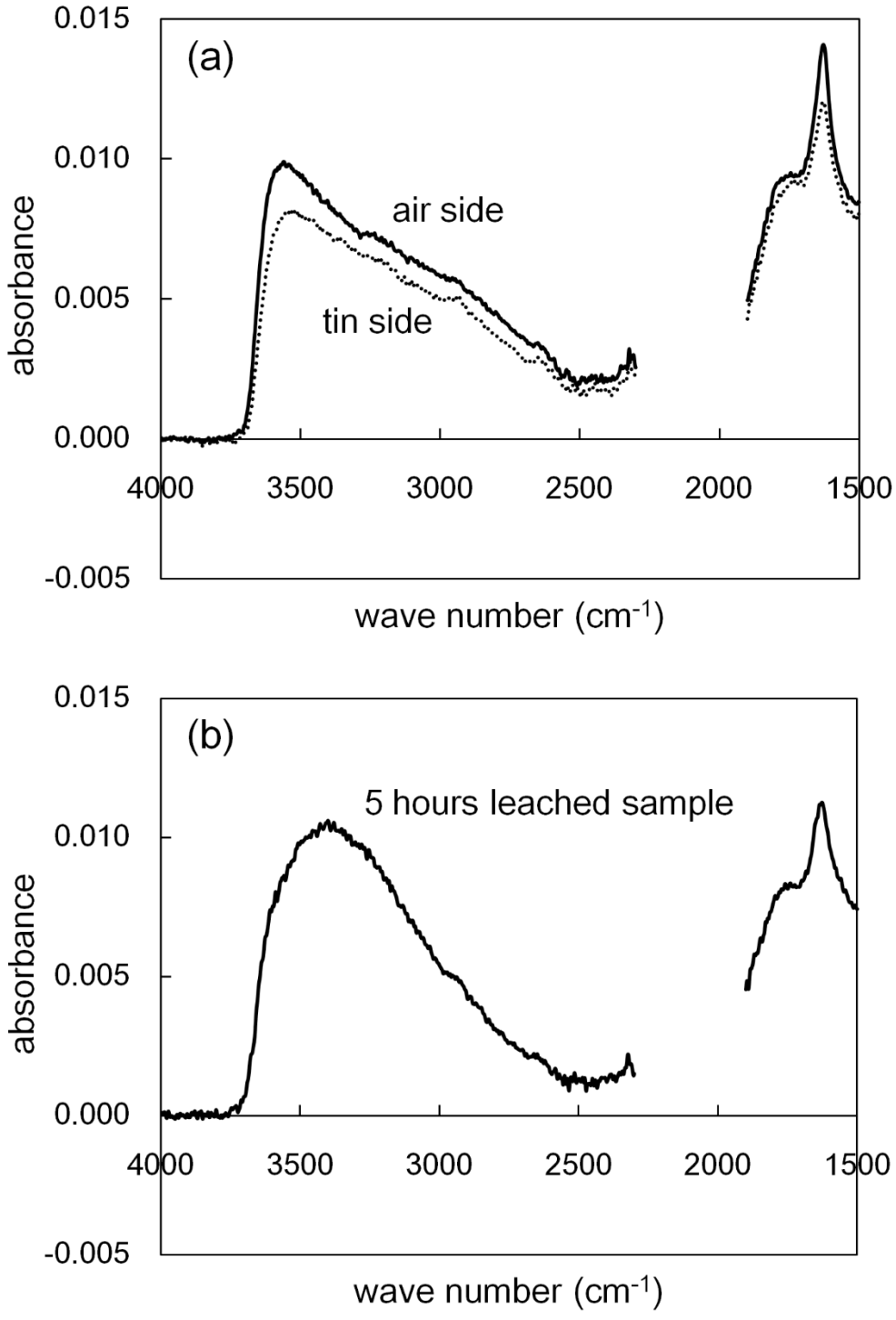

Fig. 3-3 ATR-IR spectra of (a) air and tin sides of the float sample and (b) surface of the polished and leached sample.

3.3.2. Water speciation in glass surfaces by ATR-IR

The broad band within the 3800-2500 cm^{-1} region can be attributed to the OH and H_2O species with varying degrees of hydrogen bonding interactions [4]. In transmission IR analysis, the hydroxyl versus molecular water species can be differentiated by two bands in the near IR region: 4500 cm^{-1} originating from the combination the OH stretch and the Si-OH bending vibrations and 5200 cm^{-1} from the combination of the OH stretch and the H-O-H bending vibrations of H_2O (Fig. 3-1 (a)). However, the combination and overtone bands in the near IR region (>4000 cm^{-1}) have very low absorption coefficients; thus, these bands cannot be detected in the ATR-IR analysis where the probe depth is only on the order of several hundred nm, which is much thinner than the entire sample thickness (3.9 mm for float glass or 5.0 mm for polished sample in our case) in the transmission analysis. Instead, the presence of the H-O-H bending vibration peak at ~1650 cm^{-1} can be used to check for the presence of molecular water in ATR-IR (Fig. 3-3) [32]. Note that this H_2O bending mode cannot be detected in the transmission analysis because the bulk glass absorbs strongly below 2000 cm^{-1} (Fig. 3-1 (b)). In any case, all ATR-IR spectra of as-received float glass and polished samples indicate the presence of molecular H_2O in the near-surface region (Fig. 3-3), which is absent or negligible in the bulk region (Fig. 3-1).

In contrast to the transmission mid-IR spectra showing two bands with comparable intensities at ~3500 cm^{-1} and ~2800 cm^{-1} (Fig. 3-1 (b)), the ATR spectra exhibit quite different shapes in Fig. 3-3 (a) and (b), which are dominated by the broad band spanning from 3700 cm^{-1} to 2500 cm^{-1}. The broad band is strong in the high wave number region and becomes weaker in the lower wave number region. It is known that the 2800 cm^{-1}

band is prominent in the IR spectra of the glasses containing non-bridging oxygen such as alkali silicate glasses, but very weak in those of silica and aluminosilicate glasses where non-bridging oxygen is negligible [4,20]. Thus, the difference in relative intensities of the weakly- and strongly-associated OH bands (3500 cm^{-1} and 2800 cm^{-1}) in the ATR spectra (Fig. 3-3 (a) and (b)) and the transmission spectra (Fig. 3-1 (b)) might be related to the difference in distribution of non-bridging oxygen species between the surface and bulk regions. This interpretation is reasonable since the SO_2, polishing and leaching treatments reduce the concentration of the network modifiers (primarily, sodium ions) in the surface region. Also the concentration of Si-OH groups in the bulk is so low (H/Si < 0.003; from Fig. 3-1 (b)) that all OH groups are isolated from each other and have hydrogen bonding with the network oxygen atoms or the non-bonding oxygen ions. But in the surface region, the population of the Si-OH and H_2O groups are so high (H/Si > 0.02; from Fig. 3-2) that some of them are hydrogen-bonded with each other. Thus, the distribution of hydrogen bonding interactions is expected to be much broader for the surface region than the bulk region.

It is intriguing to note that the shape of the OH stretching peak in the ATR spectra of the air and tin side of float glass (Fig. 3-3 (a)) is quite different from that of the leached sample (Fig. 3-3 (b)), which indicates that the degree of hydrogen bonding interactions of OH and H_2O species in the glass surface varies with the processing and environmental history of the surface. Fig. 3-4 shows the spectral difference between the air-side of the float sample and the 5 hour leached sample. The difference spectrum reveals that the weakly and strongly hydrogen-bonded species (~3600 cm^{-1} and ~2750 cm^{-1}) are more abundant in the float glass surface and the hydrogen-bonded species with intermediate strengths are more prominent in the polished and leached glass surface. It is reasonable

that the degree or distribution of hydrogen bonding interactions would vary with the silicate network connectivity and network modifier concentration as well as the H_2O and OH concentration.

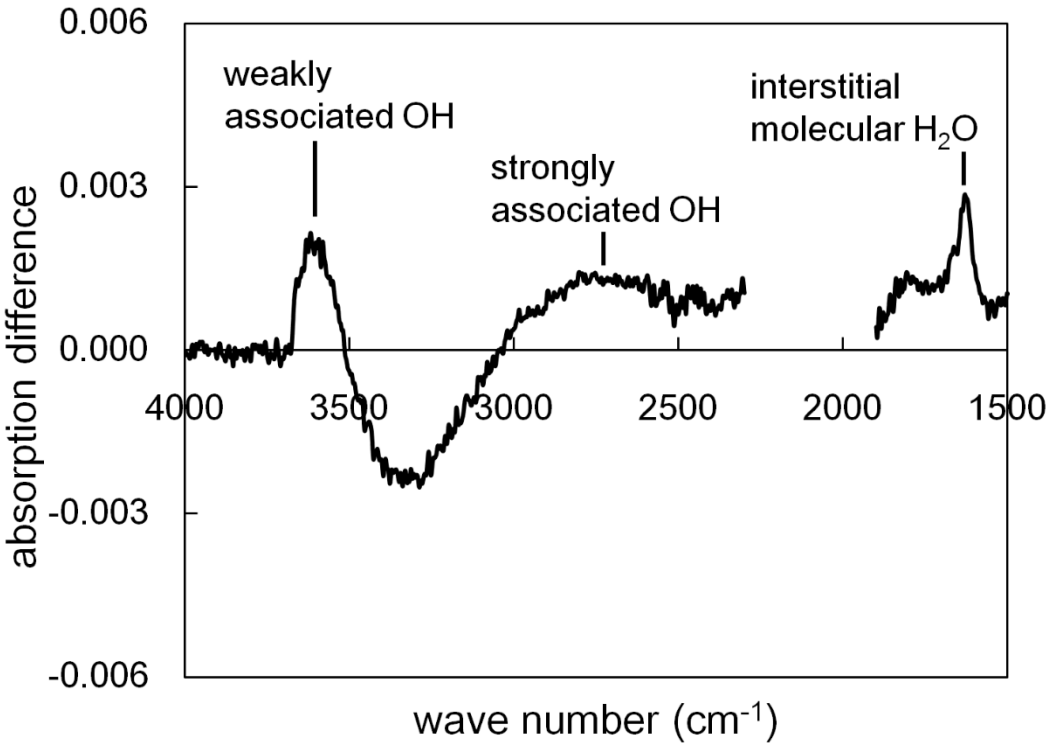

Fig. 3-4 The difference spectrum obtained by subtracting the ATR spectrum of the 5 hour leached sample (Fig. 3-3 (b)) from that of the air side of float sample (Fig. 3-3 (a)).

Davis and Tomozawa reported that for silica glass, the bands near 3673 cm^{-1} and 2820 cm^{-1} can be assigned to the OH stretching of silanol groups, while the band extending from 3450 cm^{-1} to 3225 cm^{-1}, as well as the band at 1611 cm^{-1}, to the stretching and bending modes of molecular water [4]. Studying alkali silicate glasses, Efimov assigned the peak at 3600 cm^{-1} to the stretching vibration of SiOH with weak hydrogen bonding to an oxygen from the neighboring hydroxyl group and the 2750 cm^{-1} peak to the stretching vibration of SiOH with strong hydrogen bonding to the non-bridging oxygen [56,57]. He also assigned other bands near 3400 cm^{-1} and 3200 cm^{-1} to symmetric stretching of interstitial molecular H_2O and the band at 1674 cm^{-1} to bending vibration of interstitial molecular H_2O. If, in Figure 3-4, the negative portion in the 3500-3000 cm^{-1} region is solely due to the decrease in the molecular H_2O content, then the 1650 cm^{-1} H_2O bending peak should also be negative; but that is not the case. Thus, the negative portion in Figure 3-4 must be due to the decrease in the SiOH species whose hydrogen bonding interaction strengths are similar or comparable to molecular water in the liquid state.

3.3.3. Effects of SO_2, thermal tempering, and chemical strengthening treatments

The as-received float glass is treated with SO_2 in the continuous production line [2,52,53]. This could be the reason for the difference in the OH stretching peak shape in the 3600-2500 cm^{-1} region. In order to test this hypothesis, we treated the polished glass sample with SO_2 in a laboratory furnace. Fig. 3-5 (a) compares the ATR-IR spectra of the polished glass sample before and after the SO_2 treatment. It is noted that after the SO_2 treatment, the ATR-IR spectrum becomes similar to that of the ‘as-received’ float glass (Figure 3-3 (a)). The difference spectrum in Fig. 3-5 (b) clearly shows that the weakly

bound SiOH species are increased after the SO_2 treatment. This must be a consequence of the ion exchange reaction of sodium with hydrogen in the SO_2 treatment process at a temperature (540 ^oC) near the glass transition temperature. It has been reported that in hydrous silicate glasses, the $SiOH/H_2O$ ratio increases significantly if the glass is treated at temperatures higher than its glass transition temperature [58]. There is also a densification effect in the high temperature reaction which could alter the ratio of strong to weak hydrogen bonding. In acid leached samples, both molecular water and SiOH exist and hydrogen bonding between them can possibly be formed. On the other hand, most water exist as SiOH in SO_2 treated sample and hydrogen bonding between SiOH and molecular water cannot be formed, which can cause higher ratio of weakly associated SiOH in SO_2 treated sample.

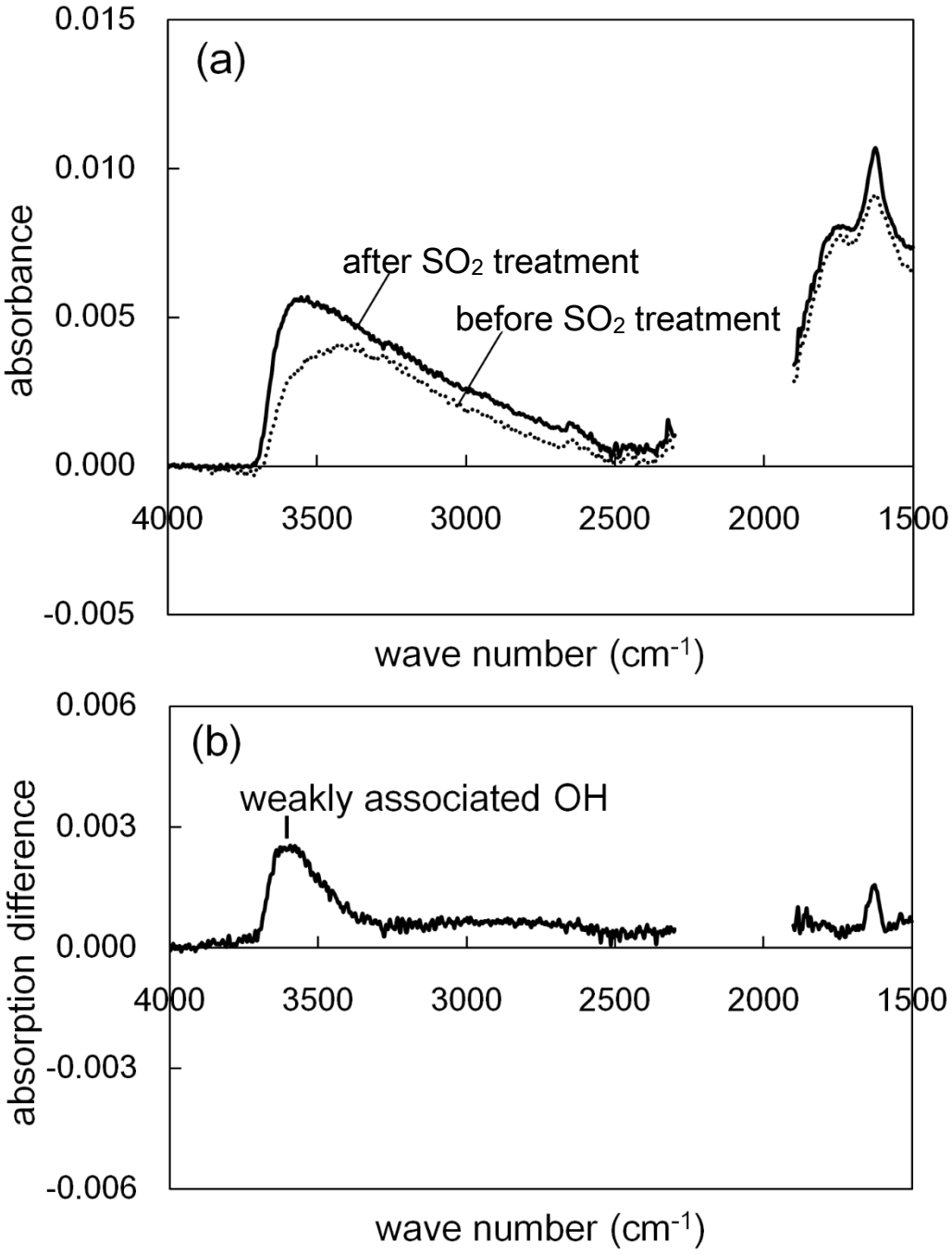

Fig. 3-5 (a) ATR-IR spectra of before (dash line) and after (solid line) SO_2 gas treated samples. (b) The differential spectrum obtained by subtracting the polished sample spectrum from the SO_2 treated sample spectrum

Fig. 3-6 shows that the thermal tempering process causes a decrease in water content in the glass surface. It is expected that this decrease of water is caused by evaporation to the gas phase or diffusion into the bulk at high temperature during the tempering process. Also the peak shape after the process is somewhat closer to those of float glass and SO_2 treated samples. It can be speculated that it is due to the high process temperature which the thermally tempered sample has experienced.

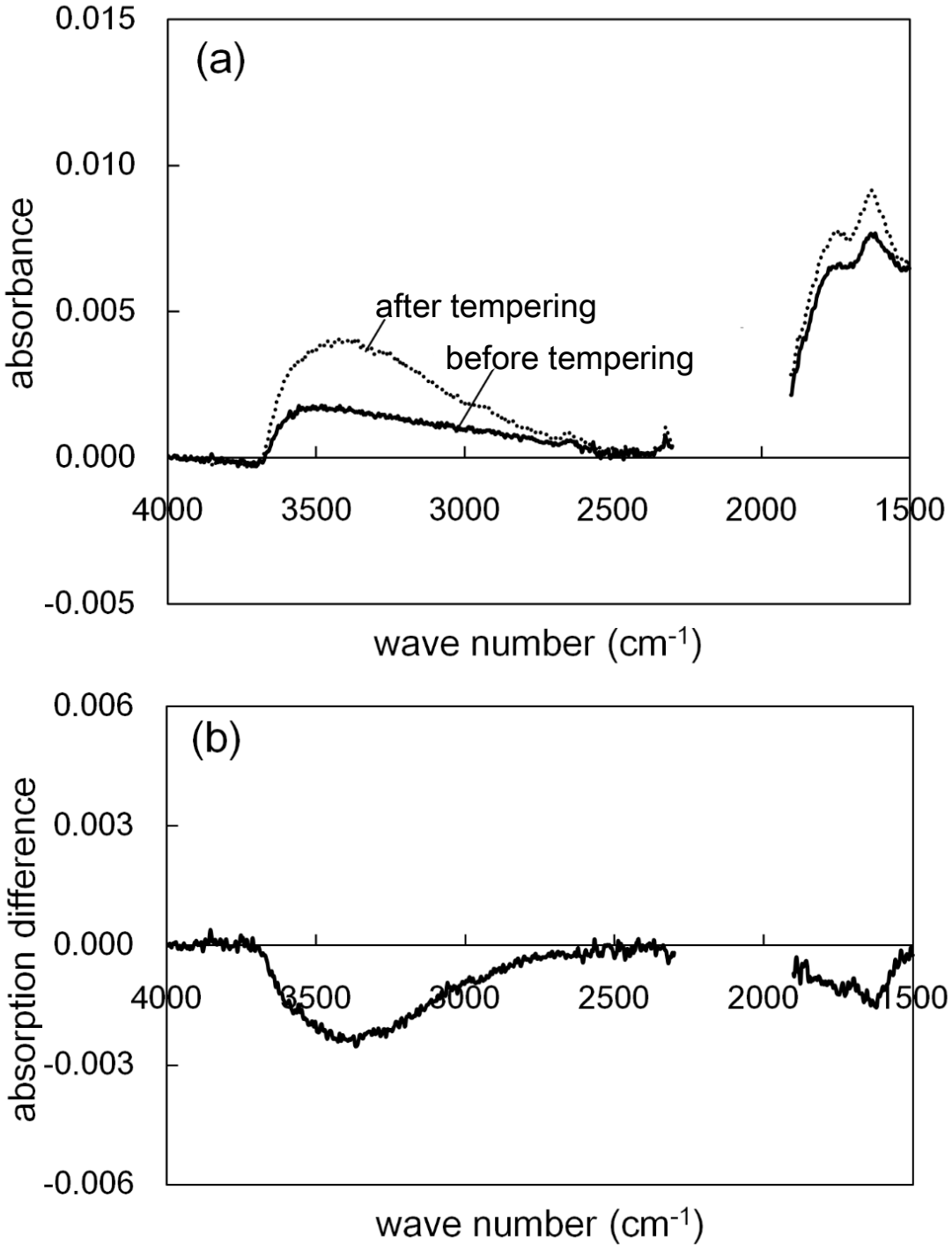

Fig. 3-6 (a) ATR-IR spectra of before (dash line) and after thermally tempered (solid line) samples. (b) The difference between thermally tempered and polished samples.

In the case of the chemically tempered/strengthened samples, the OH peak intensity change in the ATR-IR spectrum (Fig. 3-7) was much smaller compared to the SO_2 and thermal tempering cases. It is known that the exchange of Na^+ with K^+ could increase the refractive index by 0.003 in typical strengthening condition [59]; but, this change is too small to reduce the ATR-IR probe depth. Thus, its refractive index effect on the ATR-IR intensity would be negligible. Instead, it is more likely that a small fraction of water is dissolved into the molten salt during the chemical strengthening process.

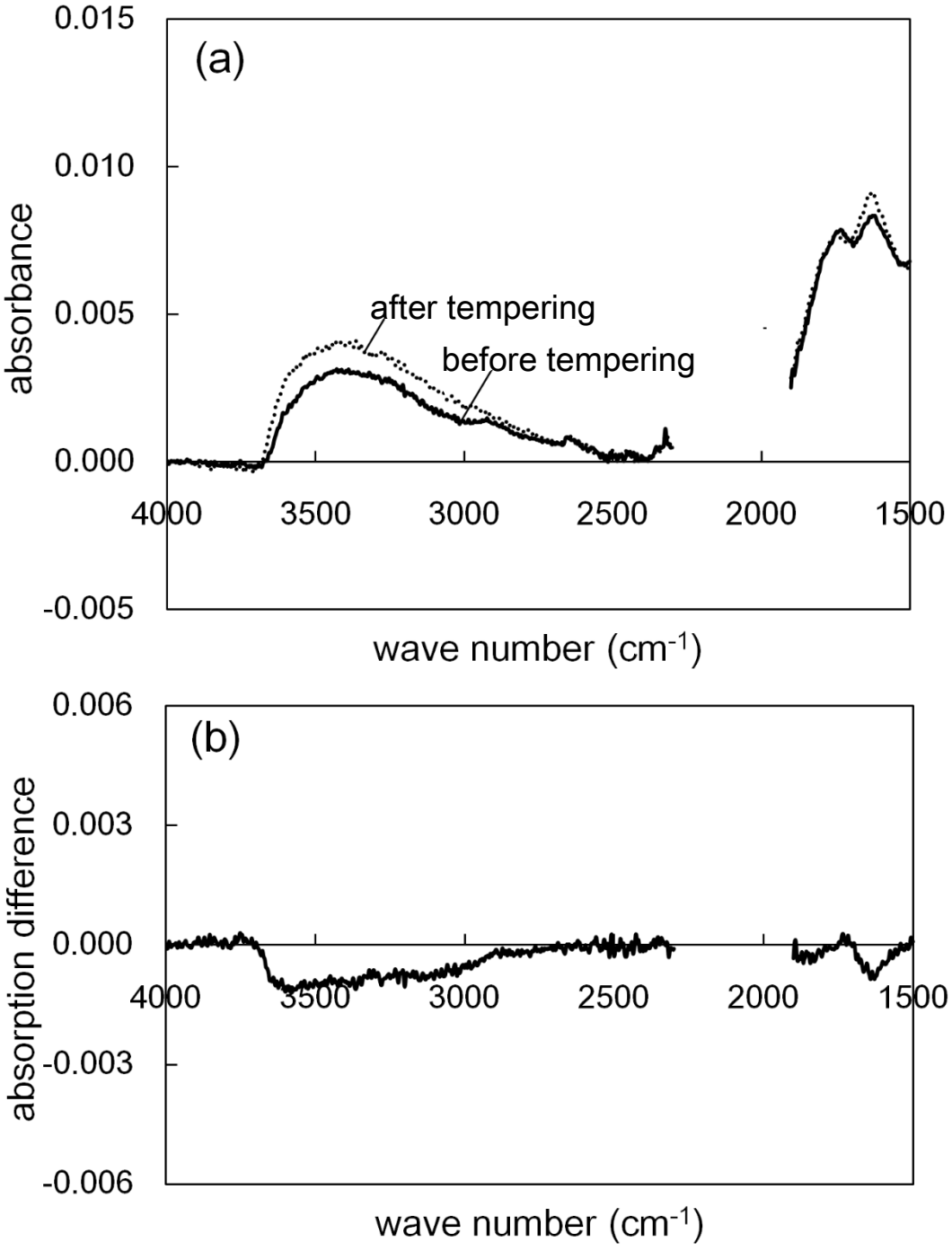

Fig. 3-7 (a) ATR-IR spectra of before (dash line) and after chemically strengthened (solid line) sample. (b) The differential spectra between chemically strengthened and polished samples.

3.4. Summary

Qualitative and quantitative evaluation of water speciation in glass surfaces has been conducted with ATR-IR. Transmission spectra were used to differentiate bulk versus surface contributions to the ATR spectra, and confirm the surface sensitivity of ATR for determination of water speciation. It was demonstrated that differences in water speciation could be detected in the ATR spectra for various surface treatments.

The ATR-IR analyses show that the concentration of strongly bound SiOH species are decreased in the surface of these glasses due to depletion of network modifier elements by SO_2 treatment, polishing or leaching processes. The SiOH and H_2O species in the glass surface showed a wide range of hydrogen bonding interactions and their distributions varied with SO_2, polishing, acid leaching, thermal tempering, and chemical strengthening treatments.

4 Effect of Fictive Temperature on Formation of Surface Layer on Soda Lime Glass

4.1. Introduction

Silicate glass surfaces often contain a high concentration of hydrous species, including silanol groups (Si-OH; also called 'hydroxyl' broadly without distinction) and interstitial molecular water (H_2O), due to the glass-forming conditions used in industrial manufacturing processes [2,52,53], as well as to polishing, acid treatment [3,41] or weathering [3]. Silanol groups and interstitial molecular water in silicate glasses can have different degrees of interaction, so-called hydrogen bonding, in the disordered network and surface of glass [60]. In Chapter 3, we have shown that the degree of hydrogen bonding interactions of these species in the glass surfaces varies with the surface formation and/or treatment history [41]. For example, soda lime silica glass treated by SO_2 gas was found to contain more free-OH (or weakly associated OH) compared to the polished surface of the same glass composition. The ratios of SiOH to molecular water in silicate glasses are known to depend on the local concentration of water in the glass [5], temperature [15,61] and glass composition [22]. However, the mechanism causing this difference in speciation of hydrous species in the glass surface is unclear. The fictive temperature of a glass is a measure of the disorder (entropy) frozen into the glass at the glass transition. Glasses cooled at different rates have different fictive temperatures; in general, a glass cooled at a higher rate has a higher fictive temperature. Industrially manufactured flat glasses have different fictive temperatures depending on the forming

and cooling processes. For example, a glass produced by the float method is known to have a lower fictive temperature than the one produced by the fusion process due to its lower cooling rate [62]. This difference can affect the dimensional stability of the glass upon re-heating and perhaps surface chemical reactivity.

Behrens and Nowak [61] conducted experiments by quenching glasses, containing different amounts of water, at various cooling rates. Their results showed that the ratio of $SiOH/H_2O$ is higher in glasses with higher fictive temperature. This indicates that the speciation of hydrous species is coupled to the degree of relaxation of the silicate network during cooling through the glass transition. In the case of commercially manufactured glass, the fictive temperature can vary with the production process. When these glasses are exposed to ambient air or subjected to secondary processing such as polishing, acid treatment and weathering, additional hydrous species can be introduced. The speciation of the hydrous products formed via reactions of glass with water in ambient conditions may depend on the fictive temperature of the glass, i.e. the disorder frozen in the glass network during the cooling. The effect of fictive temperature on the distribution of the water-related species in surfaces has not been studied and is an objective of the work reported here.

In this chapter, we investigated the effect of fictive temperature on water reactivity by leaching in pH 1 acid. The samples with different fictive temperatures were prepared by quenching soda lime silica glasses from different temperatures. ATR analyses in both the mid-IR and near-IR regions, along with specular reflectance (SR) IR and secondary ion mass spectrometry (SIMS), were used to quantitatively evaluate the effect of fictive temperature on leaching rate and the resulting water speciation.

4.2. Experiment

4.2.1. Sample preparation

Soda lime silica float glasses, supplied by AGC Inc. (Tokyo, Japan), were used in this study. The glass samples with original thickness of 0.7 mm were thinned to 100 um thickness by etching with HF and strong acid at 35 ºC for 1 hour. This reduced the heat capacity of the sample, enabling the sample cooling at a high rate in the quenching experiment described below.

The thin glass samples were annealed at 600 ºC for 5 hours and slowly cooled to room temperature at a cooling rate of 1 ºC/min. The fictive temperature of this sample would be close to the glass transition temperature. For preparation of samples with higher fictive temperatures than glass transition temperature, two of the samples were hung by a wire in an electric furnace and heated to 600 ºC and 700 ºC, respectively. The heated samples were kept there for 15 min to relax their network structures. The samples were then taken out of the furnace and quenched in air to room temperature. To fabricate the samples with lower fictive temperatures than glass transition temperature, the thin glass samples were annealed at 500 ºC for 36 and 60 hours. The refractive indices measured for the 36 hours and 60 hours samples were the same within the accuracy of the measurement, indicating the fictive temperature of the sample reached an equilibrium state at 500 ºC after the 36 hour treatment. The 60-hour-annealed sample was used as the sample with the fictive temperature of 500 ºC in other experiments.

These samples with different fictive temperatures ranging from 500 ºC to 700 ºC were then reacted in HCl acid (pH = 1, 90 ºC) for 600 hours to incorporate hydrous species in

the glass surface. The surface area of each sample was 7.5 cm^2 and the volume of HCl solution was 50 ml.

4.2.2. Refractive index measurement

Refractive indices at the He d-emission line, n_d, of the samples with different thermal histories were measured to evaluate the effect of fictive temperature. The measurements were done by the Becke line method using a series of standard matching oils (Cargille Laboratories, Cedar Grove, NJ), with refractive indices varying from 1.500 to 1.520, separated by increments of 0.0005 (all with standard error of ±0.0002). The accuracy of the measurement is estimated as 0.0003. The measured refractive index was used to estimate the density of the sample using the Clausius–Mossotti relation.

4.2.3. Secondary Ion Mass Spectroscopy (SIMS)

SIMS analyses of the leached samples with different fictive temperatures were carried out using a PHI ADEPT1010 system (ULVAC-PHI Inc., Chigasaki, Japan). The acceleration voltage of the Cs^+ primary beam was 5 kV and the beam current was 100 nA. The scanning area was 60 × 60 μm^2 for negative secondary ion detection with an incidence angle of 60^o to the sample surface normal. The secondary ions, ^1H and ^{30}Si, were monitored during depth profiling. The samples were charge-compensated with an electron gun.

4.2.4. Fourier Transform - Infrared Spectroscopy (FT - IR)

4.2.4.1. Specular reflectance (SR) - IR measurements

SR-IR spectra of the samples described above were collected in order to evaluate fictive temperature before leaching and to investigate an effect of acid treatment on the spectra after the treatment. Bruker Hyperion 3000 micro-FT-IR system equipped with a 15× infrared microscope objective lens and MCT detector (Bruker Optics Inc., Billerica, MA) was used for the measurement. Incidence angle was 20^{o} from the surface normal direction. SR-IR spectra were obtained in the range of 600 – 1300 cm^{-1}. Spectra were acquired for three spots per sample in 400 scan passes at a 4 cm^{-1} resolution. Each SR-IR spectrum was normalized by its largest peak around 1050 cm^{-1} for comparison. Peak positions around 1050 cm^{-1} were obtained from the intercept in the first differential curve of each spectrum. A gold mirror was used as a standard reference for all measurements.

4.2.4.2. Attenuated total reflectance (ATR) - IR measurements

A Bruker Vertex70 system (Bruker Optics Inc., Billerica, MA) equipped with a MCT detector was used for ATR-IR analysis. In the ATR-IR measurements, an attachment using a diamond crystal with incident angle of 45° (MVP-Pro, Harrick Scientific Products Inc., Pleasantville, NY) was used. Spectra were collected from 6000 to 1500 cm^{-1} and were processed and plotted as the log of the inverse reflectance, log (1/R), which is dimensionally equivalent to the absorbance as explained in chapter 2. Each spectrum was obtained by averaging 3200 scans with a spectral resolution of 6 cm^{-1}. Before the ATR-IR measurements, the samples were cleaned with distilled water and ethanol in an

ultrasonic cleaner, followed by UV ozone cleaning. The samples were pressed against the ATR diamond crystal with a force of 420 N over a 1.5 mm^2 sampling area during analyses. All measurements were conducted at room temperature.

4.3. Results and Discussion

4.3.1. Density of glass samples with different thermal history

The results of the Becke line measurements for the samples cooled at different temperatures are shown in Table 1. The samples treated at higher temperature have lower indices, which indicates that the soda lime glasses with higher fictive temperature have lower density [64]. The density of the samples were estimated using the Clausius–Mossotti relation between refractive index and density [65] as shown in Table 4-1. Hereafter, the density values in Table 4-1 will be used for sample identification.

Table 4-1 Analyzed samples with different fictive temperature. The error associated with the refractive indices and densities are approximately ±0.00025 and 0.001 g/cm^3, respectively.

Sample ID	Description	Refractive index (n_d)	Estimated density (g/cm^3)
SLG700Q	Air-quenched after annealing in 700^{o}C for 15 min.	1.51425	2.486
SLG600Q	Air-quenched after annealing in 600^{o}C for 15 min.	1.51525	2.490
SLG600S	Annealed in 600 ^{o}C for 5 hours and cooled to RT at 1 ^{o}C/min.	1.51675	2.496
SLG500A	Annealed in 500 ^{o}C for 60 hours	1.51775	2.500

4.3.2. Hydrogen depth profiles of glass samples with different thermal history

The hydrogen depth profiles obtained for the leached glass samples with different fictive temperatures were normalized by the maximum concentration observed at the outermost surface and shown as symbols in Fig. 4-1. The near-surface data (within 20 nm from the surface) were deleted in the plot because SIMS analysis in this region is considered unreliable [66]. In all samples, the hydrogen concentrations in the surface regions are much higher than in the bulk regions, which indicates that the acid treatment introduced a significant amount of hydrogen as a result of the interdiffusion reaction between sodium and water. The data shows that the hydrogen concentrations in the surface, to a depth of ~300 nanometers, are about two orders of magnitude higher than those in the bulk of the glass.

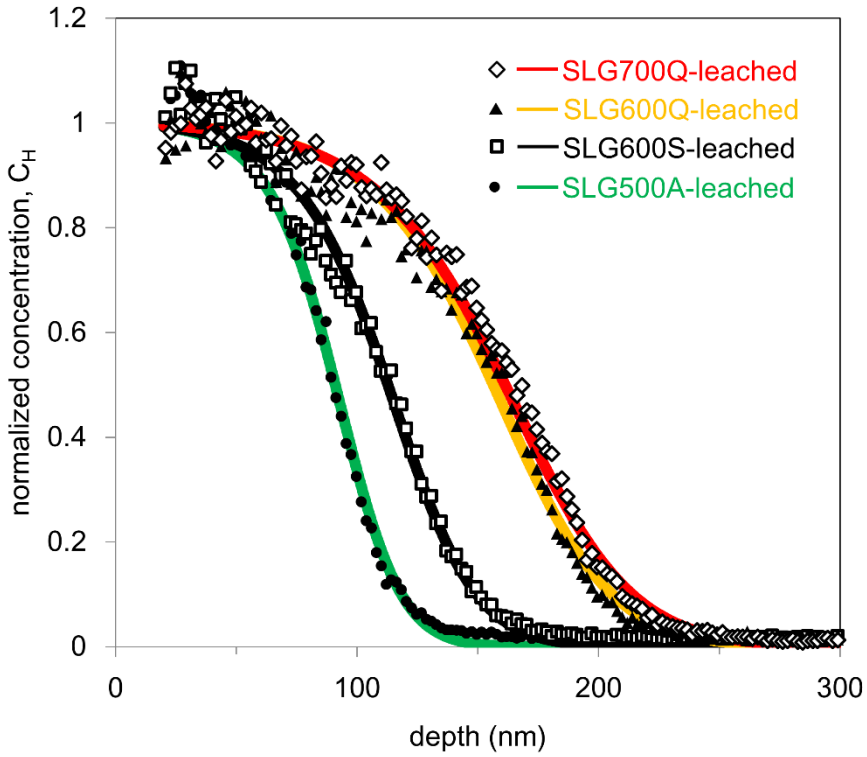

Fig. 4-1 (Symbols) normalized hydrogen concentration profiles evaluated by dynamic SIMS for the acid treated samples with different fictive temperatures. (Solid lines) the fitted curves obtained from numerical calculation.

To evaluate the rate-limiting diffusion coefficient during the leaching of the samples, the hydrogen depth profiles from the SIMS analyses were fit to an inter-diffusion model. The inter-diffusion model for soda lime silica glass, reported by Doremus [67] and Lanford [3], has been shown to describe the leaching process of soda lime glass very well. In this model, the effective diffusion coefficient $\tilde{D}$ is given by:

$$\tilde{D} = \frac{D_H D_{Na}}{C_H D_H + (1 - C_H) D_{Na}} = \frac{D_H}{1 + C_H \{(D_H / D_{Na}) - 1\}} \qquad (1)$$

where D_H and D_{Na} are the diffusion coefficient of hydrogen and sodium ions, respectively; C_H is the normalized concentration of hydrogen ions by the maximum concentration at the surface in each profile. Then, based on Lanford's study, the diffusion-driven acid leaching process can be described as follows [3]:

$$\frac{d^2 C_H}{dy^2} = -2y[1 + (D_H / D_{Na} - 1) C_H] \frac{dC_H}{dy} + \frac{D_H / D_{Na} - 1}{1 + (D_H / D_{Na} - 1) C_H} \left(\frac{dC_H}{dy} \right)^2 \qquad (2)$$

where *y* is the Boltzmann transform using leaching depth, *x*, and leaching time, *t*, as

$$y = x \sqrt{4 D_H t} \qquad (3)$$

Therefore, the hydrogen depth profiles for the glasses with different fictive temperatures can be fit numerically with equation (2) by assuming a D_H / D_{Na} ratio. We fit the data using D_H / D_{Na} ratios ranging from 0.001 to 0.01 with increments of 0.0001. These ratios are within the acceptable range reported previously [3]. The best fitting curves were obtained when D_H / D_{Na} ratio was from 0.003 to 0.005; it was difficult to differentiate the fit quality within this D_H / D_{Na} range because the SIMS hydrogen profiles were

scattered in the surface region and the variance with D_H / D_{Na} was small in this range.

The best-fit curves are displayed as solid lines in Fig. 4-1 while the diffusion coefficients of hydrogen determined for the best D_H / D_{Na} ratio range (0.003~0.005) are plotted against the estimated densities of the samples in Fig. 4-2. The results clearly show that the diffusion is faster in the glass samples with lower densities which correspond to higher fictive temperatures. To the best of our knowledge, this is the first experimental data reporting direct correlation between the diffusion coefficient and the fictive temperature. Since the soda lime silica glass with a higher fictive temperature has a lower density value [64], they must have a more open structure which facilitates higher diffusion coefficients.

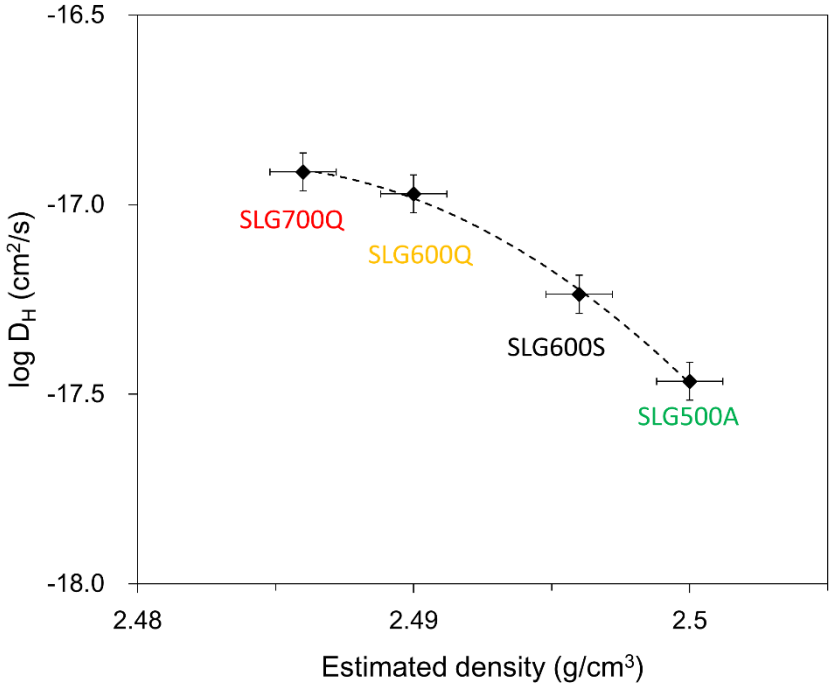

Fig. 4-2 Diffusion coefficients of hydrogen plotted against the estimated densities of the samples as measures of their fictive temperatures. A line is a guide to the eye.

3.3 FTIR analyses of the glasses with different fictive temperature

3.3.1 SR-IR analysis of silicate network

To analyze the effects of fictive temperature and sodium leaching on the network structures, we evaluated the SR-IR spectra of the samples with different fictive temperatures before and after acid treatment. Fig. 4-3 (a) presents the SR-IR spectra for glass samples listed in Table 4-1 before and after acid leaching treatment. It is shown that after leaching the peak around 1050 cm^{-1}, which is assigned to asymmetric vibration modes of the Si-O-Si network [33,35], shifts towards high wavenumber while the shoulder at 940 cm^{-1}, which corresponds to the stretching vibration of the $Si-O^-$ (NBO) and Si-OH groups [33,38], grows and becomes more distinct. These changes can be considered to be the result of dealkalization in the glass surfaces during the leaching [33,35]. The band around 770 cm^{-1}, which is attributed to symmetric vibration mode of the Si-O-Si network [38], does not show a significant shift with acid treatment.

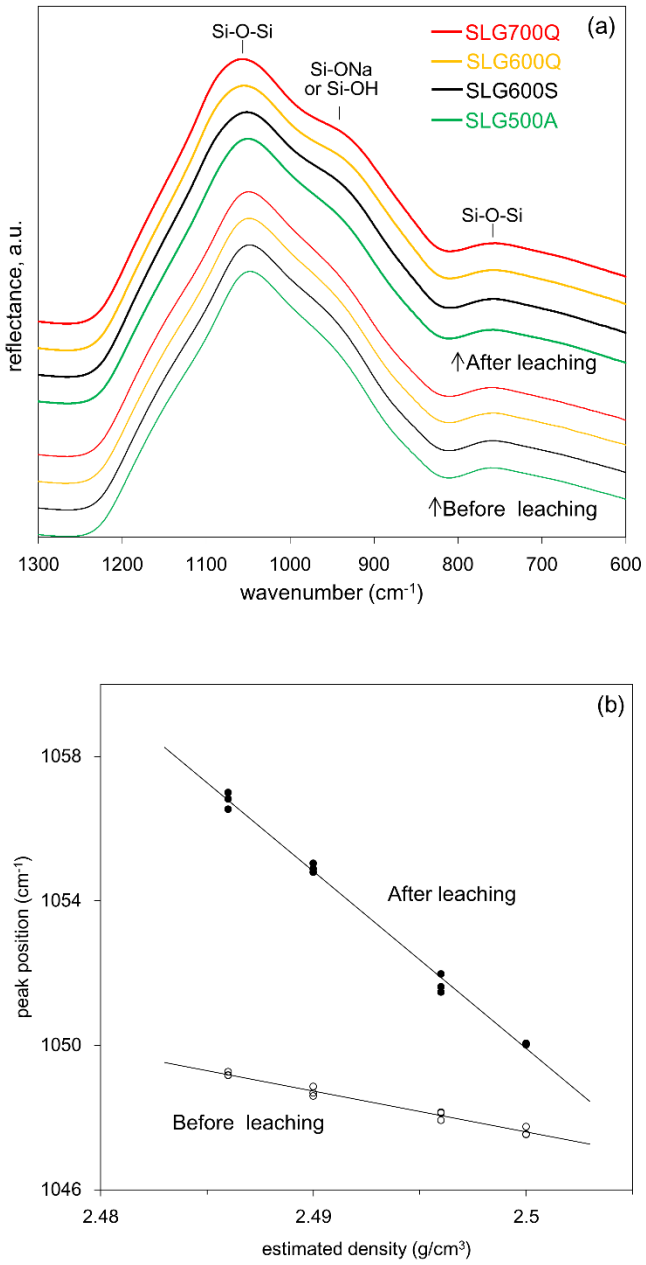

Fig. 4-3 (a) SR-IR spectra of samples with different fictive temperature before (thin lines) and after (bold lines) leaching. Spectra are plotted with an offset for clarity. (b) Peak position of 1050cm^{-1} band in the samples before and after leaching versus the estimated densities of the samples. Lines are guides to the eye.

For the further investigation of the network structure, we evaluated the positions of the Si-O-Si vibration peak around 1050 cm^{-1} in each sample in more detail. Agarwal and Tomozawa showed empirically that the Si-O-Si peak position shifts to high wavenumber with the increase of fictive temperature, although the mechanism of the peak shift is still not been fully understood [68]. The open symbols in Fig. 4-3 (b) plot the peak position of Si-O-Si vibrations of the samples before leaching against their density. The samples with higher fictive temperatures (lower densities) show higher peak positions, which confirms that the samples annealed at higher temperatures have higher fictive temperatures.

The closed symbols in Fig. 4-3 (b) display the peak positions of the Si-O-Si vibrations of the acid-treated samples. The peak position shifts to higher wavenumber in the leached glass surfaces, which can be attributed to dealkalization during acid leaching [35]. Interestingly, the extent of the peak shift before and after leaching is larger for higher fictive temperature samples. It seems likely that this is associated with the more intense dealkalization in the samples with higher fictive temperatures, as revealed by the SIMS hydrogen profiles shown in Fig. 4-1.

3.3.2 ATR-IR analysis of hydrous species in the leached glass surfaces

Fig. 4-4 (a) presents the ATR-IR spectra obtained from the samples with different fictive temperatures after acid treatment. The ATR-IR spectra in the region between 2300 and 1900 cm^{-1} are not shown in the plot because the IR signal in this region is very weak due to the absorption by the diamond ATR crystal itself. In the mid-IR region, the H-O-

H bending (δ_{HOH}) vibration peak at 1650 cm^{-1} is evidence for the presence of molecular water in the glass surface [4]. The 1650 cm^{-1} peak shape is not changed much. The broad band spanning over the 3700 - 2500 cm^{-1} region (centered at ~3400 cm^{-1}) can be attributed to the OH stretching vibration (ν_{O-H}) of SiOH and H_2O species with varying degrees of hydrogen bonding interactions [4,41,60].

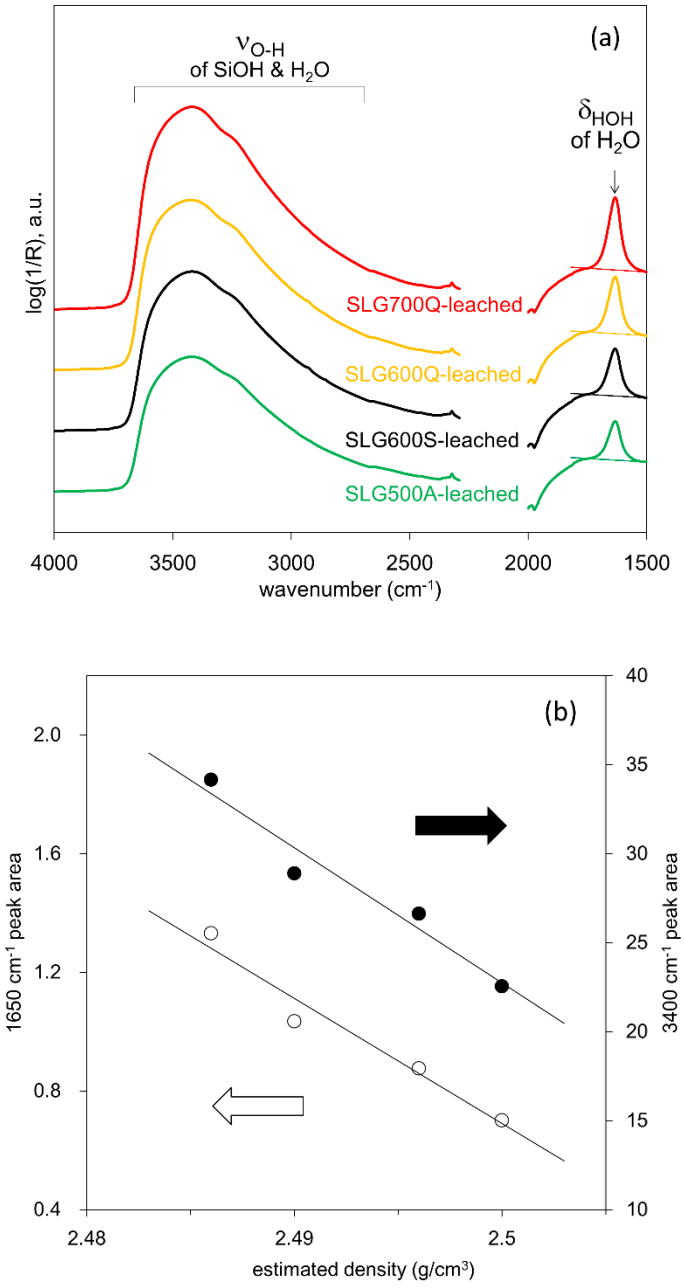

Fig. 4-4 (a) ATR mid-IR spectra of the leached samples with different fictive temperatures. The spectra are plotted with an offset for clarity. The tangential baseline for 1650 cm^{-1} bands is shown as solid thin lines. (b) Absorption peak area of 1650 cm^{-1} and 3400 cm^{-1} band plotted against the estimated densities of the samples. Lines are guides to the eye.

To measure intensities of the absorption bands, we used baselines consisting of two linear tangents which were reported previously as a TT baseline by Withers et al [69]. To evaluate the intensities of the H-O-H bending vibration peaks at 1650 cm^{-1}, we drew a tangent line connecting the minimum on the lower wavenumber side and its inflection point on the higher wavenumber side (shown as thin lines in Fig. 4-4). The intensities of the δ_{HOH} peak at 1650cm^{-1} and the ν_{O-H} peak centered at 3400 cm^{-1} are plotted against the sample density in Fig. 4-4 (b). The data shows more hydrous species in the samples with lower densities (higher fictive temperatures), which is consistent with the SIMS hydrogen profiles shown in Fig. 4-1. The amount of molecular H_2O, as measured from the 1650 cm^{-1} peak intensity, is higher for glasses with higher fictive temperature because the peak at 1650 cm^{-1} is only due to H-O-H bending vibrations. It is difficult to measure the amount of SiOH or determine the SiOH/H_2O ratio from the mid-IR analysis (Fig. 4-4) because both the ν_{O-H} bands of both SiOH and molecular water H_2O contribute to the peak in the 3700 - 2500 cm^{-1} region.

The spectral overlap in the ν_{O-H} region can be avoided in the near-IR analysis. Fig. 4-5 displays ATR spectra in the near-IR region from 6000 cm^{-1} to 4000 cm^{-1}. The peak around 5250 cm^{-1} is the combination of stretching and bending modes ($\nu_{O-H} + \delta_{HOH}$) of molecular water [17]. The small peak at 4500 cm^{-1} is attributed to the combination of O-H and Si-OH stretch modes ($\nu_{O-H} + \nu_{Si-OH}$) of the Si-OH species [17]. Since the ν_{Si-OH} peak is at ~940 cm^{-1}, the main ν_{O-H} contributor to the 4500 cm^{-1} appears to be the OH band at ~3360 cm^{-1}, which might suggest that OH groups with weak hydrogen bonding interactions can contribute to this combination band in near IR [18]. The combination band of the strongly hydrogen bonded OH groups (which appears at ~2800 cm^{-1} in the mid-IR region [18,20]) proved difficult to identify (data not shown).

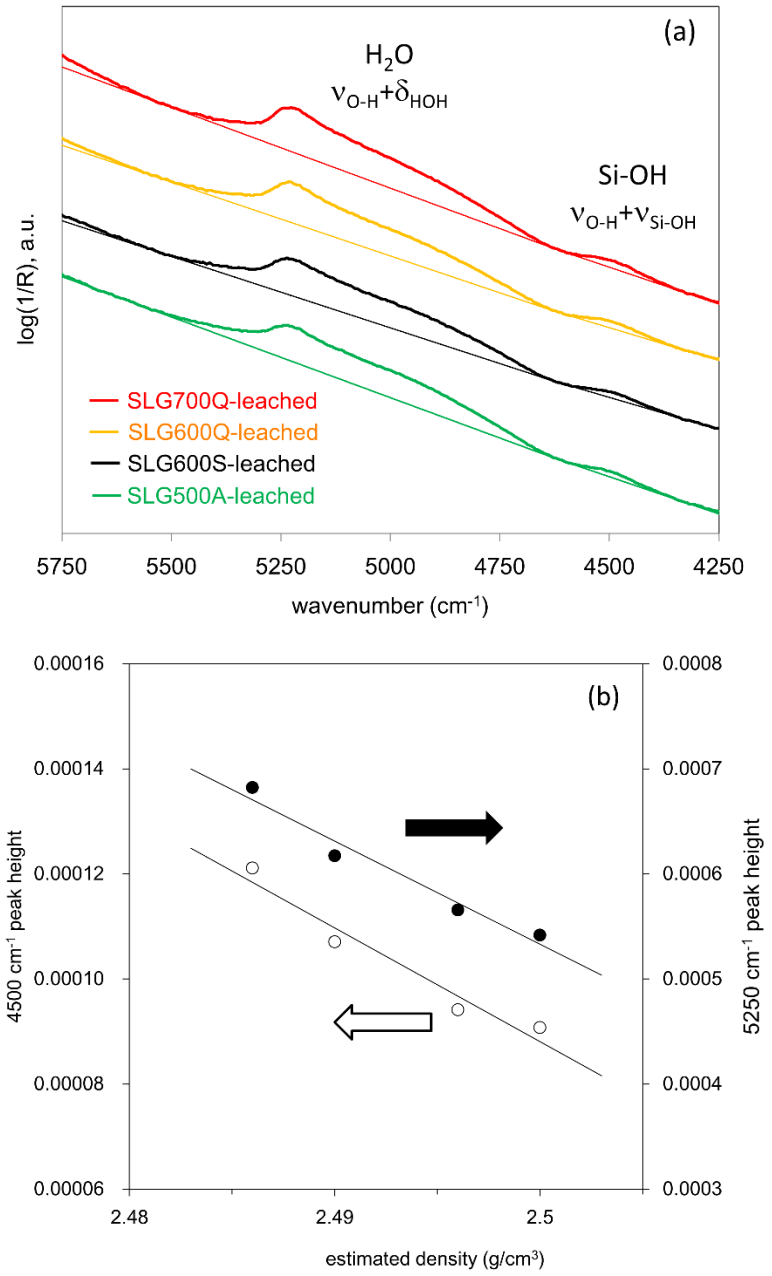

Fig. 4-5 (a) ATR near-IR spectra including H_2O and SiOH combination band of the leached samples with different fictive temperature. The spectra are plotted with an offset for clarity. The tangential baseline for 4500 cm^{-1} band and 5250 cm^{-1} band are shown as solid thin lines. (b) Peak intensities of 4500 cm^{-1} band to 5250 cm^{-1} band plotted against the estimated densities of the samples. A line is a guide to the eye.

The 5250 cm^{-1} bands are somewhat broader than the previous reported data by Stuke [5] while the shoulder around 5000 cm^{-1} becomes more prominent with the decrease of the glass fictive temperature. The mechanism of this peak shape change is unclear; but, since the shape of the δ_{HOH} peak at 1650 cm^{-1} does not vary with thermal history, the peak shape change of the $\nu_{O-H} + \delta_{HOH}$ band at 5250 cm^{-1} might be interpreted as being due to local changes in the ν_{O-H} vibration of molecular water in the glass surface [60]. It is well known that the OH stretch peak position is red-shifted as the hydrogen bonding interaction increases and the O-H···O distance decreases [60]. Such changes in the hydrogen bonding interactions could be manifest as shifts in the combination band in near-IR. This result indicates that, even for the same composition of the glass and the same method to introduce water into glass surface, the speciation of water is affected by the original network structure into which water enters.

The peak intensities of the 5250 cm^{-1} ($\nu_{O-H} + \delta_{HOH}$) and 4500 cm^{-1} ($\nu_{O-H} + \nu_{Si-OH}$) bands are shown in Fig. 4-5 (b). The peak height was calculated after applying the TT baseline method. The peak heights of both bands increase with fictive temperature, similar to the ν_{O-H} and δ_{HOH} bands in the mid-IR region (Fig. 4-4 (b)). These results indicate that both molecular H_2O and SiOH with weak hydrogen bonding increased with fictive temperature of the samples. Although Behrens and Nowak stated that the ratio of $SiOH/H_2O$ is higher in glasses with higher fictive temperature in their study [61], it is difficult to obtain the *relative abundance change* for H_2O and SiOH species from the ATR-IR data obtained in this paper alone. This is because of the data scatter and uncertainty of the baseline correction in Fig. 4-4 and Fig. 4-5 and the hydrogen bonding interactions which may change with the water content. Overall, this data does indicate that the glass network structure changes associated with the fictive temperature (or density) does affect the

speciation of hydrous species, but to further understand the ATR spectra and the mechanism of change, experimental study must be combined with computer simulation.

4.4. Summary

After acid leaching a set of glasses with different fictive temperature, the analysis of hydrous species (Si-OH and molecular H_2O) in the resulting leached layer was conducted using ATR-IR, SR-IR and dynamic SIMS. In general, larger amounts and deeper penetration of hydrous species were observed for the higher fictive temperature glasses. This can be attributed to the lower density/more open structure of the glasses with higher fictive temperatures. ATR-IR analyses in the near IR region enabled differentiation of hydroxyl and molecular water species in the glass surfaces. This revealed that not only the total amounts, but also the relative amounts (ie, hydrous speciation), of SiOH (with weak hydrogen bonding) and molecular H_2O vary with the fictive temperature of the glass before leaching. More work is needed to fully explain these observations.

5 Effect of Water and Glass Composition on the Hardness of Surface Layers on Aluminosilicate Glasses Formed through Reaction with Strong Acid

5.1. Introduction

The aluminosilicate glass system is important for industrial glass products, nuclear waste glass and for understanding natural glasses in the Earth's crust. For some applications, high durability in strong chemical solution is required. Although the incorporation of aluminum oxide improves the durability of glasses to some extent, too much aluminum is known to degrade the acid durability of glasses [70–72]. This can be attributed to the high solubility of Al^{3+} in strong acid and the low activation energy for bond rupture in the AlO_4 structural unit [73]. However, the properties of the leached surface layer formed through strong acid treatment is not well investigated. In Hamilton's study [72], it was found that in strong acid, the most important parameter controlling the leaching and dissolution behavior of aluminosilicate glasses was the number of Al-O-Si linkages present in the bulk glass structure. In the glasses containing high amounts of aluminum (which also have a large number of Al-O-Si linkages), dissolution is dominant over leaching in acid conditions. Mellott reported that, although a silica-rich layer was formed on aluminosilicate glass surfaces after strong acid treatment, no evidence supporting the diffusion-controlled reaction was reported [74]; i.e., both Al and network modifier ions were all depleted to the same depth, and with continued exposure to acid, they became completely devoid of all components except silica and hydrous species.

Although the altered surface layer on aluminosilicate glasses formed after acid treatment was reported to contain 6-coordinated Al species from nuclear magnetic resonance (NMR) studies [71,72], the existing state of hydrogen and the speciation of hydrous constituents in the surface layer have not been analyzed so far.

Several methods have been reported for the analysis of water, hydroxyl and hydrogen in glass, all of which rely largely on vibrational spectroscopies such as IR and Raman analyses. Although the speciation of water in the bulk glass is commonly evaluated with transmission IR or NMR [4,18–20,56,57], the methods lack the surface sensitivity needed to reveal the speciation of water in the surface region of a flat glass. Attenuated total reflection infrared (ATR-IR) spectroscopy is a method that can provide a surface-sensitive analysis in the outermost micron of the surface [28]. We reported that Si-O-Si network alterations at surfaces, for example, due to acid leaching [63] and other surface treatments of glass [41] can be analyzed through ATR-IR analysis.

In this chapter, we investigated surface layers formed through strong acid treatment of three simple glasses chosen from the SiO_2-Al_2O_3-MgO-CaO-Na_2O glass system with a focus on composition (especially aluminum content) and properties of the surface layer. ATR-IR analyses, along with depth profiling using secondary ion mass spectroscopy (SIMS) and X-ray photoelectron spectroscopy (XPS), were used to evaluate the bulk glass composition effect on the leaching, structure and water-related species in the surface layers. Finally, we performed nano-indentation experiments to study the resulting mechanical properties of the surface layers with thickness up to several hundred nanometers.

5.2. Experiment

5.2.1 Sample preparation

Three glass compositions listed in Table 5-1 containing different amounts of aluminum were evaluated in this study. SLG is a typical soda lime silica glass widely used industrially and NAS glass has a composition corresponding to a feldspar (albite) mineral. NCAS glass is designed from simple SiO_2-Al_2O_3-CaO-Na_2O glass system to have similar amount of sodium to both SLG and NAS glasses. The bulk compositions of these glasses were evaluated by XRF (ZSX100e, Rigaku Corporation, Tokyo, Japan) and are shown in Table 5-1. The relative standard deviations of the analyses were about 1 % of each value.

Table 5-1 Evaluated glass composition and acid treatment time of each sample

	Glass composition (mol%)					Treatment time (h)
	SiO_2	Al_2O_3	MgO	CaO	Na_2O	
SLG	70.8	1.0	6.2	9.1	12.9	320
NCAS	74.4	4.1	0.0	8.5	12.9	500
NAS	75.0	12.9	0.0	0.0	12.1	100

The bulk glass samples were prepared by the conventional melt-quench method. The mixed batch materials (analytical reagent-grade) SiO_2, Al_2O_3, Na_2CO_3, MgO and $CaCO_3$ were melted in an electric furnace at 1650 °C in a Pt90Rh10 crucible for 3 h. The melt was quenched into water to produce small fragments, and then mixed and re-melted in a crucible at 1680 °C for 3 hours to further homogenize the glasses. Na_2SO_4 was added to the batch in order to remove the bubbles efficiently. The second melt was cast onto a carbon plate to obtain cylindrical glass plates with 7 cm width and 10 mm thickness. The prepared glasses were annealed 50 °C above their respective glass transition temperatures for 1 hour and then cooled down to room temperature at a rate of 1 °C/min. The glasses were lapped with SiC powder and polished with CeO_2 dispersed in water to 1.6 mm in thickness. All of the experiments described below were performed on this polished glass.

HCl-treated samples were prepared by acid treatment of the polished glasses in a 90 ^oC HCl solution (pH=1). Treatment times were varied in order to obtain the OH stretching vibration with similar intensities in ATR-IR spectra and are listed in Table 5-1.

To distinguish incorporated hydrous species during acid treatment from pre-existing hydrous species in the glass samples, D_2O-HCl treatments were performed. D_2O-HCl solution (pH=1) was prepared by diluting HCl reagent with D_2O of 99.8 % purity. The polished glasses were treated in the D_2O-HCl solution for the same treatment time as HCl-treated samples.

The surface area of each sample was 7.5 cm^2 and the volume of solution was 50 ml for both HCl and D_2O-HCl treatment.

5.2.2 Secondary Ion Mass Spectroscopy (SIMS)

SIMS analyses of the HCl-treated samples were carried out to obtain hydrogen profiles using a PHI ADEPT1010 system (ULVAC-PHI Inc., Chigasaki, Japan). The acceleration voltage of the Cs^+ primary beam was 5 kV and the beam current was 100 nA. The scanning area was 60 x 60 um^2 for negative secondary ion detection with an incidence angle of 60^o to the sample surface normal. The secondary ions, ^1H and ^{30}Si, were monitored during depth profiling. The samples were charge-compensated with an electron gun.

5.2.3 X-ray Photoelectron Spectroscopy (XPS)

XPS analyses of the treated glass surfaces were conducted to obtain the depth profiles of the elements. The SLG and NCAS samples in Table 1 were analyzed by a Kratos Analytical Axis Ultra instrument (Chestnut Ridge, NY) with Ar ion sputtering. After initial surface scans, samples were sputtered in 40 - 100-s cycles, with 4 keV Ar^+ ions rastered over a 1 mm x 1 mm area in order to access successive in-depth regions. After each sputter cycle, XPS spectra were acquired at 80 eV pass energy using a 200 mm diameter X-ray beam centered within the sputter crater. To minimize potential effects of surface charging, a low-energy electron flood gun was directed at the surfaces during spectral acquisition. Scans were performed over narrow binding energy ranges corresponding to the O 1s, Ca 2p, C 1s, Si 2p, Al 2p and Mg 2s photoelectron peaks as well as the Na KLL Auger series.

The average sputtering rate in this configuration was of the order 0.1 nm/s, as

determined by optical profilometer measurements of sputter craters in leached samples after XPS analyses. The sputter rate was assumed to be constant and was used to determine an approximate depth scale for the XPS profiles.

The leached NAS glass in Table 1 was analyzed by an ESCA-5500 (Physical Electronics) with a C_{60} ion gun (IonOptika 06-C_{60} type). We could not analyze the distribution of sodium ions in this NAS glass by means of XPS depth profiling through Ar ion sputter because of the extremely high (beam-induced) mobility of sodium in NAS glass. Previously, we studied the glass composition effect on the Na ion mobility in aluminosilicate glass and showed that sodium aluminosilicate glass containing equal amounts of aluminum and sodium ion have significantly higher Na ion mobility [75]. Compared with Ar ion sputtering, C_{60} ion sputtering is known to be able to suppress the migration of mobile ion in glass due to sputtering [23]. The detection angle was 75^{o} using the monochromatic Al Kα line (1486.6 eV). The irradiation condition was optimized as 10 kV, 10 nA and incident angle: 67^{o} for C_{60} ion beam. The depth profiling was performed by sequential XPS measurements with 1 min sputter intervals. Neutralization of the surface charge was performed using low energy electrons. Quantification was performed using the software of MultiPak (Ulvac-phi) on selected peak areas. The error was estimated for the concentration determination to be less than 15 %.

5.2.4 Fourier Transform Infrared Spectroscopy (FTIR)

A Bruker Vertex70 system (Bruker Optics Inc., Billerica, MA) equipped with a MCT detector was used for transmission-IR and ATR-IR analyses. For FTIR transmission analysis, 100 scans were collected for each sample with a spectral resolution of 6 cm^{-1}.

Spectra were collected from 6000 to 2000 cm^{-1} and spectra were processed and evaluated as absorbance vs. wavenumber.

For the ATR-IR measurements, an attachment using a diamond crystal with an incident angle of 45° (MVP-Pro, Harrick Scientific Products Inc., Pleasantville, NY) was used. Spectra were collected from 6000 to 1500 cm^{-1} and were processed and plotted as the log of the inverse reflectance, log (1/R), which is dimensionally equivalent to the absorbance. 3200 scans were collected for each sample with a spectral resolution of 6 cm^{-1}. Before the ATR-IR measurements, the samples were cleaned with distilled water and ethanol in an ultrasonic cleaner, followed by UV ozone cleaning. The samples were pressed against the ATR diamond crystal with a force of 420 N over a 1.5 mm^2 sampling area during analyses. All measurements were conducted at room temperature.

The evanescent wave in ATR analysis decays exponentially with the distance from the surface within the sample. Its penetration depth is usually expressed as the distance at which the electric field intensity in the sample falls to 37 % (e^{-1}) of the surface value. This is calculated as shown below for the case of a media with a low extinction coefficient, *k*:

$$d_p = \lambda \Big/ \left\{ 2\pi n_1 \left[\sin^2\theta - (n_2/n_1)^2 \right]^{1/2} \right\} \quad \cdots (1)$$

where λ = wavelength of the IR beam, θ = incident angle of the IR beam, n_1 = the refractive index of the ATR crystal, and n_2 = the refractive index of the sample [28]. To calculate the penetration depth, we used the refractive indices of soda lime glass [29] and diamond [43] (reported elsewhere) as those of the sample and an ATR crystal, respectively. It increases monotonically with a decrease of wavenumber from about 350 nm at 6000 cm^{-1} to about 900 nm at 1500 cm^{-1}.

5.2.5 Nano-indentation

Nano-indentation analysis was used to evaluate the mechanical properties of the surface layer, which was formed after leaching in acid solutions, of the samples shown in Table 1. A nano-indenter (Hysitron TI 950, Minneapolis, MN) with a Berkovich tip was used during the analysis. The indentation depth was controlled in the range from 50 nm to 200 nm. 40 indents were averaged for each sample and each indentation condition.

5.3. Results and Discussion

5.3.1. Depth profiling of hydrogen and glass matrix elements with SIMS and XPS

The depth profiles of hydrogen (closed symbols) and elements in glass matrix (open symbols) obtained for each treated glass samples with different glass compositions were shown in Fig. 5-1 (a), (b) and (c). The hydrogen profiles obtained through SIMS analyses were normalized by the maximum concentration observed in the outermost surface. The near-surface data (to 10 nm) were deleted in the plot because SIMS analysis in this region is considered as unreliable [66]. In all samples, the hydrogen concentrations in the surface regions are much higher than in the bulk regions, which indicates that the acid treatment introduced a significant amount of hydrogen. The thickness of the hydrogen-rich layers of SLG, NCAS and NAS glass surfaces can be defined as the depth where the hydrogen concentration decreases to 5% of its maximum value, which is 160 nm, 210 nm and 130 nm, respectively. The distribution of hydrogen in the surface layer is caused by hydrogen

diffusion and network dissolution [72]. In the case of SLG, dissolution is expected to be negligible, whereas NAS is subject to dissolution at pH 1 due to large aluminum content.

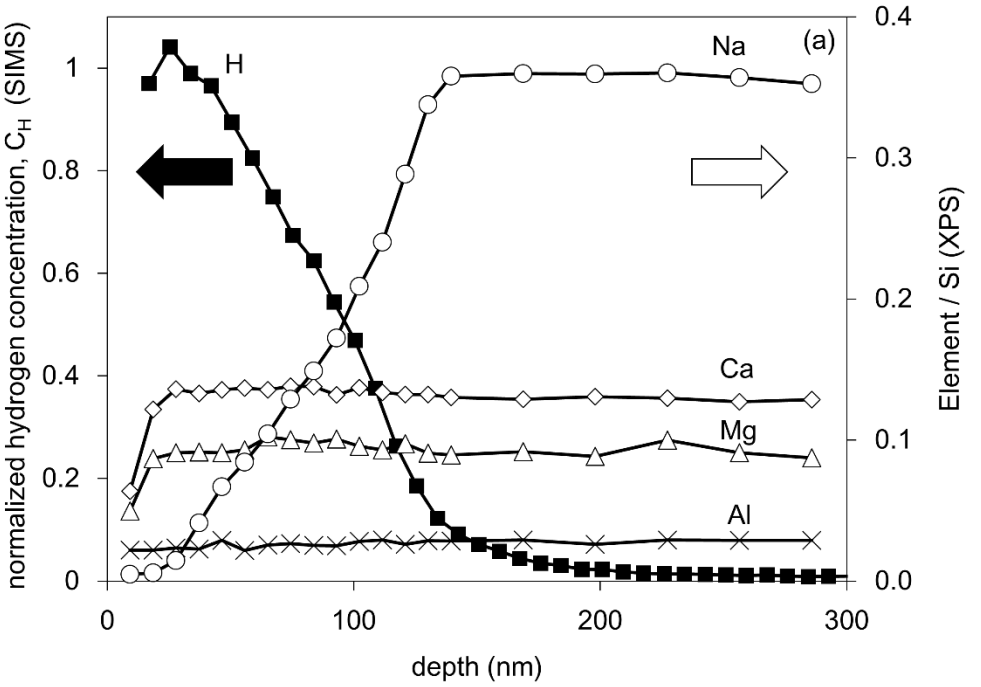
(a)
H
Na
Ca
Mg
Al
normalized hydrogen concentration, C_H (SIMS)
Element / Si (XPS)
depth (nm)
0
0.2
0.4
0.6
0.8
1
0.0
0.1
0.2
0.3
0.4
0
100
200
300

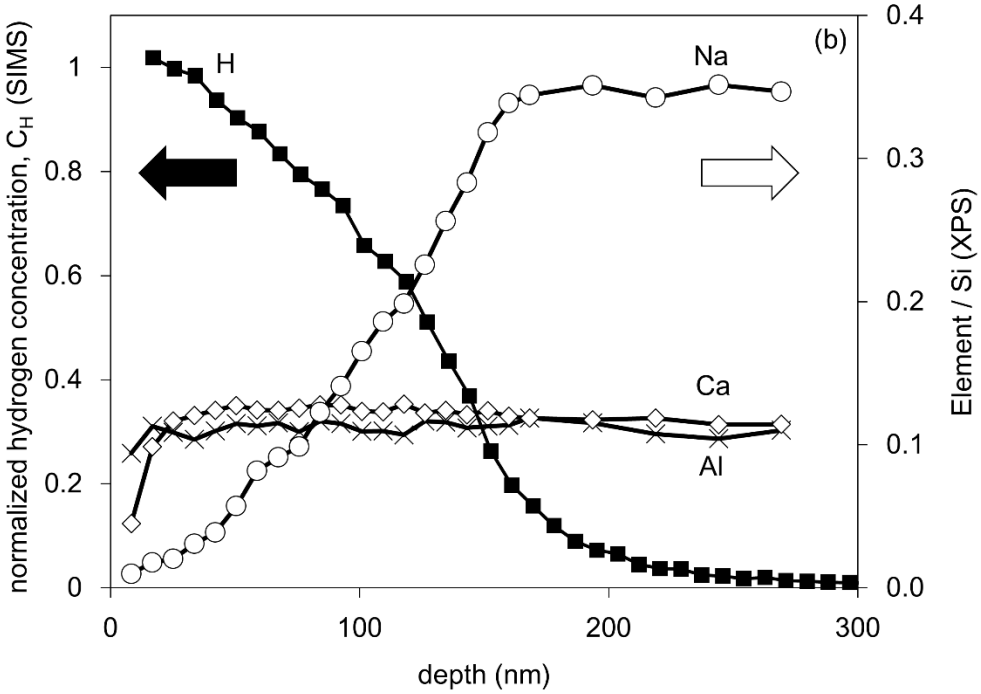
(b)
H
Na
Ca
Al
normalized hydrogen concentration, C_H (SIMS)
Element / Si (XPS)
depth (nm)
0
0.2
0.4
0.6
0.8
1
0.0
0.1
0.2
0.3
0.4
0
100
200
300

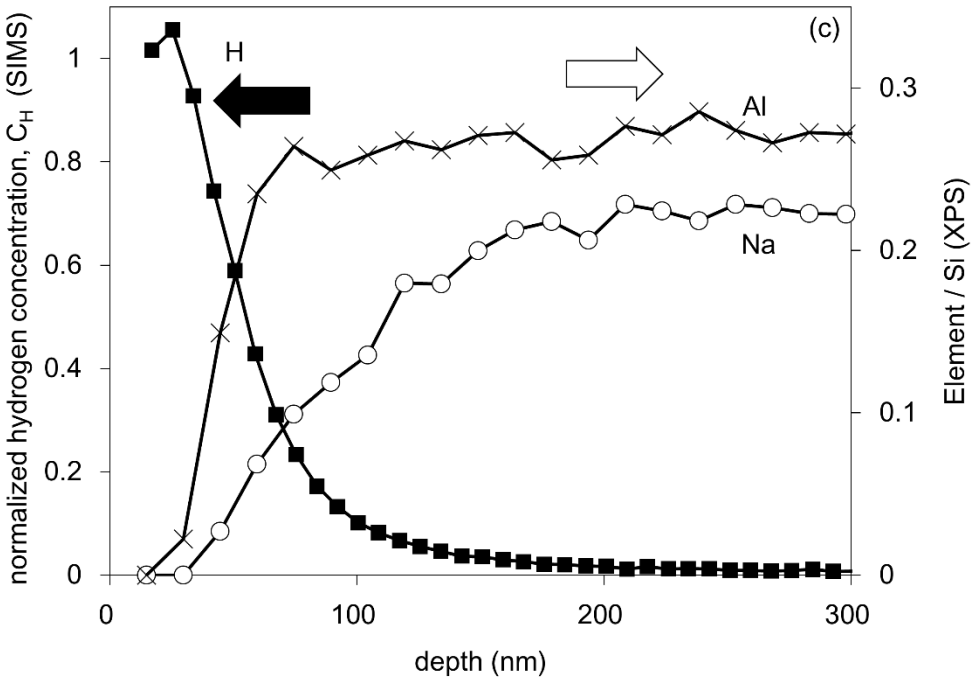

Fig. 5-1 Normalized depth profiles of hydrogen (closed symbol)(from SIMS) and glass matrix ions (open symbols)(from XPS) for (a) SLG, (b) NCAS, and (c) NAS glass after leaching in pH 1 solution.

Fig. 5-1 (a) also shows depth profiles for leached SLG samples obtained with Ar ion sputtering. The sodium depth profile shows a completely depleted regions near the outermost surface followed by a gradual increase to a plateau value at ~130 nm below the surface. In the case of multicomponent glasses with mobile ions such as sodium ions, it is known that the concentration of mobile elements analyzed by XPS gradually changes in depth with Ar ion sputtering even for homogeneous glass due to migration of mobile ions [23]. With further sputtering, the concentration tends to achieve a stable value where knock-on effects by Ar sputtering achieve a steady-state equilibrium. In this study, we normalized the concentration of each element to make the steady-state equilibrium value equal to the analyzed bulk composition of the glasses in Table 5-1.

Fig. 5-1 (a) shows that the thickness of the depleted layer for sodium in SLG is similar to the thickness of the hydrogen-rich layer in the SIMS profile, which confirms that the leached layer was formed mainly through inter-diffusion between sodium in the glass and hydrogen in HCl solution [3]. The depleted layers for the divalent cations (calcium and magnesium) are less than 40 nm, which is much shallower than that of sodium. This result is due to the lower reactivity and diffusion coefficient of the divalent cations compared to sodium ions. Aluminum was not leached out from the surface of SLG, which means that the network connectivity between Si and Al elements is mostly conserved during the leaching.

Fig. 5-1 (b) displays the depth profiles of the leached NCAS glass sample, which shows a trend similar to the leached SLG glass sample. Namely, the thickness of the Na depleted layer is comparable with the thickness of its hydrogen rich layer. Moreover, the depleted layer of calcium is much shallower than that of sodium. It is also evident that there is no detectable leaching of aluminum from the NCAS glass. These features indicate

that the leached layer on the NCAS glass was formed mainly through inter-diffusion between sodium and hydrogen during acid treatment and the network connectivity between Si and Al elements was not altered from its original one. SLG and NCAS behave similarly in these aspects.

Fig. 5-1 (c) displays the XPS depth profiles for the NAS glass obtained using the C_{60} sputtering. The composition profiles for the treated NAS glass surface are quite different from those of SLG and NCAS glass. In the case of NAS, not only the sodium ions (network modifier), but also a large amount of aluminum ions (network former) were leached out. It means that the outermost region of the leached NAS glass consists of silica network and hydrous species.

The results of depth profile analyses through SIMS and XPS were summarized in Table 5-2. It was found that in all glass samples sodium were leached out from the surface while the other modifier ions in SLG and NCAS samples were not changed significantly. At the same time hydrogen were diffused to similar thickness of the sodium-depleted layer. Aluminum ion as network former were not changed in the surface of SLG and NCAS samples, while it was substantially depleted in the surface of NAS sample which has highest ratio of Al/Si aluminum ion.

Table 5-2 Summary of chemical changes in the leached surface layer

	Al/Si in the bulk	Compositions in the leached surface layer				ν_{OH} area in ATR-MIR (cm^{-1})	Relative concentration of hydrous species in the modified layer (ν_{OH} area/*d*) (10^7 cm^{-2})
		Surface layer (*d*) thickness (nm)	Na^+ modifier	Other modifier ions	Al network former		
SLG	0.03	~160	leached	No change	No change	23.3	0.15
NCAS	0.11	~210	leached	No change	No change	22.2	0.11
NAS	0.3	~130	leached	Not present	Leached (<70nm)	26.7	0.21

5.3.2. Hydrous species probed with FTIR

To analyze the effects of glass composition on hydrous species, we performed transmission-IR analysis for evaluation of the bulk regions and ATR-IR analysis for evaluation of the surface layers. Fig. 5-2 (a) and (b) illustrate the transmission-IR spectra in the near- and mid- IR region, respectively. In Fig. 5-2 (a), the absorption bands at 4000 and 4500 cm^{-1} are observed [17,76]. The 4500 cm^{-1} band is assigned to the combination of OH stretching and bending modes of SiOH with weak hydrogen bonding [18]. If the samples contain molecular water, the combination band of stretching and bending modes of molecular water groups is expected at 5250 cm^{-1} [17]. The broad background spanning from 4700 cm^{-1} to 5700 cm^{-1} in the near-IR spectrum of SLG glass is due to the iron impurity in the glass [48]. Thus, the absence of the 5250 cm^{-1} peak in Fig. 5-2 (a) for all three glasses indicates that almost all hydrogen in the bulk is associated with OH groups, and not molecular water.

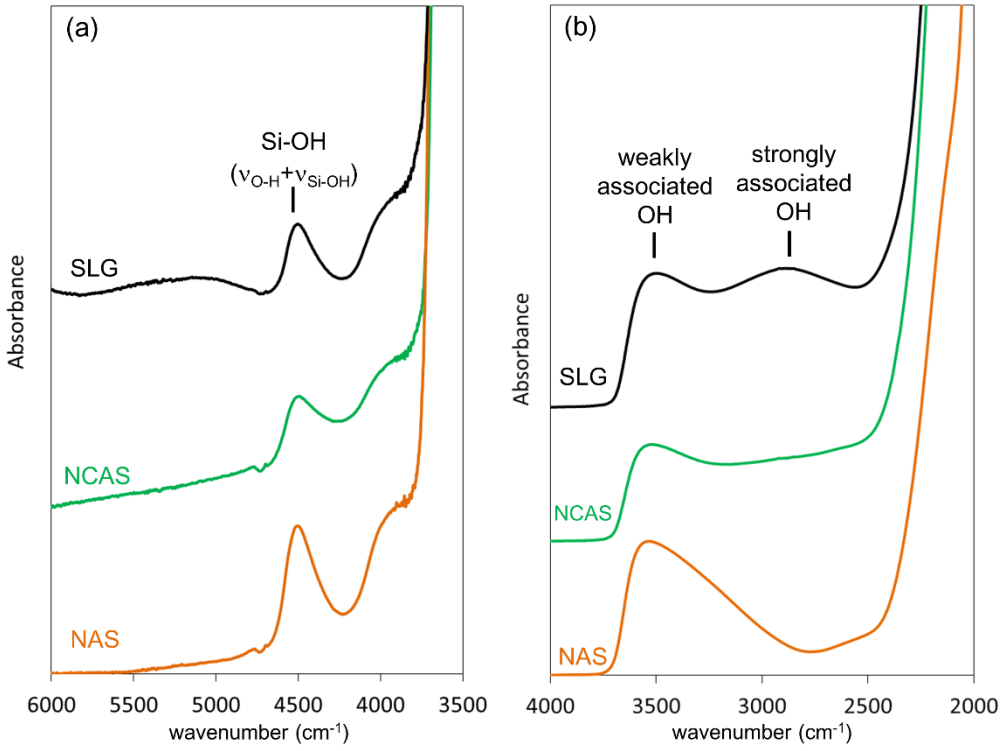

Fig. 5-2 Transmission-IR spectra of the polished SLG, NCAS and NAS glasses in (a) NIR and (b) MIR region

The two broad peaks in Fig. 5-2 (b) observed at 3500 cm^{-1} and 2800 cm^{-1} are assigned to stretching vibrations of the Si-OH (ν_{OH}), which are hydrous species weakly and strongly bound to non-bridging oxygen sites in alkali silicates, respectively [16,20]. Fig. 5-2 (b) indicates that the strongly associated OH peak around 2800 cm^{-1} is less prominent in NCAS and NAS glasses with higher aluminum content.

Fig. 5-3 (a), (b) and (c) display the ATR mid-IR spectra of the acid-treated SLG, NCAS and NAS glass surfaces, respectively. Here, black lines indicate the ATR-IR spectra obtained from the as-polished control sample. Blue and red (dotted) lines are obtained from the HCl and the D_2O-HCl treated samples, respectively. In the lower wavenumber region, the peaks at 1650 cm^{-1} observed in all glass compositions are the H-O-H fundamental bending vibration (δ_{H2O}) indicating the presence of molecular water [4,18] in the surface region, which is absent in the bulk region. In the D_2O-HCl treated samples, additional sharp peak around 1450 cm^{-1} was observed, which is assigned to HDO bending vibrations (δ_{HDO}) [77] and supports the assignment of 1650 cm^{-1} peaks in HCl treated samples to molecular water.

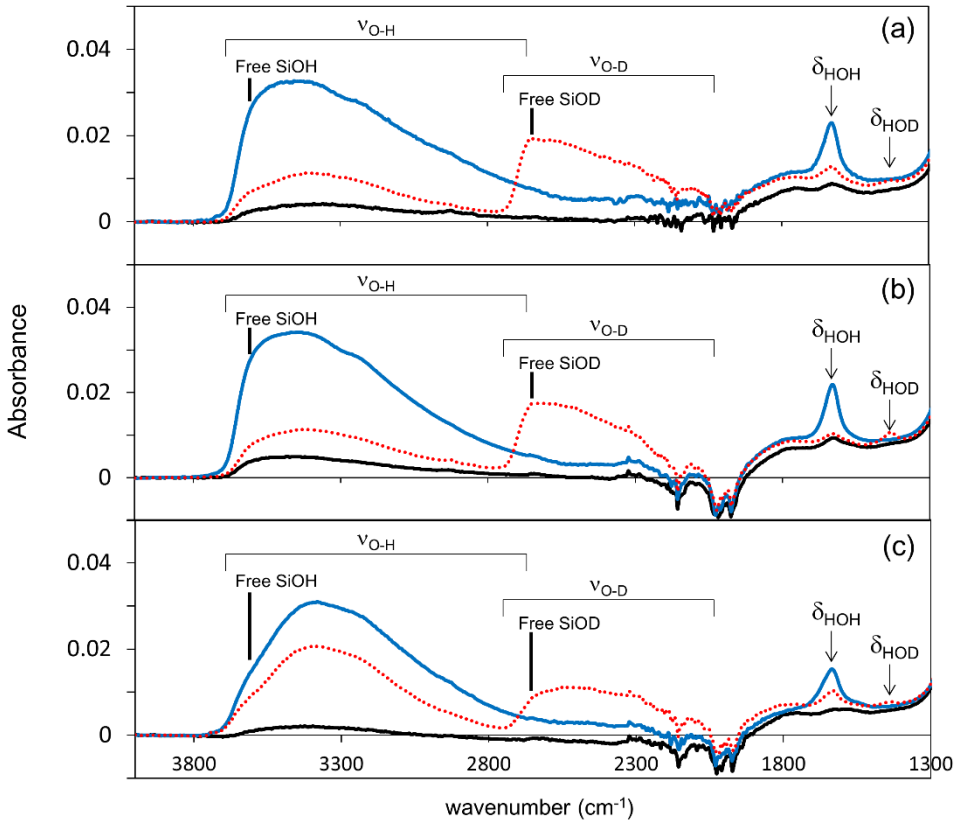

Fig. 5-3 ATR-MIR spectra of the polished (black line), the HCl treated (blue line) and the D_2O-HCl treated (red line) samples of (a) SLG, (b) NCAS and (c) NAS glass. The spectra in the region between 2300 and 1900 cm^{-1} are noisy because the IR transmission in this region is very weak due to the absorption by the diamond ATR crystal itself.

To confirm the presence of molecular H_2O in the surface layer, ATR-IR spectra of the HCl-treated samples in near-IR region (6000-3500 cm^{-1}) were investigated because the combination bands of SiOH and molecular water were expected to be observed more distinctly in this wavenumber region. Fig. 5-4 displays ATR spectra in the near-IR region. The peak around 5250 cm^{-1} is attributed to the combination of stretching and bending modes of molecular water groups [17], and the peak around 4500 cm^{-1} originates from the combination of OH stretching and bending modes of SiOH with weak hydrogen bonding [18]. The TT baseline method by Withers [69] band was applied for background correction. Note that the 5250 cm^{-1} band is negligible in transmission-NIR (Fig. 5-2 (a)), but dominant in ATR-NIR (Fig. 5-4). While the transmission signal is the integral of bulk species over the entire thickness (1.6 mm), ATR confirms the high concentration of molecular water species within a very thin surface layer (~200 nm). Fig. 5-4 also indicates that the 4500 cm^{-1} band in NAS is much smaller than those in the other two glasses.

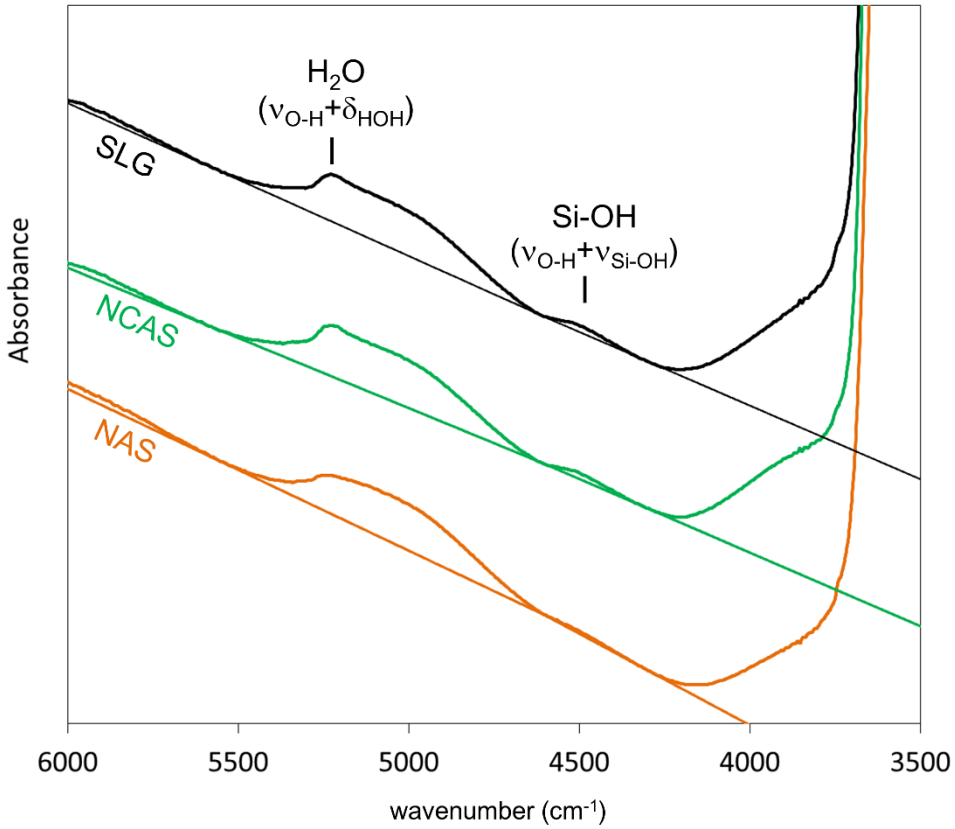

Fig. 5-4 ATR-NIR spectra showing H_2O and SiOH combination bands of the leached samples of (a) SLG, (b) NCAS and (c) NAS glass.

In the ATR-mid IR spectra (Fig. 5-3), the broad band within the 3700 - 2500 cm^{-1} region can be attributed to the OH stretching vibration (ν_{OH}) of OH and H_2O species with varying degrees of hydrogen bonding interactions [4,41]. In the D_2O-HCl treated samples, the broad band within the 2700 - 2200 cm^{-1} region is assigned to OD stretching vibrations (ν_{OD}) in OD, D_2O and HDO species with varying degrees of hydrogen bonding interactions [77]. Here, a clearly discernable difference is noted in the peak shape of the ν_{OH} and ν_{OD} bands of the altered surface layers. The higher wavenumber components of the peak around 3650 cm^{-1} (OH) and 2650 cm^{-1} (OD) are weak in NAS samples compared with the other two glasses. Based on hydrous species reported for bulk silicate glass, this peak around 3650 cm^{-1} can be assigned to the vibration of free or weakly hydrogen-bonded SiOH [4,18]. This indicates that the relative abundance of free or weakly-associated SiOH and H_2O species in the leached layers is decreased with the increase of aluminum content in the bulk glass composition, which is consistent with the ATR near-IR spectra in Fig. 5-4 showing that the band around 4500 cm^{-1} is less significant in surfaces of NAS glass. Moreover, the shape of ATR-IR spectra of leached NAS glass seems similar to absorption spectrum of silica gel reported before [78]. The XPS data that outermost region of the leached NAS glass consists of silica network and hydrous species also can imply that the altered layer has analogous properties and structure to silica gel. For further investigation, other analysis with a method which can probe network structure in glass surface, such as UV Raman spectroscopy, is needed.

The amount of total hydrous species is proportional to the peak area of the ν_{OH} band within the 3700 - 2500 cm^{-1}. Then, the relative concentration of hydrous species in the modified layer could be compared by dividing the ν_{OH} peak area with the thickness of the modified layer (obtained from the SIMS hydrogen profiles). These values are shown in

Table 5-2; the data indicate that the concentration of hydrous species is the largest in the surface layer on NAS samples, which is believed to be associated with the leaching of aluminum ion observed only in NAS samples.

5.3.3. Mechanical properties of the altered surface layer

So far, we have evaluated the leached layer on glasses with different aluminum contents and shown that only the glass with high aluminum content, NAS sample, show aluminum leaching; as shown in Table 5-2, relative concentration of hydrous species in the surface layers is the largest in the NAS glass. To evaluate the mechanical properties of these leached layers, we conducted nanoindentation measurements with varying indentation depths.

Fig. 5-5 (a), (b) and (c) show the reduced moduli calculated from the Oliver-Pharr analysis of the force-displacement curves for the SLG, NCAS and NAS glass surfaces, respectively, before and after leaching in acid solutions. Since the Poisson's ratio was not known for the surface layer altered after leaching, only the reduced modulus (rather than elastic modulus) is reported for the polished and leached surfaces. Fig. 5-5 (d), (e) and (f) display the hardness for the SLG, NCAS and NAS glass surfaces, respectively, before and after leaching. As can be seen from the Fig. 5-5, the hardness and reduced modulus of the leached surfaces are smaller than the polished surfaces.

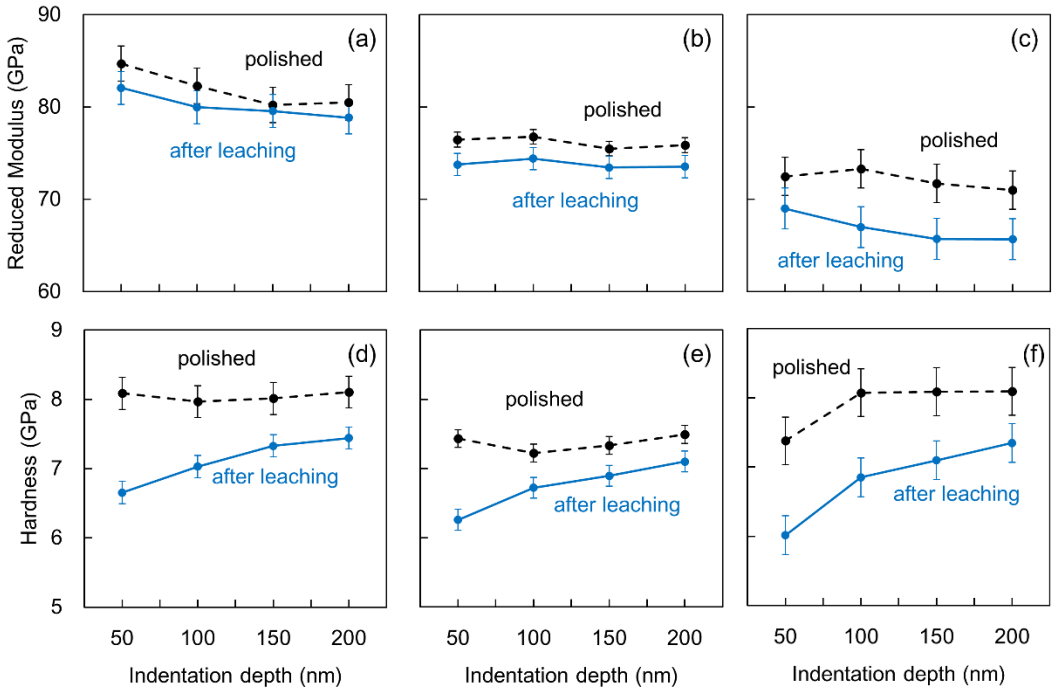

Fig. 5-5 Reduced moduli of (a) SLG, (b) NCAS and (c) NAS glass and hardness of (d) SLG, (e) NCAS and (f) NAS glass evaluated with nano-indentation. Data from polished (black dotted line) and leached (blue solid line) sample are shown.

Since the leached layer thickness determined from the SIMS profile (Table 5-1) is larger than 10 % of the indentation depth, the mechanical properties determined from these nano-indentation tests are a composite of the leached layer and the substrate [79]. If the leached glass surface can be considered as a soft layer on top of the hard substrate, the mechanical properties of the leached layer can be evaluated based on analytical models for soft coatings with known mechanical properties on a hard substrate. Here, a model developed by Tuck et al. was applied to evaluate the hardness of the leached layer [80]. The hardness of the soft layer can be deconvoluted from the composite hardness obtained from indentation as a function of relative indentation depth (*R*), which represents the ratio of indentation depth over the thickness of the leached layer. The model is described as follows:

$$H_C = H_S + \frac{H_l - H_S}{1 + [R/\beta_0]^X}$$

where H_c, H_s *and* H_l denote the hardness of composite, substrate and leached layer, respectively; β_0 and X are the fitting parameters for the model.

In Fig. 5-6, the hardness of the leached layer estimated from the model fit is compared with that of the bulk. In all samples, reduced moduli and hardness are decreased after acid treatment as shown in Fig 5-5. Inaba suggested [28] expression prediction Vicker's hardness, H_v, and Young's modulus, E, as

$$H_v = 0.13 m V_p G_t$$

$$E = 2 m V_p G_t$$

where m is Madelung constant, V_p is ionic packing factor and G_t is dissociation energy of the oxide constituents per unit volume. These expression indicate glasses with higher m, V_p and G_t should have higher hardness and moduli. However m and G_t in the altered layer in glass surfaces are difficult to be expected since the structure of the

layers is altered after acid leaching. Therefore here we discuss the change of hardness and moduli after leaching considering the change of ionic packing factor, V_p, of glasses.

Ratio of ionic packing factor before and after acid treatment, V_{p2}/V_{p1}, is expressed as

$$V_{p2}/V_{p1} = \sum r_j^3 n_j / \sum r_i^3 n_i$$

where V_{p1} and V_{p2} are ionic packing factors before and after acid treatment and r_i, r_j are ionic radius of each element and n_i, n_j are molar fraction in glass surfaces before and after acid treatment respectively. According to depth profiling through XPS and SIMS shown in Fig. 5-1 ion exchange between Na^+ and H^+ expressed as

$$Si-O^-Na^+ + H_3O^+ \rightarrow Si-OH + Na^+ + H_2O$$

should occur in all samples. Moreover aluminum ions are depleted from NAS glass surface. Assuming that volumes of surface layer before and after acid treatment and all Na^+ ions have been substituted by H^+ ions in the layer of SLG, NCAS and NAS and all aluminum ions have been depleted from the layer in NAS, V_{p2}/V_{p1} are calculated and displayed in table 5-3. The ionic radii are taken from Shannon et al [82].

Table 5-3 Calculated ratio of ionic packing factors in surface layers before and after acid treatment

SLG	NCAS	NAS
0.94	0.94	0.77

This result indicates that the ionic packing factors in surface layers of all samples decreased after leaching and the degree of the decrease is most significant in that of NAS samples, which are consistent with trend of the moduli and the hardness obtained through

nano-indenter experiments. Therefore the decrease of ionic packing factors in surface layers through leaching can be one of the origin of the decrease of the moduli and the hardness.

The difference between the leached layer and the bulk is the largest for the NAS glass. In the leached NAS glass surface, not only sodium ion but also aluminum has been depleted (Fig. 5-1 (c)), which resulting in a “silica-rich” surface layer with the largest concentration of hydrous species as shown in Table 5-2. The hydrolysis of Al-O-Si sites and removal of Al ions could lead to either Si-OH or Si-O-Si. Unless the entire network collapses to a higher density state, the remaining layer would have a larger porosity to accommodate more hydrous species, which could cause the large decrease of hardness in the NAS glass. Based on the elemental composition depth profiles shown in Fig. 5-1 (a) and (b), the network connectivity between Si and Al elements is believed to be conserved for the SLG and NCAS; thus, the result shown in Fig. 5-6 may imply that the effect of simple ion exchange (replacing the modifier ions with hydrogen) does not affect the mechanical property as severely as the case where one of the network former elements is depleted.

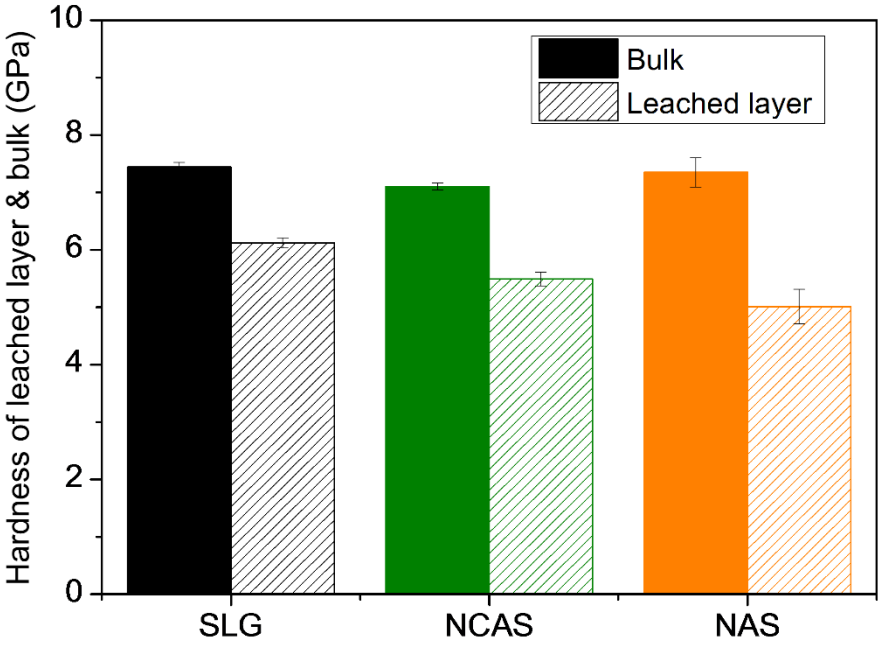

Fig. 5-6 Hardness difference between before and after HCl leaching analyzed by nano-indentation experiments

5.4. Summary

In this chapter, we have evaluated the surface layer formed by strong acid treatment of SLS, NACS, and NAS glasses with different aluminum contents through SIMS, XPS, transmission-IR, ATR-IR and nanoindentation analyses. It was found that the glass with the highest aluminum content (NAS) showed aluminum depletion and incorporation of molecular water in the surface layer, and correspondingly, the larger decrease in hardness of the leached surface layer.

6 Summary and Future Works

Glass surface usually contains much more concentration of hydrous species, including interstitial molecular water and hydroxyl (SiOH) groups, due to interactions with environments in production process or usage than its bulk region. However, existing state of the species in the surface had not been understood because there was no adequate way to analyze the species in outermost several nanometers of glass. In this research, we first evaluated capability of attenuated total reflection (ATR) - IR spectroscopy as a surface-sensitive analytical method to investigate hydrous species in glass surface and showed it can reveal qualitative and quantitative information of the species. Then, we utilized the method to reveal the different existing state of water in glass surfaces depending on surface treatment technique, fictive temperature of glass and glass compositions.

We first described the features of specular reflection (SR) and ATR - IR spectroscopy and displayed that both of them are useful methods for glass surface analyses. Especially ATR - IR was demonstrated to be useful method to probe hydrous species in glass surface with a depth of several tens or hundreds of nanometers, which showed both molecular water and hydroxyl group existed in polished and acid treated glass surfaces because of their high concentration of water. Then SIMS analysis of the hydrogen concentration - depth profiles for the acid-leached soda lime silica glass samples was used to provide independent information to validate and quantify the ATR signal. Thus we proved ATR – IR is the appropriate method to analyze the hydrous species in glass surfaces qualitatively and quantitatively.

Then we evaluated the ATR-IR spectra of various surface treated float glass samples

(as-produced, polished, leached by acid, treated by SO_2 gas, and strengthened by thermal or chemical methods) in conjunction with depth profiles analyses of the glass composition by SIMS and XPS and discovered the shapes of spectra obtained from these samples were depending on the treatment method, which means the relative speciation of hydrous species varied with different surface treatment. Especially, SO_2 gas-treated glass surface was found to have higher ratio of weakly associated SiOH which possess weak hydrogen bonding to molecular water or strongly associated SiOH, compared with acid-leached glass surface. This is the first study which unveil the effect of surface treatment method on the speciation of hydrous species in glass surface.

To understand the mechanism we investigated the effect of fictive temperature on leaching in strong acid using series of soda-lime silica glass samples with different fictive temperatures. Hydrogen depth profiles by SIMS showed that the higher fictive temperature the glass had the more water can diffused into the surface. ATR-IR analyses in near IR region provide differentiation of hydroxyl and molecular water species by using well-separated absorption peak due to those species in the region. The fictive temperature of the glass before leaching affect the relative amounts of SiOH (with weak hydrogen bonding) and molecular H_2O but the effect on the water speciation was not significant to explain the difference between SO_2 gas-treated and acid-leached surface.

Effect of the aluminum content in glass composition on formation of altered layer through reaction with strong acid were investigated through combined glass surface analyses by SIMS, XPS, ATR-IR and nano-indenter experiments. It was showed that in the glass with high aluminum content not only mobile alkali ion, such as sodium ion, but also aluminum are leached out from surface. Nano indenter experiments indicated larger decrease of hardness after acid treatment in the glass containing high amount of aluminum

compared with other glasses with less aluminum including soda lime glass. ATR-IR revealed that relative amount of weakly associated SiOH among hydrous species decreased with aluminum content. This study demonstrated that glass composition affect the formation of altered layer through the glass's reaction with solution.

We showed the availability to analyze the hydrous species in surface of glass monolith qualitatively and quantitatively through multiple analytical method including ATR-IR for the first time. This work deepened our knowledge of the species which should affect the properties of glass materials governed by its surface properties. This knowledge is also expected to be applied to a development of new glass product with new functionality which cannot be realized only by optimization of properties of glass bulk and help understand and resolve the phenomena provoked by hydrous species in glass surface.

For instance, different hydrous species should have different impacts on mechanical responses in glass surfaces, such as stress corrosion or stress relaxation. Through deep understanding of the relationship between the quantities of each hydrous species and these properties, we can provide a guideline to obtain glasses with optimized mechanical properties. Also, in the scheme of the chemical strengthening of glass, hydrous species in surface affect diffusion of alkali elements, such as Li, Na and K, as well as relaxation of compressive stress caused by the ion exchange. To control the product characterization it is necessary to know how each hydrous specie affect these properties.

We have showed ATR helps understanding of the hydrous species in glass surface and their effect on the properties, but still have problem with its sensitivity. For example, although the species on outermost surface have significant effect to interaction between

glass and other materials, such as adhesion or reaction, it cannot be distinguished from same specie existing at inner region of surface through ATR-IR spectroscopy itself. This is because the signals from each region of the samples within information depth of the measurement are integrated and appear in ATR spectra. This issue should be solved by combined analyses with other surface-sensitive methods, such as sum frequency generation (SFG) IR spectroscopy.

7 Reference

[1] J.E. Shelby, Water in glasses and melts, in: Introd. to Glas. Sci. Technol., 2nd Editio, The Royal Society of Chemistry, Cambridge, UK, 2005: pp. 222–236.

[2] Y. Yamamoto, K. Yamamoto, Precise XPS depth profile of soda–lime–silica float glass using C_{60} ion beam, Opt. Mater. (Amst). 33 (2011) 1927–1930. doi:10.1016/j.optmat.2011.03.026.

[3] W.A. Lanford, K. Davis, P. Lamarche, T. Laursen, R. Groleau, R.H. Doremus, Hydration of Soda-lime Glass, J. Non-Cryst. Solids. 33 (1979) 249–266.

[4] K.M. Davis, M. Tomozawa, An infrared spectroscopic study of water-related species in silica glasses, J. Non-Cryst. Solids. 201 (1996) 177–198. doi:10.1016/0022-3093(95)00631-1.

[5] A. Stuke, H. Behrens, B. Schmidt, R. Dupree, H_2O speciation in float glass and soda lime silica glass, Chem. Geol. 229 (2006) 64–77. doi:10.1016/j.chemgeo.2006.01.012.

[6] J. Deubener, R. Müller, H. Behrens, G. Heide, Water and the glass transition temperature of silicate melts, J. Non-Cryst. Solids. 330 (2003) 268–273. doi:10.1016/S0022-3093(03)00472-1.

[7] M. Tomozawa, D. Kim, A. Agarwal, K.M. Davis, Water diffusion and surface structural relaxation of silica glasses, J. Non-Cryst. Solids. 288 (2001) 73–80.

[8] T.A. Michalske, S.W. Freiman, A molecular interpretation of stress corrosion in silica, Nature. 295 (1982) 511–512. doi:doi:10.1038/295511a0.

[9] G. Soraru, R.D. Maschio, G. Della Mea, Correlation between surface modification and resistance to the formation of radial craks in soda lime glass, Glas. Technol. 7

(1986) 69–71.

[10] L.C. Bradley, Z.R. Dilworth, A.L. Barnette, E. Hsiao, A.J. Barthel, C.G. Pantano, S.H. Kim, Hydronium ions in soda-lime silicate glass surfaces, J. Am. Ceram. Soc. 96 (2013) 458–463. doi:10.1111/jace.12136.

[11] N.D. Surdyka, C.G. Pantano, S.H. Kim, Environmental effects on initiation and propagation of surface defects on silicate glasses : scratch and fracture toughness study, Appl. Phys. A. (2014) 519–528. doi:10.1007/s00339-014-8552-7.

[12] H. He, L. Qian, C.G. Pantano, S.H. Kim, Mechanochemical wear of soda lime silica glass in humid environments, J. Am. Ceram. Soc. 97 (2014) 2061–2068. doi:10.1111/jace.13014.

[13] J.H. Seaman, P.J. Lezzi, T. a. Blanchet, M. Tomozawa, Degradation of ion-exchange strengthened glasses due to surface stress relaxation, J. Non-Cryst. Solids. 403 (2014) 113–123. doi:10.1016/j.jnoncrysol.2014.07.016.

[14] S.M. Wiederhorn, T. Fett, G. Rizzi, S. Fünfschilling, M.J. Hoffmann, J.P. Guin, Effect of water penetration on the strength and toughness of silica glass, J. Am. Ceram. Soc. 94 (2011) 196–203. doi:10.1111/j.1551-2916.2011.04530.x.

[15] S.M. Wiederhorn, F. Yi, D. LaVan, L.J. Richter, T. Fett, M.J. Hoffmann, Volume Expansion Caused by Water Penetration into Silica Glass, J. Am. Ceram. Soc. 98 (2015) 78–87. doi:10.1111/jace.13264.

[16] H. Scholze, Der Einbau des Wassers in Gläser, Glas. Ber. 32 (1959) 81–88.

[17] E. Stolper, Water in silicate glasses: An infrared spectroscopic study, Contrib. to Mineral. Petrol. 81 (1982) 1–17. doi:10.1007/BF00371154.

[18] D.P. Zarubin, Infrared spectra of hydrogen bonded hydroxyl groups in silicate glasses; A re-interpretation, Phys. Chem. Glas. 40 (1999) 184–192.

[19] A.M. Efimov, V.G. Pogareva, Water-related IR absorption spectra for some phosphate and silicate glasses, J. Non-Cryst. Solids. 275 (2000) 189–198. doi:10.1016/S0022-3093(00)00250-7.

[20] T. Suzuki, J. Konishi, K. Yamamoto, S. Ogura, K. Fukutani, Practical IR extinction coefficients of water in soda lime aluminosilicate glasses determined by nuclear reaction analysis, J. Non-Cryst. Solids. 382 (2013) 66–69.

[21] C. Le Losq, R. Moretti, D.R. Neuville, Speciation and amphoteric behaviour of water in aluminosilicate melts and glasses: high-temperature Raman spectroscopy and reaction equilibria, Eur. J. Mineral. 25 (2013) 777–790. doi:10.1127/0935-1221/2013/0025-2322.

[22] S. Yamashita, H. Behrens, B.C. Schmidt, R. Dupree, Water speciation in sodium silicate glasses based on NIR and NMR spectroscopy, Chem. Geol. 256 (2008) 230–240. doi:10.1016/j.chemgeo.2008.06.029.

[23] Y. Yamamoto, K. Yamamoto, Precise XPS depth profile of soda-lime-silica glass using C_{60} ion beam, J. Non-Cryst. Solids. 356 (2010) 14–18. doi:10.1016/j.jnoncrysol.2009.09.027.

[24] D. Sprenger, H. Bach, W. Meisel, P. Gutlich, XPS study of leached glass surfaces, J. Non-Cryst. Solids. 126 (1990) 111–129. https://www.sciencedirect.com/science/article/pii/002230939091029Q#!

[25] J. Banerjee, S.H. Kim, C.G. Pantano, Elemental areal density calculation and oxygen speciation for flat glass surfaces using x-ray photoelectron spectroscopy, J. Non-Cryst. Solids. 450 (2016). doi:10.1016/j.jnoncrysol.2016.07.029.

[26] S. Hashimoto, A. Tanaka, Alteration of Ti 2p XPS spectrum for titanium oxide by low-energy Ar ion bombardment, Surf. Interface Anal. 34 (2002) 262–265.

doi:10.1002/sia.1296.

[27] Z.M. Khoshhesab, Reflectance IR Spectroscopy, in: T. Theophanides (Ed.), Infrared Spectrosc. - Mater. Sci. Eng. Technol., InTech, 2012: pp. 233–244. doi:10.5772/37180.

[28] M. Milosevic, Internal Reflection and ATR Spectroscopy, First Edit, Wiley & Sons, Inc., Hoboken. New Jersey, 2012.

[29] M. Rubin, Optical properties of soda lime silica glasses, Sol. Energy Mater. 12 (1985) 275–288. doi:10.1016/0165-1633(85)90052-8.

[30] T. Uchino, T. Sakka, K. Hotta, M. Iwasaki, Attenuated Total Reflectance Fourier-Transform Infrared Spectra of a Hydrated Sodium Silicate Glass, J. Am. Ceram. Soc. 72 (1989) 2173–2175.

[31] H. Hosono, Fourier transform infrared attenuated total reflection spectra of ion-implanted silica glasses, J. Appl. Phys. 69 (1991) 8079. doi:10.1063/1.348925.

[32] J.B. Lowenstern, B.W. Pitcher, Analysis of H_2O in silicate glass using attenuated total reflectance (ATR) micro-FTIR spectroscopy, Am. Mineral. 98 (2013) 1660–1668. doi:10.2138/am.2013.4466.

[33] F. Geotti-Bianchini, L. De Rui, G. Gagliardi, M. Guglielmi, C.G. Pantano, New interpretation of the IR reflectance spectra of SiO_2 rich films on soda lime glass, Glas. Berichte. 64 (1991) 205–217.

[34] M. Tomozawa, Y. Lee, Surface fictive temperature of annealed and rate-cooled soda lime glasses, J. Non-Cryst. Solids. 253 (1999) 119–125.

[35] F. Geotti-Bianchini, M. Preo, M. Guglielmi, C.G. Pantano, Infrared reflectance spectra of semi-transparent SiO_2 rich films on silicate glasses: Influence of the substrate and film thickness, J. Non-Cryst. Solids. 321 (2003) 110–119.

doi:10.1016/S0022-3093(03)00154-6.

[36] R.M. Almeida, T.A. Guiton, C.G. Pantano, Characterization of silica gels by infrared reflection spectroscopy, J. Non-Cryst. Solids. 121 (1990) 193–197. doi:http://dx.doi.org/10.1016/0022-3093(90)90130-E.

[37] N.J. Smith, C.G. Pantano, Leached layer formation on float glass surfaces in the presence of acid interleave coatings, J. Am. Ceram. Soc. 91 (2008) 736–744. doi:10.1111/j.1551-2916.2007.02079.x.

[38] T. Uchino, T. Sakka, M. Iwasaki, Interpretation of Hydrated States of Sodium Silicate Glasses by Infrared and Raman Analysis, J. Am. Ceram. Soc. 74 (1991) 306–313. doi:10.1111/j.1151-2916.1991.tb06880.x.

[39] A.B. Kuzmenko, Kramers-Kronig constrained variational analysis of optical spectra, Rev. Sci. Instrum. 76 (2005) 1–9. doi:10.1063/1.1979470.

[40] S. a Macdonald, C.R. Schardt, D.J. Masiello, J.H. Simmons, Dispersion analysis of FTIR reflection measurements in silicate glasses, J. Non-Cryst. Solids. 275 (2000) 72–82. doi:10.1016/S0022-3093(00)00121-6.

[41] S. Amma, S.H. Kim, C.G. Pantano, Analysis of Water and Hydroxyl Species in Soda Lime Silica Glass Surfaces using Attenuated Total Reflection (ATR) - IR spectroscopy, J. Am. Ceram. Soc. (2015). doi:DOI: 10.1111/jace.13856.

[42] M.E. Pemble, P. Gardner, Infrared Spectroscopy from Surfaces, in: J.C. Vickerman, I.S. Gilmore (Eds.), Surf. Anal. – Princ. Tech., 2nd Editio, John Wiley & Sons, Ltd, Chichester, West Sussex, PO19 8SQ, United Kingdom, 2009: pp. 334–361.

[43] A.M. Zaitsev, Optical properties of diamond, A data handbook, Springer, 2011.

[44] N.P. Barnes, M.S. Piltch, Temperature-dependent Sellmeier coefficients and nonlinear optics average power limit for germanium, J. Opt. Soc. Am. 69 (1979)

178. doi:10.1364/JOSA.69.000178.

[45] P.B. McGinnis, J.E. Shelby, Diffusion of water in float glass melts, J. Non-Cryst. Solids. 177 (1994) 381–388. doi:10.1016/0022-3093(94)90552-5.

[46] J.E. Shelby, Protonic species in vitreous silica, J. Non-Cryst. Solids. 179 (1994) 138–147. doi:10.1016/0022-3093(94)90691-2.

[47] F. V Natrup, H. Bracht, S. Murugavel, B. Roling, Cation diffusion and ionic conductivity in soda-lime silicate glasses., Phys. Chem. Chem. Phys. 7 (2005) 2279–2286. doi:10.1039/b502501j.

[48] E.N. Boulos, L.B. Glebov, T. V Smirnova, Absorption of iron and water in the Na_2O–CaO–MgO–SiO_2 glasses. I. Separation of ferrous and hydroxyl spectra in the near IR region, J. Non-Cryst. Solids. 221 (1997) 213–221. doi:10.1016/S0022-3093(97)00334-7.

[49] D.B. Asay, S.H. Kim, Evolution of the adsorbed water layer structure on silicon oxide at room temperature., J. Phys. Chem. B. 109 (2005) 16760–3. doi:10.1021/jp053042o.

[50] A. Novak, Hydrogen bonding in solids correlation of spectroscopic and crystallographic data, in: Large Mol. SE - 4, Springer Berlin Heidelberg, 1974: pp. 177–216. doi:10.1007/BFb0116438.

[51] M. Milosevic, Depth Profiling, in: Intern. Reflect. ATR Spectrosc., First Edit, Wiley & Sons, Inc., Hoboken, New Jersey, 2012: pp. 92–96.

[52] R.W. Douglas, J.O. Isard, The Action of Sulphur Dioxide and of Water on Glass Surfaces, J. Soc. Glas. Technol. 33 (1949) 289.

[53] W.E. Dirkes, W.A. Rubey, C.G. Pantano, The formation of a silica-rich surface using sulfur dioxide in drawn glass capillaries, J. High Resolut. Chromatogr. 3

(1980) 303–305. doi:10.1002/jhrc.1240030611.

[54] R. Gardon, Variation of Densities and Refractive Indices in Tempered Glass, J. Am. Ceram. Soc. 61 (1978) 143–146. doi:10.1111/j.1151-2916.1978.tb09258.x.

[55] Y. Zhang, E.M. Stolper, G.J. Wasserburg, Diffusion of water in rhyolitic glasses, Geochim. Cosmochim. Acta. 55 (1991) 441–456. doi:10.1016/0016-7037(91)90003-N.

[56] A.M. Efimov, V.G. Pogareva, A. V. Shashkin, Water-related bands in the IR absorption spectra of silicate glasses, J. Non-Cryst. Solids. 332 (2003) 93–114. doi:10.1016/j.jnoncrysol.2003.09.020.

[57] G. Navarra, I. Iliopoulos, V. Militello, S.G. Rotolo, M. Leone, OH-related infrared absorption bands in oxide glasses, J. Non-Cryst. Solids. 351 (2005) 1796–1800. doi:10.1016/j.jnoncrysol.2005.04.018.

[58] A. Shen, H. Keppler, Infrared spectroscopy of hydrous silicate melts to 1000℃ and 10 kbar : Direct observation of H_2O speciation in a diamond-anvil cell, Am. Mineral. 80 (1995) 1335–1338.

[59] R. Gy, Ion exchange for glass strengthening, Mater. Sci. Eng. B Solid-State Mater. Adv. Technol. 149 (2008) 159–165. doi:10.1016/j.mseb.2007.11.029.

[60] J. Luo, J. Banerjee, C.G. Pantano, S.H. Kim, Vibrational Sum Frequency Generation (SFG) Spectroscopy Study of Hydrous Species in Soda Lime Silica (SLS) Float Glass, Langmuir. (2016) acs.langmuir.6b00706. doi:10.1021/acs.langmuir.6b00706.

[61] H. Behrens, M. Nowak, Quantification of H_2O Speciation in Silicate Glasses and Melts by IR Spectroscopy - in situ versus Quench Techniques, Phase Transitions. 76 (2003) 45–61. doi:10.1080/0141159031000076048.

[62] A. Ellison, I.A. Cornejo, Glass Substrates for Liquid Crystal Displays, Int. J. Appl. Glas. Sci. 1 (2010) 87–103. doi:10.1111/j.2041-1294.2010.00009.x.

[63] S. Amma, J. Luo, C.G. Pantano, S.H. Kim, Specular Reflectance (SR) and Attenuated Total Reflectance (ATR) Infrared (IR) Spectroscopy Analyses of Soda-lime Glass Surfaces: an Experimental and Comparative Study, J. Non-Cryst. Solids. 428 (2015) 189–196. doi:http://dx.doi.org/10.1016/j.jnoncrysol.2015.08.015.

[64] M. Hara, S. Suetoshi, Density Change of Glass in Transformation Range, Res. Rep. Asahi Glas. Co. Ltd. 5 (1955) 126–135.

[65] A. Edgar, Optical properties of Glasses, in: J. Singh (Ed.), Opt. Prop. Condens. Matter Appl., John Wiley & Sons, Ltd, Hoboken, New Jersey, 2006: pp. 159–196.

[66] Y. Kataoka, K. Yamazaki, M. Shigeno, Y. Tada, K. Wittmaack, Surface roughening of silicon under ultra-low-energy cesium bombardment, Appl. Surf. Sci. 203–204 (2003) 43–47. doi:10.1016/S0169-4332(02)00650-5.

[67] R.H. Doremus, Interdiffusion of Hydrogen and Alkali Ions in Glass Surfaces, J. Non-Cryst. Solids. 19 (1975) 137–144. doi:10.1016/0022-3093(79)90022-X.

[68] A. Agarwal, M. Tomozawa, Determination of fictive temperature of Soda-lime glass, J. Am. Ceram. Soc. 78 (1995) 827–829.

[69] A.C. Withers, H. Behrens, Temperature-induced changes in the NIR spectra of hydrous albitic and rhyolitic glasses between 300 and 100 K, Phys. Chem. Miner. 27 (1999) 119–132. doi:10.1007/s002690050248.

[70] J.P. Hamilton, C.G. Pantano, Effects of glass structure on the corrosion behavior of sodium-aluminosilicate glasses, J. Non-Cryst. Solids. 222 (1997) 167–174. doi:10.1016/S0022-3093(97)90110-1.

[71] N. Tsomaia, S.L. Brantley, J.P. Hamilton, C.G. Pantano, K.T. Mueller, NMR

evidence for formation of octahedral and tetrahedral Al and repolymerization of the Si network during dissolution of aluminosilicate glass and crystal, Am. Mineral. 88 (2003) 54–67. doi:10.2138/am-2003-0107.

[72] J.P. Hamilton, Effects of Structure, Composition and pH on the Corrosion Behavior of Sodium-Aluminosilicate Glasses and Crystals, Ph. D dessertation, The Pennsylvania State University, 1999. http://scholar.google.com/scholar?hl=en&btnG=Search&q=intitle:No+Title#0.

[73] A. Paul, Chemical durability of glasses; a thermodynamic approach, J. Mater. Sci. 12 (1977) 2246–2268. doi:10.1007/BF00552247.

[74] N.P. Mellott, Multicomponent aluminosilicate glasses: structure and acid corrosion, Ph. D dessertation, The Pennsylvania State University, 2003.

[75] S. Amma, M.T. Lanagan, S.H. Kim, C.G. Pantano, Ionic Conductivity in Sodium – Alkaline Earth – Aluminosilicate Glasses, J. Am. Ceram. Soc. 99 (2016) 1239–1247. doi:10.1111/jace.14101.

[76] J. Stone, G.E. Walrafen, Overtone vibrations of OH groups in fused silica optical fibers, J. Chem. Phys. 76 (1982) 1712–1722. doi:10.1063/1.443210.

[77] M. Leschik, G. Heide, G.H. Frischat, H. Behrens, M. Wiedenbeck, N. Wagner, K. Heide, H. Geisler, U. Reinholz, Determination of H_2O and D_2O contents in rhyolitic glasses, Phys. Rev. Lett. 45 (2004) 238–251.

[78] A. Bertoluzza, C. Fagnano, M.A. Morelli, Raman and Infrared spectra on silica gel evolving toward glass, J. Non-Cryst. Solids. 48 (1982) 117–128. doi:10.1016/0022-3093(82)90250-2.

[79] W.C. Pharr, G.M. Oliver, Measurement of Thin Film Mechanical Properties Using Nanoindentation, Mater. Res. Soc. 17 (1992) 28–33.

[80] J.R. Tuck, A.M. Korsunsky, D.G. Bhat, S.J. Bull, Indentation hardness evaluation of cathodic arc deposited thin hard coatings, Surf. Coatings Technol. 139 (2001) 63–74. doi:10.1016/S0257-8972(00)01116-6.

[81] S. Inaba, S. Todaka, Y. Ohta, M. Kenji, Evaluation for Estimating the Young's Modulus, Shear Modulus and Vickers Hardness of Aluminosilicate Glasses, J. Japan Inst. Met. Mater. 64 (2000) 177–183.

[82] R.D. Shannon, C.T. Prewitt, Effective ionic radii in oxides and fluorides, Acta Crystallogr. Sect. B Struct. Crystallogr. Cryst. Chem. 25 (1969) 925–946. doi:10.1107/S0567740869003220.

8 Publication

1. **Shin-ichi Amma**, Jiawei Luo, Seong H. Kim, Carlo G. Pantano, *"Effect of Glass Composition on the Hardness of Surface Layers on Aluminosilicate Glasses Formed through Reaction with Strong Acid"*, Journal of American Ceramics Society, 101 (2018) 657–665, DOI: 10.1111/jace.15239
2. **Shin-ichi Amma**, Jiawei Luo, Seong H. Kim, Carlo G. Pantano, *"Effects of Fictive Temperature on the Leaching of Soda Lime Silica Glass Surfaces"*, Journal of American Ceramics Society, 100 (2017) 1424–1431, DOI: 10.1111/jace.14754
3. **Shin-ichi Amma**, Seong H. Kim, Carlo G. Pantano, *"Analysis of Water and Hydroxyl Species in Soda Lime Silica Glass Surfaces using Attenuated Total Reflection (ATR) - IR spectroscopy"*, Journal of American Ceramics Society, 99 [1] (2016) 128–134, DOI: 10.1111/jace.13856
4. **Shin-ichi Amma**, Jiawei Luo, Seong H. Kim, Carlo G. Pantano, *"Specular Reflectance (SR) and Attenuated Total Reflectance (ATR) Infrared (IR) Spectroscopy of Transparent Flat Glass Surfaces: A Case Study for Soda Lime Float Glass"*, Journal of Non-Crystalline Solids, 428 (2015) 189–196

9 Presentation

1. **Shin-ichi Amma**, Jiawei Luo, Seong H. Kim, Carlo G. Pantano, *"Surface layer formed through acid treatment of aluminosilicate glasses"*, ICG Annual Meeting 2018, Yokohama, Japan, Sep. 24th, 2018
2. **Shin-ichi Amma**, Jiawei Luo, Seong H. Kim, Carlo G. Pantano, *"ATR-IR Analysis of Water in Silicate Glass Surfaces"*, 5th Workshop of Photonic Materials 2017, Osaka, Japan, Mar. 1st, 2017 (Invited, In Japanese)
3. **Shin-ichi Amma**, Jiawei Luo, Seong H. Kim, Carlo G. Pantano, *"ATR - IR Analysis of Water in Soda Lime Glass Surfaces"*, CerSJ-GOMD Joint Symposium on Glass Science and Technologies, Kyoto, Japan, Nov. 14th, 2016
4. **Shin-ichi Amma**, Seong H. Kim, Carlo G. Pantano, *"ATR - IR Analysis of Water in Soda Lime Glass Surfaces"*, 24th International Congress on Glass, Shanghai, China, Apr. 8th, 2016.
5. **Shin-ichi Amma**, Seong H. Kim, Carlo G. Pantano, *"Attenuated Total Reflection (ATR) - FTIR Spectroscopy Analysis of Water in the Surface of Commercial Silicate Glass"*, Materials Science & Technology 2015, Columbus, OH, Oct. 6th, 2015

10 Other publications

1. Katsuaki Nakazawa, Tomohiro Miyata, **Shin-ichi Amma**, Teruyasu Mizoguchi, *"Identification of nanometer-scale compositional fluctuations in silicate glass using electron microscopy and spectroscopy"*, Scripta Materialia, 154 (2018) 197-201, DOI: 10.1016/j.scriptamat.2018.05.048
2. **Shin-ichi Amma**, Mike T. Lanagan, Seong H. Kim, Carlo G. Pantano, *"Ionic conductivity in sodium - alkaline earth - aluminosilicate glass"*, Journal of American Ceramics Society, 99 [4] 1239–1247 (2016), DOI: 10.1111/jace.14101
3. **Shin-ichi Amma**, Yuki Tokumoto, Keiichi Edagawa, Naoya Shibata, Teruyasu Mizoguchi, Takahisa Yamamoto and Yuichi Ikuhara, *"Electrical current flow at conductive nanowires formed in GaN thin films by a dislocation template technique"*, Applied Physics Letters 96 (2010) 193109
4. Yuki Tokumoto, **Shin-ichi Amma**, Naoya Shibata, Teruyasu Mizoguchi, Keiichi Edagawa, Takahisa Yamamoto and Yuichi Ikuhara, *"Fabrication of electrically conductive nanowires using high-density dislocations in AlN thin films"*, Journal of Applied Physics 106 (2009) 124307

11 Other Presentation

(Only presentations as a first author are listed)

1. **Shin-ichi Amma**, Mike T. Lanagan, Seong H. Kim, Carlo G. Pantano, *"Composition Effects on Ionic Transport in Alkali - Alkaline-Earth - Aluminosilicate Glass"*, ACerS GOMD–DGG Joint Meeting, Miami, FL, May. 20th, 2015
2. **Shin-ichi Amma**, Yuki Tokumoto, Keiichi Edagawa, Naoya Shibata, Teruyasu Mizoguchi, Takahisa Yamamoto and Yuichi Ikuhara, *"Fabrication of conductive nanowires using threading dislocation in GaN thin film"*, The 57th Japan Society of Applied Physics Spring Meeting, Kanagawa, Japan, March. 8th, 2010 (In Japanese)
3. **Shin-ichi Amma**, Nobuaki Takahashi1, Tsubasa Nakagawa, Isao Sakaguchi, Rie Takenaka, Keiichi Edagawa, Naoya Shibata, Teruyasu Mizoguchi, Yuki Tokumoto, Takahisa Yamamoto and Yuichi Ikuhara, *"Fabricating Conductive Nanowires using Dislocations in GaN Thin Films"*, MRS Fall Meeting & Exhibit, Boston, MA, December. 2nd, 2009 (poster)
4. **Shin-ichi Amma**, Nobuaki Takahashi, Tsubasa Nakagawa, Isao Sakaguchi, Yuki Tokumoto, Takahisa Yamamoto, Naoya Shibata, Teruyasu Mizoguchi and Yuichi Ikuhara, *"Cation segregation in threading dislocation in thin GaN film"*, Annual Spring meeting of The Japan Institute of Metals and Materials, Tokyo, Japan, March. 29th, 2009 (In Japanese)

12 Acknowledgment

I would like to express my deepest appreciation to Prof. Hiroyuki Inoue for his guidance on this thesis. He gave a lot of helpful comments on this thesis. I am deeply grateful to Prof. Yuichi Ikuhara who first taught me how materials science was interesting when I joined his group in my bachelor course. Through my student days, I learned a lot about an attitude against research as a scientist. I would like to my gratitude to Prof. Naoya Shibata who also always helped me valuable advice and kindness from when I was bachelor student. I liked relaxing conversation in his room at that time. I would like to offer special thanks to Prof. Teruyasu Mizoguchi who also always advised me on my research and life in general since I was student in the university. He gave many insights on this study as well as another collaborative work between us. I would like to thank Prof. Katsuyuki Fukutani for his valuable comments on this thesis.

This work has been done in collaborative program between the Pennsylvania State University and AGC Inc. under supervision of Prof. Carlo Pantano and Prof. Seong H. Kim. I would like to express my deepest appreciation to Prof. Carlo Pantano for his precious guidance. All discussion with him were highly suggestive for me and I often came up with new idea after that. He also supported my whole life in State College kindly. I really appreciate it. I would also like to express my respect to Prof. Seong H. Kim for his patient support for me. I leaned a lot from him how we should deliver my own research and ownership we should have as a researcher.

I would like to thank Dr. Josh Stapleton for his broad knowledge about spectroscopy. Most of the data in this thesis were collected in the machine he maintained carefully. I would also like to thank Vince Bojan for his support on XPS. I enjoyed

discussions about XPS with him.

I would like to express my appreciation to members in Pantano and Kim's group, Dr. Joy Banerjee, Dr. Jiawei Luo, Dan Kramer, Dr. Nisha Sheth, Dr. Hongtu He, and Nick Surdyka. They are all good friends and helped me live in Millennium Sciences Complex, without any complain on my poor English. Without the support of you, all this research would not have been possible. Especially Joy was always my good teacher on everything needed for me to live there. Jiawei taught me lots on how to use experimental instruments in our group and helped my paper. I would like to thank Donna Lucas for her continuous support.

I would like to thank former general managers of AGC research center, Mr. Tomoya Takigawa and Mr. Hiroyuki Watanabe for giving me an opportunity to study abroad. I would like to thank my bosses, Dr. Kei Maeda, Mr. Yuichi Kuroki, Dr. Yuki Kondo, Mr. Tetsuya Nakashima, for sending me Penn State and supporting me continuously. I would like to thank Mr. Kunio Masumo, Dr. Yoko Takebe, Ms. Kumiko Kobayashi and Ms. Rie Kunisada for supporting this project as R&D planning team. I would like to thank Dr. Setsuro Ito, Dr. Kiyoshi Yamamoto, Dr. Akio Koike, Dr. Shusaku Akiba and Mr. Toshio Suzuki for valuable discussion on my research. I would like to thank Mr. Daisuke Kobayashi, Ms. Tomomi Sekine and Mr. Michinori Suehara for conducting SIMS and XPS experiments in AGC. I would like to express special thanks to my senior colleagues in Penn State from AGC, Dr. Yusuke Arai, Mr. Masahiro Ohkura, and Dr. Takahira Miyagi. They helped me setting up in State College. Especially Dr. Miyagi and his wife, Soyon-san, supported me when I felt alone every day in beginning of my life there.

I would like to thank my family, particularly my parents, Mr. Masanobu Amma

and Ms. Yoko Amma, for their constant love and support and patience, even in my difficult or tough times.

Finally I would like to express my greatest appreciation to my amazing wife, Yoko, who has accompanied me every time and helped me live happy life. There are no words to tell how much your love and encouragement has helped me through each day. Thank you very much.